JAERI-M
7103

INFLUENCE OF ERROR FIELDS ON THE PLASMA CONFINING FIELD AND THE PLASMA CONFINEMENT IN TOKAMAK

May 1977

Shinzaburo MATSUDA

日本原子力研究所
Japan Atomic Energy Research Institute

JAERI - M 7103

Influence of Error Fields on the Plasma Confining Field and the Plasma Confinement in Tokamak

Shinzaburo MATSUDA

Division of the Thermonuclear Fusion Research, Tokai, JAERI

(Received May 9, 1977)

Influence of error fields on the plasma confining field and the plasma confinement is treated in the standpoint of design.

In the initial breakdown phase before formation of the closed magnetic surfaces, the vertical field properly applied is the most important. Once the magnetic surfaces are formed, the non-axisymmetric error field is important. Effect of the shell gap associated with iron core and with pulsed vertical coils is thus studied. The formation of magnetic islands due to the external non-axisymmetric error field is studied with a simple model. A method of suppressing the islands by choosing the minor periodicity is proposed.

JAERI－M 7103

トカマク装置における乱れ磁場の，プラズマ閉込め磁場およびプラズマ閉込めに及ぼす影響

日本原子力研究所東海研究所
核融合研究部

松田慎三郎

（1977年5月9日受理）

トカマク装置に於いて，乱れ磁場がプラズマ閉込め磁場及びプラズマ閉込めに及ぼす影響を，装置設計の立場からまとめたものである。放電の初期，閉じた磁気面が形成される前には垂直磁場を適切にかけることが最も重要である。一担閉じた磁気面が形成されると非軸対称の乱れ磁場が重要となる。この観点から，鉄心からの漏洩磁場やパルス垂直磁場と関連したシェルギャップの影響が調べられた。また，これらの非軸対称乱れ磁場による磁気面の島の形成が簡単なモデルに基いて検討され，トロイダル方向の周期を適切に選ぶことによって島の形成が抑えられることが判った。

この報告は「京都大学審査学位論文」と同じものである。

CONTENTS

CHAPTER 1
INTRODUCTION

A low-beta plasma confinement by tokamak devices[1] has been one of the most attractive means in the thermonuclear fusion research program. Historically, it has been studied extensively in Russia since mid-1950's. Notwithstanding the seeming simplicity of its magnetic configuration, a fairly long time was needed before its superiority has been approved. This may be attributed to the diagnostics difficulties involved in this particular devices, because of high density, high temperature of the plasma and because of the presence of plasma current. In 1968 N.J. Peacock et al[2] from Culham laboratory visited the Kurchatov institute where they measured the electron temperature in Russian tokamak T-3[3] by Thomson scattering of the laser light and confirmed the former results measured by diamagnetic loops. Since that time, the tokamak has attracted the world wide interests as an outstanding device in the low beta approach to CTR. Shortly after this confirmation, Princeton group has determined to shut down the long lasting C-stellarator experiments[5] and to convert it to a tokamak (ST)[4]. It was just under these situations that JAERI begun its activities on the design of a tokamak (JFT-2)[6].

A stabilized confinement of the tokamak plasma is attained by the complex magnetic field produced by the different types of coils and conducting shells.[3,6] One of the important characteristics of the tokamak plasma is the axisymmetry.[7] However, it is practically impossible to design devices with a complete symmetry, due to shell gaps, to the yoke of a transformer core and also to the misassembling of coils or to their current feeders. The consequence is occurrence of the error field. Its influence on the plasma confinement had been partly studied[8,9,10] mainly on Stellarator geometries before the design study on the JFT-2 tokamak started. However, only few works[11,12] were available which were useful for practical cases from designing view points. This may be due to the circumstances that very small number of tokamaks existed in the world except in Russia and therefore, those works had not been made much of on those days. Besides, geographical position of Japan had the disadvantage of getting informations which were veiled behind the published works. By these reasons, it was not clear what is the allowable limit of the error field. Furthermore, properties of the tokamak plasma were not well understood because of diagnostics difficulties and its

complexity even though the well-confined stable discharge is established. In the initial breakdown phase of the discharge, measurements might be much more difficult, since all the plasma parameters are time-dependent in a high electric field and atomic processes such as ionization, excitation and recombination as results of plasma-neutral and/or plasma-wall interactions are involved.

It was under these circumstances that this work has been started on the JFT-2 tokamak in order to evaluate the allowable error field under which the plasma can be confined throughout an entire discharge, namely, from the plasma production phase to the confinement phase.

In the JFT-2 tokamak, following magnetic fields are energized which can be devided into two groups. Namely, the one is the so-called "internal field" due to the plasma current and the other is the "external field" due to various control windings. The latter consists of toroidal field which is used to stabilize the plasma column, D.C. and pulsed vertical fields which are provided to suppress the plasma column shift, and the induction field which is applied for the ohmic heating of the plasma. There are also other mediums which are capable of producing magnetic field. Conducting shells and transformer core may be included in this category. Thus the purpose of the present paper is to investigate the influence of their error fields on the plasma confinement.

The JFT-2 tokamak has been accomplished in 1972 followed by a stable confinement of the high temperature plasma.[13,14,15] The typical dimensions of this device are listed in Table 1.1. Figure 1.1 shows a side view of the device with a dry evacuating system on the right hand. The upper view is shown in Fig. 1.2 indicating positions of diagnostics ports. Fig. 1.3 shows a quarter unit of the toroidal coil-liner system mounted on the slide base.

In Chapter 2 we treat the initial breakdown phase when the magnetic surface has not yet been formed. In this phase, escaping field lines due to error fields may almost determine the plasma confinement. Every conceivable sources producing error fields[16] are evaluated relating to the plasma confinement.

When the plasma current rises to form magnetic surfaces, deformation of the plasma column may be the primary interest. Chapter 3 is devoted to this problem including influences of axisymmetric error fields[17] and of shell gaps.[16]

The equilibrium of the plasma is also strongly influenced by the

leakage magnetic field from the iron core.[17,18] In particular, the strength of the vertical component of the leakage magnetic field is of a great concern, since its magnitude is supposed to be of the same order of the equilibrating vertical field. There were several measurements using model iron cores.[6,19] However, measurements were made in the absence of the secondary plasma current. There had been difficulties in measuring these values in the presence of even a simulated plasma current, since azimuthal field due to the plasma current overwhelms the leakage field which is to be measured. In Chapter 4, a method is presented for measuring such a leakage magnetic field.[18] Measurements are made by a special pick up coil on a model iron core of the JFT-2 tokamak. The results will be applied to the equilibrium of a shellless tokamak.

In the presence of a conducting shell, the situation is quite different, because the external field is partly shielded by the shell, and its gap effect becomes prominent. In particular, the toroidal uniformity of the vertical field is strongly influenced by the shell gap. In Chapter 5, these problems are investigated and the results are compared with the theory.[20] This makes it possible to determine the effective gap length.

These shell gaps also affect the uniformity of the control field. For instance, the pulsed vertical field is strongly influenced by the presence of shell gaps in association with finite conductivity of the shell.[21,22] This is due to the induction of the soakage current which flows in the shell. These problems are discussed in Chapter 6.

Chapter 7 is oriented to study the magnetic island formation due to error field in resonance with the rotational transform of magnetic lines of force.[16,23,24] The width of islands had been obtained analytically by M.N. Rosenbluth et al.[11,25] on the analogy of phase space analysis of the motion of particles. Their theory is confirmed here by a simple analysis which gives a physical picture more clearly. Islands which may appear due to resonant components of the pulsed vertical field are investigated numerically by means of following magnetic lines of force by the R.K.G. method and then are compared with the theory.

Magnetic islands formation is again discussed in Chapter 8 with a special emphasis on the importance of minor periodicity in the toroidal direction.[26] This periodicity, which is generally identified by the number of shell gaps, has a possibility of reducing resonant formations of magnetic islands. Several examples are presented to confirm this model by numerical calculations. Finally, Chapter 9 serves to summarize and conclude the present work.

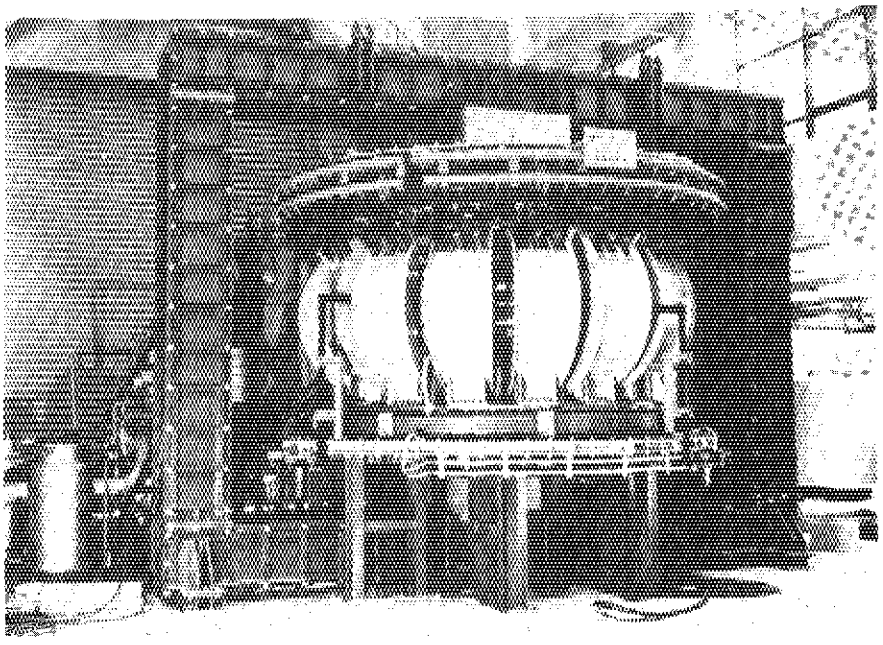

Fig. 1.1 The JFT-2 tokamak (accomplished in 1972)

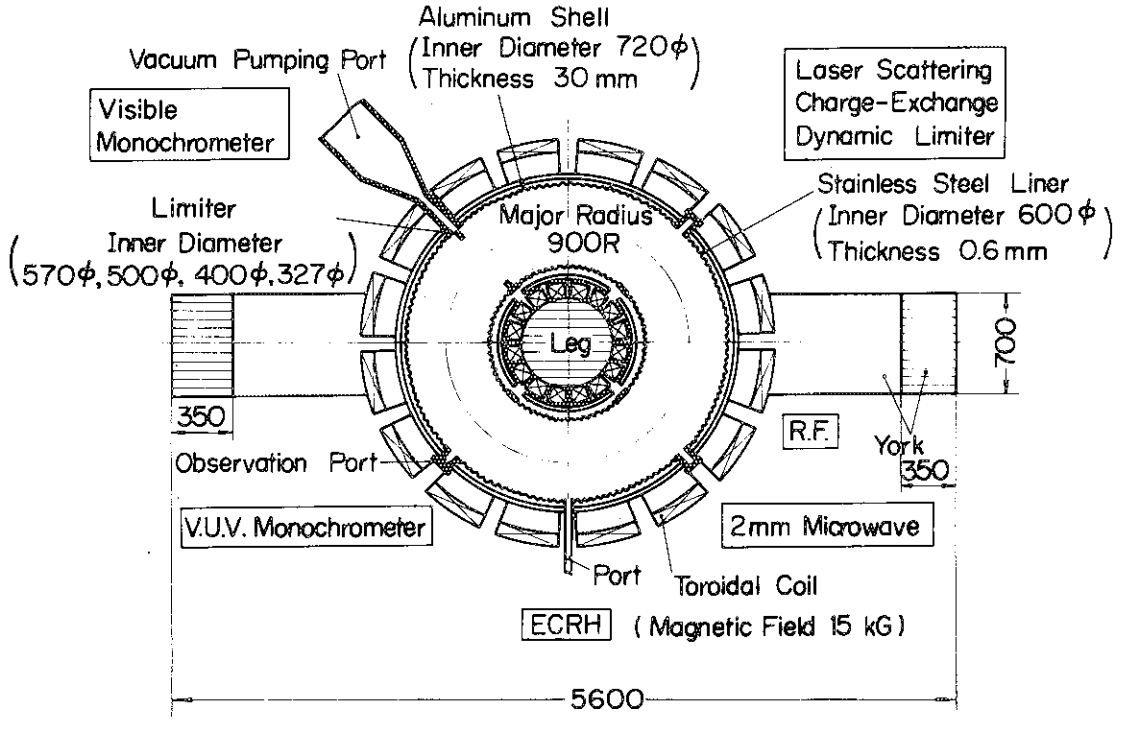

Fig. 1.2 Upper view of the JFT-2 device and the arrangement of diagnostics instruments.

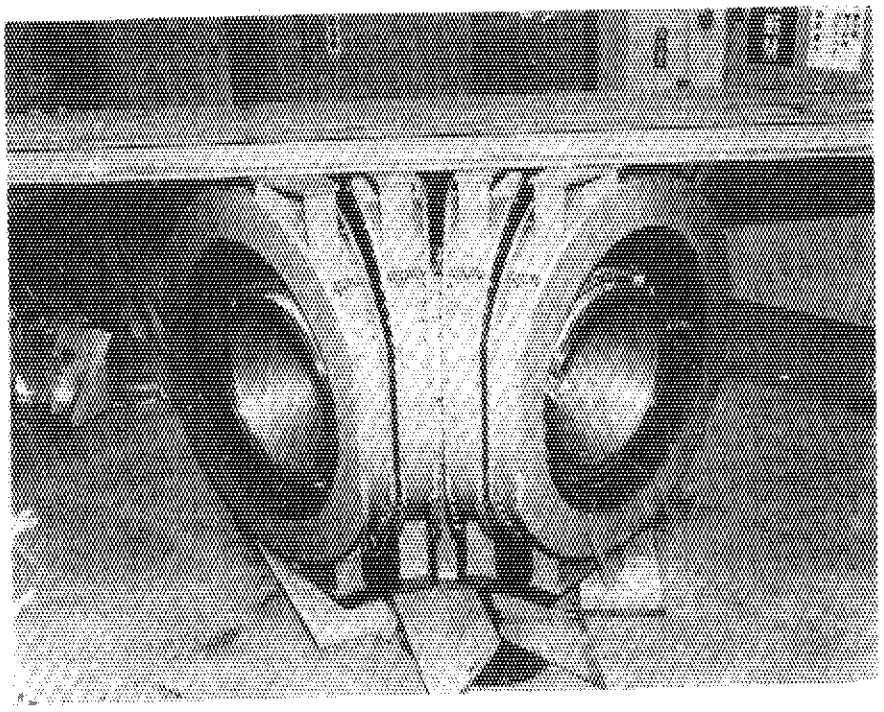

Fig. 1.3 A quarter unit of the toroidal coil and the liner mounted on the slide base.

Toroidal Field B_t	< 1.0 Wb/m^2 (phase 1) < 1.8 Wb/m^2 (phase 2)
Major Radius R	90 cm
Minor Radius a	25 cm
Core Flux	< 0.58 V.s
Vertical field	
Continuous B_{dcv}	< 350 G
Pulse B_{pv}	< 160 G
Shell (Aluminum)	
Minor Radius b	36 cm
Thickness	3 cm
Liner (Stainless Steel)	
Minor Radius r_{lin}	30 cm
Thickness	0.6 mm
Limiter (Molybdenum)	
Minor Radius	25 cm, 20cm and 16.3 cm
Plasma Current	< 210 kA

Table 1.1 Typical dimensions of the JFT-2 tokamak

CHAPTER 2
ERROR FIELD IN THE BREAKDOWN PHASE[16)]

§2.1 Introduction

First, we treat the case where the azimuthal field due to a plasma current has yet been small, and can be neglected as compared with other external fields. This is particularly the case in the initial breakdown and subsequent current rising phase. We assume that intensities of the external error fields are small compared with toroidal field B_t. In the presence of these error fields, magnetic lines of force do not close and finally intersect the chamber wall after they transit along the major circumference of the torus for many times. In these magnetic field configurations, the behavior of the charged particles is determined in terms of parallel and perpendicular diffusion along and across the field lines.[27)] The parallel motion of the plasma may be ambipolar diffusion, if the mean free path of particles is much smaller than the total length of a magnetic line of force before interception with the wall, while it may be determined by the thermal velocity of particles, if the mean free path is of the same order or longer than the magnetic lines of force. In the first place, in §2.2 we discuss the effect of perturbations of the toroidal magnetic field and investigate what kind of coil configurations would give rise to escaping field lines to the wall. In the second place, in §2.3 we describe how the plasma loss time varies with a change of error field intensity. Section 2.4 contributes to the estimate of constraint due to a presence of instability[12)] driven by the error field. In a simple toroidal field, the charged particles are subject to charge separation across the magnetic field in the vertical direction followed by a rapid $\mathbf{E} \times \mathbf{B}$ drift[28)] to the outside of the torus. This problem is discussed in §2.5.

§2.2 Error Field Produced by the Toroidal Coil Configurations

First, we suppose that each toroidal coil is composed of ideal single turn elements and hence no toroidal component of the coil current exists. This may correspond to the toroidal coil with numerous windings. If these coils are placed uniformly along the torus without separation, the magnetic field produced may be completely axisymmetric and the field lines close in consequence.

Next we consider the case where the number of coils is finite and they are regularly placed in equal separations in the toroidal direction.

In this case, magnetic lines of force near the coils become wavy due to nonuniformity of the field intensity (See Fig. 2.1). A separatrix appears which discriminates two groups of field lines.[29] Namely, those outside the separatrix close locally interinking with each coil and intersect the wall, while those inside it return to their original positions after the transit along the torus. This can be understood by the following conceptual experiment. We choose the cylindrical coordinate system (r,ϕ,z) such that $\phi = 0$ plane coincides with the plane of toroidal symmetry (Just as the $\phi = 0$ coordinate lies in a plane which includes one of the coils or in a plane halfway between two coils). Following one of the typical magnetic lines of force starting from the $\phi = 0$ plane in both directions, we find the trajectories are exactly symmetric with respect to the $\phi = 0$ plane because the magnetic field is symmetric. Consequently these field lines meet at one position on the opposite side of the torus.

With a similar consideration, magnetic lines of force close, even when the magnetic field is strengthened at one local point by the increase of ampere turns in one of the coils (See Fig. 2.2, where $\phi = 0$ plane is chosen to include the coil of the present concern). Also the magnetic lines of force remain closed when the position of this coil is displaced along z or r directions.

In the next place, we consider the case where the field intensities are increased (or decreased) by superposition of two different coils (See Fig. 2.3). In this case the plane symmetry is broken with respect to $\phi = 0$. We put these coils with a separation of $\pi/8$ (coinciding with that of the JFT-2) and coil currents of 281 kAT and 140.5 kAT, respectively, are superposed on a toroidal field of 1.0 Wb/m^2. These values correspond to 100% and 50% increase of the coil current in the 1.0 Wb/m^2 operation. Following magnetic lines of force by the R.K.G. method by selecting a step length of $\frac{1}{1600}$ times the major circumference, we obtain a result that it exactly returns to the original position after a transit of the torus within a numerical error. Since this is the basic property of the plane asymmetry, one envisages that magnetic lines of force close whatever the distribution of ampere turns is in a toroidal coil arrangement, provided each coil is precisely mounted on the ϕ = const. plane. This can be equivalently applied to the case where positions of coils (with equal ampere turns) are displaced in the toroidal direction, as long as they still remain in planes which include the axis of toroidal symmetry.

In what follows we discuss the case where one of the toroidal coils

tilts against ϕ = const. plane (See Fig. 2.4). This situation is equivalently understood by investigating the effect of a couple of coils illustrated in Fig. 2.4b which are superposed on the uniform toroidal field. On the other hand, as described above, a set of coils with opposit current directions do not break the closed magnetic field lines as long as they are on the ϕ = const. planes (See Fig. 2.4c). The coils in Figs. 2.4b and 2.4c can be deformed to the saddle coil without changing their topological nature. Namely, the coils in Fig. 2.4b can be deformed to those in Fig. 2.4e and those in Fig. 2.4c to those in Fig. 2.4f. The basic difference between these two cases is that the current direction in one of the coils is inverse. The consequence is that in the case of Fig. 2.4e, the traversing currents (toroidal component of the coil current) will double the intensity of the transverse field generated by this part, while those in Fig. 2.4f are opposite and the net effect may be canceled. Furthermore, the magnetic field produced by two saddle coils in Fig. 2.4e will drift the field lines in the same direction, while those in Fig. 2.4f in the opposite direction. Numerical calculations show that after a transit along the torus the displacement of a field line from the starting position is proportional to the tilt angle ξ of a toroidal coil when ξ is small. It is found to be 1.5 mm per transit in the radial direction under the conditions of the toroidal field intensity B_t = 1.0 Wb/m^2, coil current I_1 = 281 kAT and its tilt angle ξ = 0.01. On the other hand, a set up error of each toroidal coil may be determined by the accuracy of the knock pins and of a couple of holes which are drilled in the coil basement with a separation of 160 mm, and the tilt angle is estimated to be within $\xi = 3.5\times10^{-3}$ (0.2°) radian against ϕ = const. plane. This corresponds to 0.52 mm per transit for one coil, and the field line stays for almost 500 transits before it escapes to the wall and can confine the low temperature plasma (~10 eV) for sufficient time period (~100 msec). With these considerations, one concludes that most dangerous among the toroidal coil misassembling is the tilt angle of the coil which produces the toroidal component of the coil current. Therefore, one has to investigate the effect of current feeders, rewinding and/or geometrical accuracy of each coil in detail and actually these effects cannot be neglected in the present day tokamaks. We shall discuss this problem later in view of the plasma column displacement in Chapter 3.

§2.3 Allowable Limit of the Transverse Error Field

A mean free path of H^+-H^+ or e^--e^- collisions with energy about 10eV is 130 m

when the density is 10^{10} cm^{-3} and 13 m when it is 10^{11} cm^{-3}. On the other hand, the total length of the magnetic lines of force until it is intercepted by the wall is

$$L \sim 2\pi R \cdot \frac{r_p}{2\pi R \times 10^{-2}} \sim 25 \text{ m} \tag{2.1}$$

in the presence of 1% transverse error field all over the torus, where r_p and R are the minor radius and major radius of the plasma, respectively. Therefore, in the case of low density plasma such as $n \sim 10^{10}$ cm^{-3} or of strong error field, the mean free path is much longer than the total length of the magnetic lines of force ($\lambda \gg L$) and hence, particles can escape from the confinement region with their thermal velocity. The characteristic time of this phenomena is given by

$$\tau \sim L/v_{thi} \tag{2.2}$$

where the notation is obvious. When the plasma density increases so that it comes to satisfy the condition $\lambda \ll L$, particle losses may be determined in terms of ambipolar diffusion along the magnetic lines of force. Takeda[30] et al had shown in numerical simulations that an initial filling gas is almost fully ionized in quite a short time ($t \lesssim 0.5$ ms) and meanwhile the electron temperature stays around 10 eV. The ion sound velocity, a characteristic velocity of the ambipolar diffusion, is estimated to be

$$v_s \sim \sqrt{\frac{kT_e}{m_i}} \sim 2.9 \times 10^6 \text{ cm/sec.} \tag{2.3}$$

and the plasma loss time τ_n is given by

$$\tau_n \sim \frac{L}{v_s} \quad . \tag{2.4}$$

Until the plasma current rises to form magnetic surfaces, it is necessary for the initially produced plasma to be effectively heated, before it escapes. We define the following quantities;

$$\text{Plasma heating time} \quad : \tau_h = \frac{nkT}{jE} \simeq \frac{nkT_e}{jE} \tag{2.5}$$

$$\text{Ratio of error field to toroidal field} \quad : \alpha = \frac{b}{B_t} \tag{2.6}$$

Then the total length of the magnetic lines of force L is written as

$$L = r_p \cdot \frac{B_t}{b} = \frac{r_p}{\alpha} \tag{2.7}$$

Therefore, the condition for the effective heating of plasma before it

escapes to the wall is

$$\tau_h < \tau_n \tag{2.8}$$

namely,

$$\frac{nkT_e}{jE} < \frac{r_p}{a}\sqrt{\frac{m_i}{kT_e}} \tag{2.9}$$

or

$$a < \frac{E^2 r_p}{nkT_e \eta}\sqrt{\frac{m_i}{kT_e}} \tag{2.10}$$

Assuming the plasma parameters, $T_e \sim 10$ eV, $n \sim 10^{12}$ cm^{-3}, $E \sim \frac{2.5\text{volt}}{2\pi R}$ $\sim 4.5\times10^{-3}$ volt/cm, $r_p \sim 10$ cm, $\eta \sim 2\text{x}10^{-4}$ ohm-cm, we obtain

$$a < 1.6\times10^{-2} .$$

In the phase I operation of the JFT-2, the toroidal field intensity is 10 kG. Therefore, the transverse field should be less than 160 Gauss. This restriction would easily be satisfied in the normal operation of tokamaks.

§2.4 Instabilities Driven by Error Field[12)]

In toroidal system without closed magnetic surface, Kadomtsev[12)] has shown a possibility of an instability in the presence of a small amount of error field perpendicular to the toroidal direction. If the relative intensity of error field b/B_t is not too small, the perpendicular loss velocity is expressed by $v_t \sim v_i \frac{b}{B_t}$ as considered in the preceding section. However, if b/B_t is much smaller, the following effect is predominant. In the presence of radial electric field, the plasma drifts in the azimuthal direction with a velocity

$$v_d \sim \rho_i v_i / r_p \tag{2.11}$$

and finally an equilibrium state is obtained owing to the parallel motion of electrons along magnetic lines of force. When the inequality

$$\frac{\rho_e}{r_p} < \frac{b}{B_t} < \frac{\rho_i}{r_p} \tag{2.12}$$

holds, a rotation of plasma is determined by the drift velocity. The ions do not move appreciably along B_t during the time of one transit in the azimuthal direction. However, due to a presence of centrifugal force $m_i g \sim m_i v_d^2/r_p \sim m_i v_i^2 \rho_i^2/r_p^3$, the plasma is subject to the spreading deformation

in the b direction. Ions tend to escape in the perpendicular direction, while electrons in the parallel direction. The growth velocity of this instability is given by

$$\sqrt{gr_p} \sim \frac{\rho_i}{r_p} \quad v_i \tag{2.13}$$

and the loss time is approximately given by

$$\tau \sim \frac{r_p^2}{v_i \rho_i} = \frac{r_p^2 e B_t}{k T_i} \tag{2.14}$$

Again for the effective heating, a relation $\tau_h < \tau$ should be valid as previously described. This condition is rewritten as

$$\frac{n\, T_i^{\frac{1}{2}}}{r_p^2 B_t E^2} < 8.6 \times 10^{23} \quad \text{(in M.K.S. unit)} \tag{2.15}$$

Putting $r_p \sim 10$ cm, $B_t \sim 10^4$G, $E \sim 4.5 \times 10^{-3}$ volt/cm, $T \sim 10$ eV, one obtains a relation which may give an upper limit of the density, namely,

$$n < 5.1 \times 10^{12} \text{ cm}^{-3} \tag{2.16}$$

and the corresponding confinement time $\tau \sim 1.0$ msec when the error field b/B_t ranges between 1.2×10^{-4} and 5×10^{-3}. Thus, if the error field is small enough, one needs not seriously worry about this instability, since the plasma current perhaps rises to form closed magnetic surfaces before the density exceeds this limit.

§2.5 E×B Drift due to Charge Separation

In the initial breakdown phase where the plasma current does not exceed I_c, the critical current for the formation of closed magnetic surface which will be discussed in Chapter 3, the magnetic configuration primarily consists of a simple toroidal field and a small amount of vertical field. Therefore, electrons and ions are subject to the vertical drift due to curvature and gradient of the toroidal field (See Fig. 2.5). Since their directions are mutually opposite, they result in the build up of an electric field caused by charge separation. Although the vertical drift velocity[31]

$$v_g = \frac{\frac{1}{2} v_\perp^2 + v_{11}^2}{R\Omega} = \frac{\frac{3}{2} v_{th}^2}{R\Omega} = \frac{3}{2} \frac{\rho}{R} v_{th} \tag{2.17}$$

is a lower order quantity of v_{th}, the resulting E×B drift velocity[32]

$$v_d \sim \frac{E \times B}{B^2} \sim v_{thi} \tag{2.18}$$

is of the same order of v_{thi}.
Therefore, the confinement time τ is given by

$$\tau \sim \frac{r_p}{v_d} \sim \frac{r_p}{v_{thi}} \quad . \tag{2.19}$$

Under the condition $\tau_h < \tau$, one obtains

$$\frac{nkT}{jE} < \frac{r_p}{v_{thi}} \tag{2.20}$$

or, irrespective of temperature

$$n < r_p \cdot E^2 \times 8.1 \times 10^{17} \quad \text{(in M.K.S. unit)} \tag{2.21}$$

provided the plasma resistivity is classical.
Putting $r_p \sim 10$ cm, $E = 4.5 \times 10^{-3}$ volt cm^{-1} we get

$$n < 1.7 \times 10^{10} \ cm^{-3} \quad . \tag{2.22}$$

This condition appears most serious among the restraints discussed so far. Moreover, the drift is of an intrinsic nature of the torus irrespective to the existence of error field, it would be required to form magnetic surfaces very rapidly in the initial breakdown phase.

§2.6 Concluding Remarks

In the initial breakdown of the plasma, influence of the error field on the plasma confinement is studied. The results may be summarized as follows.

Firstly, the error field associated with toroidal coil misalignment is generated by toroidal component of the coil current. However, its vertical field component, if it ever exists, would be expected small in the ordinary set up using knock pins, and moreover, it can be compensated by the external vertical field. The radial component, on the other hand, would make a problem, if its amount is large and no compensation field is present.

Secondly, the allowable limit of the transverse field is estimated for a given plasma parameters and found to be a few percent of the toroidal field intensity. Thus it can be easily satisfied in the normal operation of tokamaks. Kadomtsev's instability may not make any serious restriction.

Finally, the $E \times B$ drift due to charge separation requires rapid formation of magnetic surfaces before the plasma density exceeds a few times $10^{10} cm^{-3}$. This restriction appears most serious, though it is not related to the presence of error field. Thus one may conclude that the influence of the error field on the plasma confinement is negligible provided the time varying vertical field is properly applied.

Recently a considerable amount of data are available which make clear the initial plasma parameters.[33] In the very early stage of the discharge the mean free path of electrons is, in fact, determined by collisions with background neutrals. In this case, the particle loss is dominated by the diffusion across the toroidal field. The energy gain of electrons accelerated in the electric field before they escape is dissipated by the ionization and/or excitation of neutral particles. Influence of the error field in this stage would be weaker.

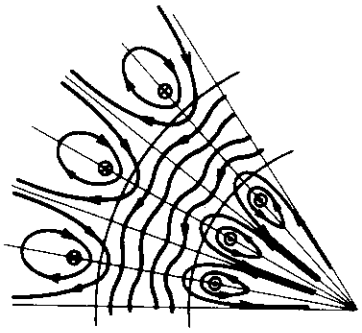

Fig. 2.1 Discrete toroidal coils and the magnetic lines of force in the median plane.

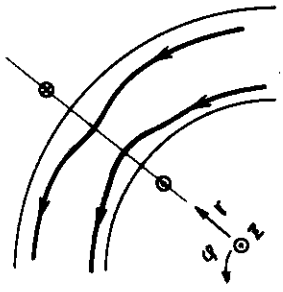

Fig. 2.2 Magnetic lines of force when the current is increased in one of the coils

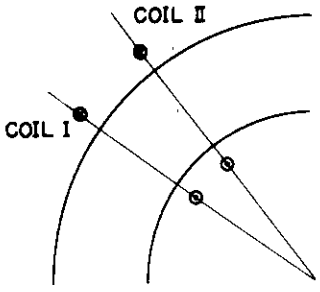

Fig. 2.3 Superposition of two coils with different ampere turns on the uniform toroidal field.

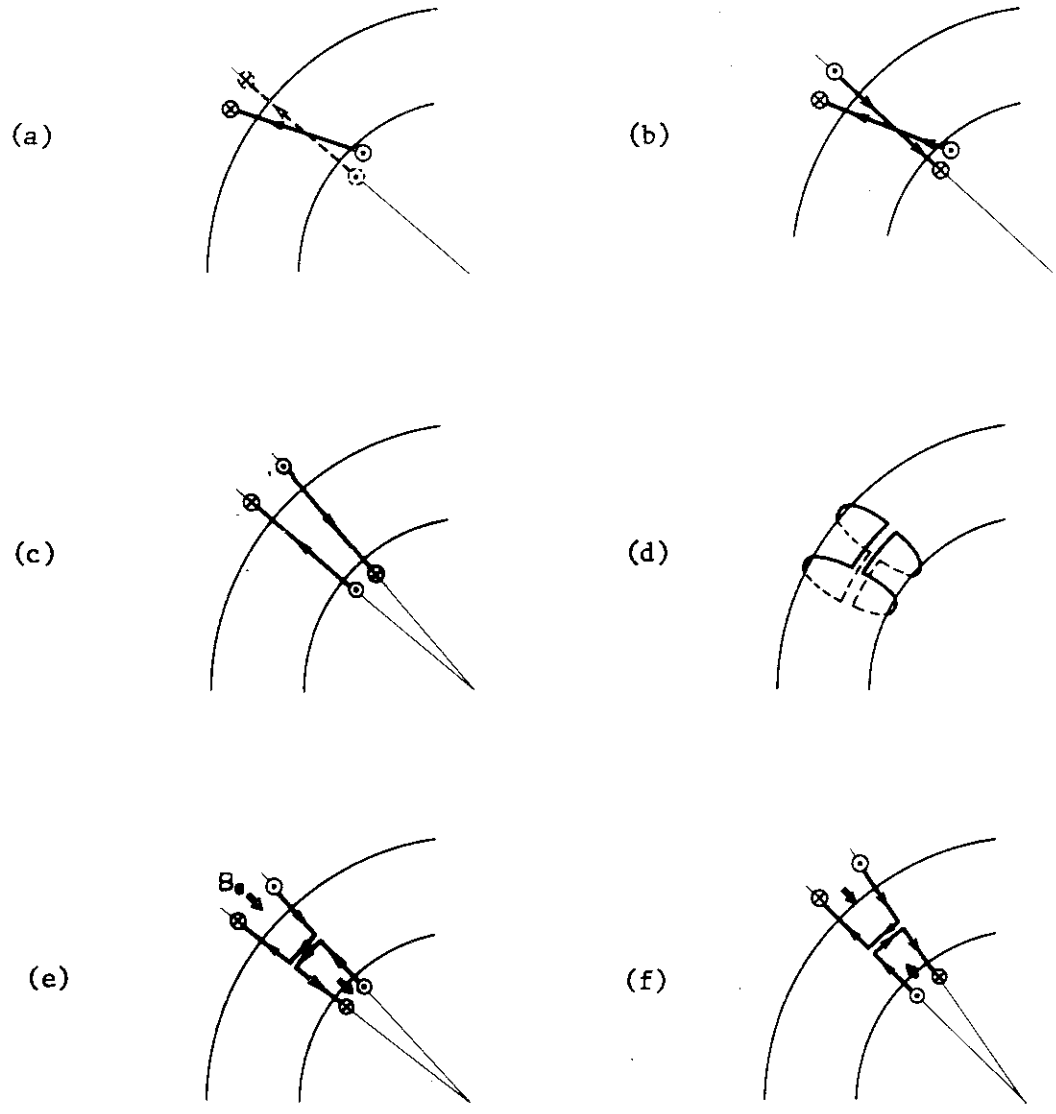

Fig. 2.4 One of the toroidal coils tilts against ϕ = const. plane.

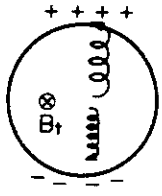

Fig. 2.5 Toroidal drift of charged particles in a simple toroidal field. The ions drift upward while the electrons drift downward.

CHAPTER 3
INFLUENCE OF ERROR FIELD ON CLOSED MAGNETIC SURFACES[16)]

§3.1 Introduction

With an increase of plasma current, the azimuthal magnetic field, in combination with the toroidal field, may give rise to a sufficient rotational transform to form closed magnetic surfaces. We shall determine a critical plasma current I_c for this condition. We consider the case where spatially uniform vertical field B_v is present. In the initial breakdown phase, the effect of a plasma pressure can be neglected in equilibrium of a plasma column. Neglecting the influence of a conducting shell, one obtains a relation necessary to keep the plasma in equilibrium in the lowest order approximation, namely.

$$B_p \sim \frac{R}{r} \cdot B_v \tag{3.1}$$

or

$$B_v \sim \frac{\mu_0 I_p}{2\pi R} \tag{3.1'}$$

where B_p is the azimuthal field by the plasma current I_p, μ_o is the permeability of the vacuum. Therefore, if B_v starts to rise from zero and is programmed in time to keep the above relation, closed magnetic surfaces could be obtained from the beginning of a discharge. However, in most present tokamaks such as T-3 (Kurchatov)[3)] ST(PPPL)[5)] and JFT-2 (JAERI)[6)] where no feedback control system of the vertical field is used, it may be very difficult to keep the above relation with time even when the vertical field is programmed to a considerable extent. As a result, a deviation of the vertical field from eq. (3.1') remains. We assume that B_v does not change during the initial break down phase. When the vertical field intensity exceeds that of eq. (3.1), the plasma is formed near the inner edge of the vacuum vessel. The condition for the existence of a closed magnetic surfaces is then given by

$$B_v < B_p = \frac{\mu_o I_p}{2\pi r_p} \tag{3.2}$$

Assuming that $B_v \sim 50$ Gauss, $r_p \sim 10$ cm, we find

$$I_p \geq I_c = 2.5 \times 10^3 \text{ Ampere} \tag{3.3}$$

Thus closed magnetic surfaces can be obtained with a small plasma current

above I_c. Once they are formed, the restrictions for the error field become lose to a considerable degree as will be discussed in the following subsections.

In §3.2, we study the deformation of a circular magnetic surface due to axisymmetric error field. In §3.3, the radial error field generated by the misalignment of a set of toroidal coils is discussed in relation to the vertical plasma shift. Section 3.4 contributes to the crude estimate of the global effect of shell gaps on the plasma shift and deformation.

§3.2 Axisymmetric Error Field

First, we consider the influence of axisymmetric error fields originated from various magnetic systems. Since the toroidicity is not intrinsic in the deformation of magnetic surfaces, a linear model is adopted. As is well known, the flux function is given by the following expressions in the lowest order approximation when a uniform transverse field is superposed on a typical circular magnetic surface,

$$\Psi_p = \beta (x^2 + y^2) \tag{3.4}$$

$$\Psi_v = \alpha \cdot x$$

where Ψ_p and Ψ_v denote the flux functions of the plasma current and vertical field, respectively, and x and y are the orthogonal coordinates. Then the superposed magnetic surface is

$$\begin{aligned} \Psi &= \Psi_p + \Psi_v = \beta (x^2 + y^2) + \alpha x \\ &= \beta \left(x + \frac{\alpha}{2\beta}\right)^2 + \beta y^2 - \frac{\alpha^2}{4\beta^2} \end{aligned} \tag{3.5}$$

namely, it can be obtained by a simple parallel shift of the circular surfaces.

Second, axisymmetric cusp type error field is considered. Near the axis, it is expressed as

$$\Psi_{cusp} = \alpha (x^2 - y^2) \tag{3.6}$$

Then we find

$$\begin{aligned} \Psi &= \Psi_{cusp} + \Psi_p = \alpha (x^2 - y^2) + \beta (x^2 + y^2) \\ &= \beta \left[\left(1 + \frac{\alpha}{\beta}\right) x^2 + \left(1 - \frac{\alpha}{\beta}\right) y^2 \right] \end{aligned} \tag{3.7}$$

Thus the superposed magnetic surfaces become elliptic or parabolic depending on the sign of $1-\frac{\alpha}{\beta}$. Since the latter occurs in the case of strong error field, we will investigate only the elliptic case. The deformation of magnetic surfaces is characterized by the ratio a/b, where a and b are the minor and major axes of the ellipse and are written as

$$a = \sqrt{\frac{\Psi}{\alpha+\beta}} \quad , \quad b = \sqrt{\frac{\Psi}{\beta-\alpha}} \quad . \tag{3.8}$$

The linear cusp field can also be expressed in terms of Bessel functions

$$\Psi = A\rho\, I_n'(n\rho) \cos n\theta \tag{3.9}$$

where ρ is the radial coordinate, θ the azimuthal coordinate, n the number of poles and A the constant. In the case of n = 2, near the axis, we get

$$I_2'(2\rho) \sim \rho \ , \qquad \text{since } I_n(n\rho) \simeq \frac{1}{ni}\left(\frac{n\rho}{2}\right)^n \qquad \text{with } \rho \to 0 \ .$$

and

$$\Psi_{cusp} = -\frac{B_{eo}}{2a}\rho^2 \cos 2\theta = -\frac{B_{eo}}{2a}(x^2 - y^2) \tag{3.10}$$

where B_{eo} is the azimuthal field at $\theta = 0$ and $\rho = a$. On the other hand the flux function for the uniform plasma current distribution is given by

$$\Psi_p = -\frac{B_{ao}}{2a}\rho^2 = -\frac{B_{ao}}{2a}(x^2 + y^2) \tag{3.11}$$

where B_{ao} is the value of B_θ at $\theta = 0$ and $\rho = a$. Then α and β in eq. (3.8) are related to B_{ao} and B_{eo} by

$$\beta = -\frac{B_{ao}}{2a} \quad , \qquad \alpha = -\frac{B_{eo}}{2a} \tag{3.12}$$

and we find

$$\frac{a}{b} = \sqrt{\left|\frac{\beta-\alpha}{\beta+\alpha}\right|} = \sqrt{\frac{B_{ao}-B_{eo}}{B_{ao}+B_{eo}}} \sim 1 - \frac{B_{eo}}{B_{ao}} \ . \tag{3.13}$$

In the JFT-2 Tokamak, B_{ao} is about 1 kG, while the cusp field, if it ever exist*), may be much smaller than the vertical control field which is of the order of 100 Gauss and hence the deformation of the superposed magnetic surfaces is much smaller than 10%. Thus the effect of cusp field is unimportant in the JFT-2 Tokamak.

---

*) Since the magnetic configuration is plane symmetric with respect to the median plane except for the slide base of the toroidal coils and for the one turn feeder and its rewinding, there is scarcely a room for the ℓ=2 cusp field to appear.

In the case of $\ell = 2$ multipole error field, the flux functions are given by

$$\Psi_{multi} = \frac{\mu_o I_e}{4\pi} \ell n \left\{ 1 + \left(\frac{\rho}{\rho_o}\right)^4 - 2\left(\frac{\rho}{\rho_o}\right)^2 \cos 2\theta \right\} \tag{3.14}$$

where ρ_o indicates the position of the multipole. Near the axis $\rho/\rho_o \ll 1$, we may write

$$\Psi_{multi} \simeq - \frac{aB_{eo}}{A} \left\{ \left(\frac{\rho}{\rho_o}\right)^4 - 2\left(\frac{\rho}{\rho_o}\right)^2 \cos 2\theta \right\} \tag{3.15}$$

where $A = 4\left(\frac{a}{\rho_c}\right)^4 - 4\left(\frac{a}{\rho_o}\right)^2 < 0$.

Then we find

$$\Psi = \Psi_P + \Psi_{multi}$$

$$= - \frac{B_{ao}}{2a}\rho^2 - \frac{aB_{eo}}{A} \left\{ \left(\frac{\rho}{\rho_o}\right)^4 - 2\left(\frac{\rho}{\rho_o}\right)^2 \cos 2\theta \right\}. \tag{3.16}$$

Putting $\rho^2/\rho_o^2 = X$, the above equation is rewritten as

$$X^2 - \left(2 \cos 2\theta - \frac{A}{2}\left(\frac{\rho_o}{a}\right)^2 \frac{B_{ao}}{B_{eo}}\right) X + \frac{\Psi \cdot A}{aB_{eo}} = 0 . \tag{3.17}$$

We assume that a radius of the magnetic surface intersecting $\theta = 0$ and $\theta = \frac{\pi}{2}$ axis as $X_1 \left(X_1 = \left(\frac{a}{\rho_o}\right)^2\right)$ and X_2, respectively.
Then the condition for $\frac{X_2}{X_1} = m^2$ $(m>1)$ to hold is

$$\frac{B_{eo}}{B_{ao}} = \frac{2\left|(1-m^2)\right| \left\{1-\left(\frac{a}{\rho_o}\right)^2\right\}}{\left\{2(1+m^2) + (m^4-1)\left(\frac{a}{\rho_o}\right)^2\right\}} \tag{3.18}$$

or in the approximation $a \ll \rho_o$, we find

$$m \sim \sqrt{\frac{B_{ao}+B_{eo}}{B_{ao}-B_{eo}}} \sim 1 + \frac{B_{eo}}{B_{ao}} \tag{3.19}$$

From this expression one may easily envisage that the deformation is in the same order of magmitude as that by cusp field and may be negligible in the confinement physics.

§3.3 Radial Error Field and Its Compensation

Error field criginated from misalignment of the toroidal coils is again important when the plasma current builds up to form closed magnetic

surfaces. The vertical component of the error field which will shift the plasma column in the radial direction,[34] if ever exists, can easily be compensated by a proper choise of the vertical field intensity prepared for the radial equilibrium of the plasma column. The radial component, on the other hand, will shift the plasma column vertically. This shift could also be suppressed by the radial compensation field in principle. However, the winding for this purpose in most cases is not prepared at the beginning, since the amount of the radial error field is not known until the device is constructed. This is due to the fact that it is fairly difficult to know the geometry of toroidal coil winding and their feeders within the accuracy described in §2.2. Therefore, temporal winding are used in many devices such as ST, ATC and JFT-2 etc. After the completion of the JFT-2, a radial field of 10 Gauss is detected, which is compensated by the 80 turn winding. It is also experienced that the radial field changed by about 10 Gauss after a process of dismantle and reconstruction of the toroidal coil assembly. This may well suggest that the radial error field is generated not by the traversing current feeder and rewinding but presumably by the accuracy of assembling. Two possible causes are considered. First, error field associated with the tilt of the toroidal coil against ϕ = const. plane. Second, error field generated due to the twist of the coil base. For the former, we consider that one of the toroidal coil tilts by angle ξ with respect to ϕ = const. plane as investigated in §2.2. The ampere turn of 281 kAT in every coils can generate the toroidal field of 10 kG. As shown in §2.2, the magnetic field line shifts by 0.15ξ meter from the starting position after a transit along the torus. This means that the effective radial field averaged over the torus

$$\langle B_r \rangle \sim \frac{0.15\xi}{2\pi R} \cdot B_t \tag{3.20}$$

is generated. On the other hand, assuming that the mechanical accuracies of the knock pin, holes on the coil and coil base being ± 0.1 mm, we estimate a probable set up error to be

$$\xi = \frac{(0.2+0.2+0.2)}{160} = 3.75 \times 10^{-3} \text{ radian} \tag{3.21}$$

since the separation of a couple of knock holes is 160 mm. Thus, one obtains for the misalignment of one of the coils

$$\langle B_r \rangle \sim \frac{0.15 \times 3.75 \times 10^{-3}}{2\pi \times 0.9} \times 10^4 = 1.0 \text{ Gauss} \tag{3.22}$$

Namely, it is necessary for ten coils to tilt in producing the error field of 10 Gauss. Since each coil is set up independently, it is conceivably improbable (although cannot be excluded completely) for such a large number of coils out of 16 to tilt to their extremes in one direction. For the latter cause, we suspect that the stainless steel upper base which fixes a quarter of the coils without knock bolt in one unit is set up in a twisted manner with respect to the lower base. For instance, we assume that the twist is such that the outer edge of each coil is displaced by 2 mm in the toroidal direction. Since the coil is 150 cm high and 40 cm wide in the radial direction, the effective tilt angle ξ is given by

$$\xi = \frac{1}{2} \times \frac{2}{400} = 2.5 \times 10^{-3} \tag{3.23}$$

with a corresponding error field

$$< B_{error} > \sim \frac{0.15\xi}{2\pi R} \times 10^4 \times 16 = 10.6 \text{ Gauss}, \tag{3.24}$$

if all the bases tilt in the same manner. Thus in any case, it would be probable for the amount of error field to vary within 10 Gauss, when the coil assembly is dismantled.

§3.4 Bending of a Plasma Column due to Shell Gaps

3.4.1 Plasma Column Shift due to Shell Gaps

In this subsection, we briefly discuss the influence of the shell gap on the plasma column equilibrium. In addition to the normal shift,[17,34] the plasma column is exposed to the further outward shift due to the presence of shell gaps. In the ideal shell where the influence of the shell gap is negligibly small, the shift δ_o is expressed as[34]

$$\frac{\delta_o}{b} = \frac{b}{2R}\left[\ell n \frac{b}{a} + \left(1 - \frac{a^2}{b^2}\right)\left(\Lambda + \frac{1}{2}\right) \right] - \frac{B_v}{B_p} \tag{3.25}$$

$$\text{with } \Lambda = \beta_p + \frac{\ell_i}{2} - 1$$

, where, a is the minor radius, R is the major radius of the plasma, b is the minor radius of the shell, β_p is the poloidal beta, ℓ_i is the internal inductance, B_p is the azimuthal field at r = a, and B_v is the externally applied vertical field.

In the ideal case where the width of the shell gap is negligibly small, one chooses the external vertical field to satisfy the relation

$$B_v = B_{v1} = B_p \cdot \frac{b}{2R}\left(\ln\frac{b}{a} + (1 - \frac{a^2}{b^2})(\Lambda + \frac{1}{2})\right) \tag{3.26}$$

in order to put the plasma at the center of the shell, mamely, $\delta_0 = 0$.

In the presence of shell gaps, however, the plasma is exposed to the outward force, since the vertical field produced by the shell is reduced. Therefore, the plasma column shifts from the ideal equilibrium position by δ where it finds a new equilibrium state as illustrated in Figs. 3.1 and 3.2. We evaluate δ in this configuration where the outward force acts on the plasma at the gap due to the plasma hoop force which can be compensated by the inward force from the shell (See Fig. 3.3).

Firstly, we evaluate the aditional expanding force due to the presence of shell gaps. It is composed of a couple of forces, that is, one by the magnetic pressure F_m and the other by the plasma pressure F_p

$$F = F_m + F_p \tag{3.27}$$

with

$$\begin{aligned} F_m &= \iint \frac{B_p^2}{2\mu_o} r d\theta R d\varphi \\ &= \frac{B_{po}^2}{2\mu_o} R_o r \int_0^{\delta\varphi}\int_0^{2\pi} (1-2\varepsilon\cos\theta)\cos\theta\,(1+\frac{r}{R_o}\cos\theta)\,d\theta d\varphi \\ &= \pi\varepsilon \cdot \frac{B_{po}^2}{2\mu_o} r\cdot g \end{aligned} \tag{3.28}$$

and

$$\begin{aligned} F_p &= \iint p\, r d\theta R d\varphi = p_o R_o r \int_0^{\delta\varphi}\int_0^{2\pi} \cos\theta\,(1+\varepsilon\cos\theta)\,d\theta d\varphi \\ &= \pi\varepsilon\, p_o r\cdot g \end{aligned} \tag{3.29}$$

where $p_o = nkT$, $\varepsilon = \frac{r}{R}$ and g is the gap distance. Therefore F is written as

$$F = (p_o + \frac{B_{po}^2}{2\mu_o})\pi\varepsilon r\cdot g \tag{3.30}$$

On the other hand, the compensation force due to the plasma shift is evaluated as follows;

The external field necessary for the equilibrium is written as

$$B_v = B_{v2} = \left(\frac{b}{2R} \left(\ln \frac{b}{a} + \left(1 - \frac{a2}{b^2} \right)\left(\Lambda + \frac{1}{2} \right) \right) - \frac{\delta}{b} \right) \cdot B_p \qquad (3.31)$$

provided that g is small enough as compared with $2\pi R$. The increment of the inward force due to the shift δ is then given by

$$F = 2\pi R\, I_p (B_{v1} - B_{v2}) = \frac{2\pi R\, I_p B_p \delta}{b} \qquad (3.32)$$

Combining eqs.(3.30) and (3.32), one obtains

$$\left(p_0 + \frac{B_{p0}^2}{2\mu_0} \right) \pi \varepsilon r g = \frac{2\pi R\, I_p B_p \delta}{b} \,. \qquad (3.33)$$

Using a relation $I_p = 2\pi r \cdot B_{p0} / \mu_0$, we find

$$\frac{\delta}{b} = \frac{\varepsilon g}{8\pi R} (1 + \beta_p)$$

namely δ is proportional to the total gap length. Putting the JFT-2 dimensions for instance, $\varepsilon = 1/3.6$, $g/2\pi R = 20/140$ *) $\beta_\theta \sim 1$, and $b = 36$ cm, we find

$$\delta = 0.02 \cdot b \sim 0.7 \text{ cm} \qquad (3.35)$$

However, one can be optimistic on this problem, because the plasma shift can also be compensated simply by increasing the vertical field of the order

$$\Delta B_v \sim \frac{\delta}{b} \cdot B_p \sim 0.02 \cdot B_p \,. \qquad (3.36)$$

3.4.2 Local Bending of the Plasma Column

In the preceding subsection, we consider the plasma column as a rigid

*) This value is increased if one uses the effective gap length which will be discussed in Chapter 5.

body. However, the plasma may be subject to a local expanding force at the shell gap due to the plasma pressure and the magnetic pressure, because there are no counter force present at this position. Thus, the purpose of this subsection is to estimate the local bending of the plasma column near the shell gap. Besides the well known deformation of magnetic surfaces due to islands formation,[8,16,24] there may have another possibility of local deformation. We assume that the plasma is frozen in the toroidal magnetic field and that the bending of the plasma is associated with that of toroidal magnetic field. In the ideal configuration without shell gaps, the tension on a toroidal flux is given by

$$F_t \simeq \frac{B_t^2}{2\mu_o} \pi r^2 \tag{3.37}$$

where the notation is obvious. This force is balanced with the radial pressure. Near the gap, the expanding force is added which results in a local deformation shown in Fig. 3.4. The motive force originating from the radial pressure difference of the magnetic field at both sides of the plasma at the gap, is approximated by eq. (3.31). The counter force which will be balanced with this force is the radial component of the tension by the toroidal magnetic field. A simplified model is adopted where χ determines the amount of deformation. For the force balance,

$$2 F_t \cdot \sin \chi \simeq F \tag{3.38}$$

with $F_t \simeq \frac{B_t^2}{2\mu_o} \cdot \pi r^2$ and $F \simeq (p_o + \frac{B_{po}^2}{2\mu_o}) \pi \varepsilon r g$

Then we find

$$\chi \simeq \frac{g}{2r} \frac{\varepsilon^3}{q^2} (1 + \beta_p) \tag{3.39}$$

Putting the JFT-2 dimensions

$$\frac{g}{r} \sim 1, \quad \varepsilon = \frac{1}{3.6}, \quad q \sim 2 \quad \text{and} \quad \beta_p \simeq 1$$

one finds

$$\chi \sim 5.36 \times 10^{-3} \text{ radian} \sim 0.31^{\circ} \tag{3.40}$$

which is a negligibly small amount. Thus it may be concluded that the bending of the magnetic field line due to the presence of shell gaps can be neglected and that the plasma column can be regarded as a rigid body in the force balance equation.

§3.5 Concluding Remarks

Global effect of the error field on the plasma column deformation is studied when closed magnetic surfaces are formed. Deformation of the circular magnetic surface in the presence of axisymmetric cusp or multipole field is fairly small even when its intensity is considerably large. Roughly, the elongation of the circular magnetic surface is given by the ratio of the error field to the azimuthal field by the plasma current.

Generation of the radial error field due to toroidal coil misalignment is investigated in some detail. The experience in the JFT-2 suggests the possible source for the change of error field intensities after the process of assembling. A slight twist of the coil basements may be the primary cause, but a possibility of coil tilt with respect to toroidal axis may not be completely excluded because it is still within the accuracy of knock pins. However, it could be decreased by elongating the separation distance between knock pins.

A local bending of the plasma column due to shell gaps is roughly estimated with an indication that this effect is very weak and that the plasma can be treated like a rigid body. The further outward shift of the plasma due to shell gaps, however, cannot be neglected. It is found to be proportional to the gap length and is easily compensated by the additional vertical field.

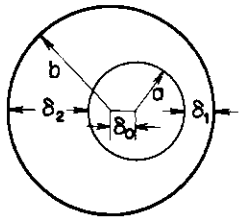

Fig. 3.1 The outward shift of the plasma in equilibrium due to the toroidal effect, where a is the minor radius of the plasma, b is the minor radius of the shell, and δ_0 is the plasma shift from the axis of the shell.

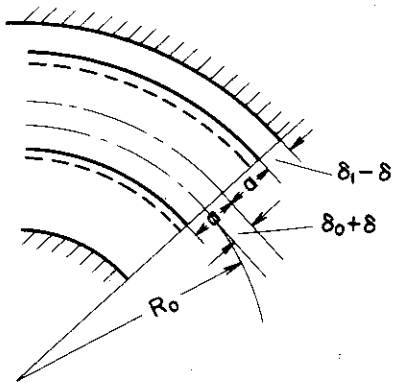

Fig. 3.2 Further shift of the plasma column due to the presence of shell gaps. The center of the plasma column is displaced from the center of the shell by $\delta + \delta_0$.

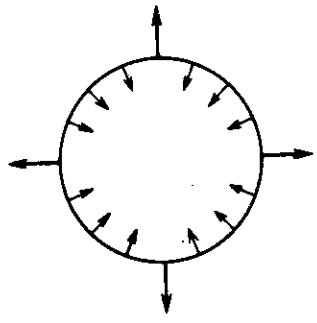

Fig. 3.3 Equilibrium obtained by the inward force at the shell and the outward force at the gap.

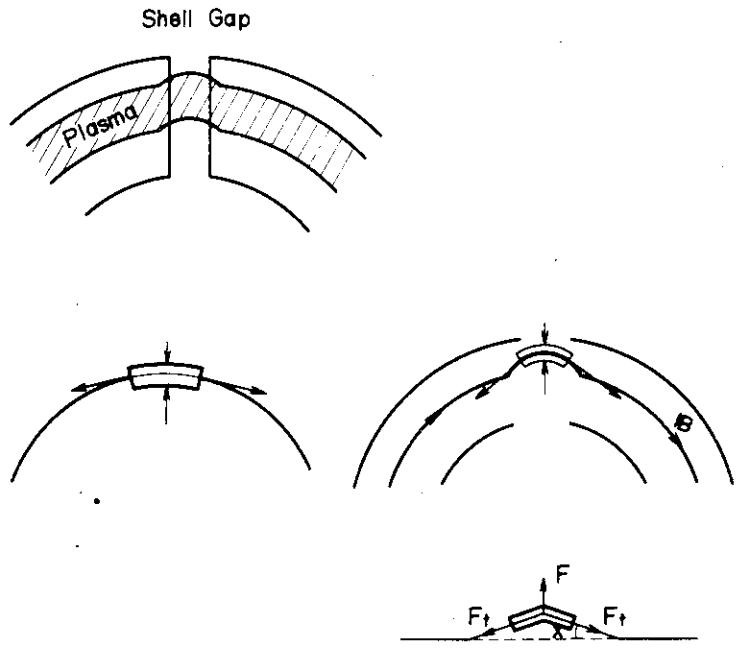

Fig. 3.4 Sketch of the force balance in connection with the local bending of the plasma column. The residual outward force F is balanced by the inward force $F_t \sin \chi$ which is generated by the bending of toroidal field.

CHAPTER 4
LEAKAGE MAGNETIC FIELD ASSOCIATED WITH AN IRON CORE[18)]

§4.1 Introduction

Measurements of the leakage magnetic field from an iron core in tokamak devices in the presence of both primary coil current and secondary plasma current has not been reported so far. The reason seems to lie in the fact that the strength of the magnetic field produced by the plasma current is one or two orders of magnitude greater than that of leakage field to be measured[17)] so that it is difficult to measure the latter separately from the former with a good accuracy.

The leakage field, however, is important in its effect on the displacement of plasma column[17,34)] and on the formation of islands in magnetic surfaces.[8,11,16)] The generation of the leakage field may be attributed to the following three sources.

(1) The primary winding current in the absence of the core

(2) The core magnetized by the primary current

and

(3) The core magnetized by the plasma current.

The leakage magnetic field to be measured is the superposition of these three components. The source (3) was examined to some extent[17)], but the model adopted seems to be inappropriate for practical use. For instance, the theory considers neither non-axisymmetry due to the yokes nor infinite permeability of the iron core. Of course, there are some measurements in the absence of a secondary current[6,19)] and some informations are obtained related to the sources (1) and (2). However, we do not know how it varies in the presence of the secondary current because of the spacial variety of the magnetic permeability in the iron core. On the other hand, the scaling law of ampere turns NI, magnetic field strength B and self- or mutual- inductance ℓ in magnetic systems which have different sizes but the same geometrical configuration can easily be deduced from Maxwell's equations. Namely, relations $NI \propto BL$ and $\ell \propto L$ hold. Hence, we can scale the leakage magnetic field including the effect (3) at the position of the plasma column, if we measure it on some model with a simulated plasma current.

Although magnitude of the leakage field in such a configuration is very large, usual tokamak devices are equipped with conducting shells which plays role of shielding against external leakage field to influence on

the plasma equilibrium.[34] However, as far as the shellless tokamak[17] with the iron core is concerned, the plasma is directly influenced by this field. Therefore, it is very important to obtain informations about strength and uniformity of the leakage field.

It will be shown later that a direction of this field is the same as that of the usual vertical field necessary for the plasma equilibrium, and hence this field can be utilized as one of the equilibrating field of the plasma column. It will be also shown that its strength is somewhat weaker than what is necessary.

§4.2 Method of Measurements

A ring conductor with a small cross section is substituted for the plasma. It serves as one turn secondary winding of the transformer. The ring is made such that the current can be fed through a coaxial feeder and is also induced by excitation of the primary winding.

At first, in the absence of the core, a current is fed through a coaxial feeder from an external capacitor bank. Since the cross section of the ring conductor is very small, the current flowing through it can be approximated by a line current. Therefore, magnetic surfaces can easily be calculated.

A special form of pick up coils is chosen to eliminate the influence of the magnetic field produced by the ring current as shown in Figs. 4.1 and 4.2, with its radial ends coinciding with the intersection of one of the magnetic surfaces with the median plane. In this configuration, a signal to noise ratio of this pick up coil system is expressed by

$$\frac{\Phi_S}{\Phi_N} = \frac{\langle B_V \cdot S \rangle}{\langle B_p \cdot \Delta S \rangle} \tag{4.1}$$

where B_v is the vertical field of the present concern, B_p is the azimuthal field by the simulated plasma current, S and ΔS is the effective area of the pick up coil for B_v and B_p, respectively. Note that ΔS is much smaller than S because ΔS is only a result of misassembling of the pick up coil. Therefore, it is easy to set the pick up coil such that $S/\Delta S \gtrsim 10^3$ can be satisfied. Thus one can measure Φ_s within an error of 1 - 10%, if B_v ranges between 10 to 1% of the azimuthal field B_p. Although the radial positions A and B in Fig. 4.1 can easily be calculated in the case of line current, they do not meet with actual intersection positions. Therefore, we fix the radial position of the pick up coil experimentally by moving and adjusting it minutely until the magnitude of the magnetic flux picked up by this coil

becomes smaller than a critical value (See Fig. 4.2). This value in turn is determined from the required accuracy of the measurement.

In the next place, we assemble the ring conductor and pick up coil system with the above accuracy in the presence of the core (See Fig. 4.3). The ring conductor is short-circuited electrically, and the current is induced by excitation of the primary winding. Thus we can measure the leakage field averaged over the pick up coil area in the presence of simulated plasma current.

§4.3 Apparatus

The ring conductor which is a substitution for the plasma is made of a single turn copper ring of 8 mm in minor diameter and 36 cm in major diameter. A coaxial current feeder 40 cm long is attached to this ring in order to minimize the influence of error field by the feeder (See Fig. 4.2). The ring conductor is fixed to a base which can be disassembled into two parts and reconstructable in the median plane within an error of ±0.1 mm by knock pins.

Each pick up coil is made of ten turns with a form shown in Fig. 4.2.*) It can also be fixed to the base. Once the positions of its radial ends are adjusted experimentally on a magnetic surface, they can be reproduced within an error of ±0.1 mm by knock pins after disassembling. Eight pick up coils are used, and are set up in the toroidal direction.

The size of the transformer core is just 1/5 of that of JFT-2 and its material is also the same as used in the JFT-2 (See Fig. 4.6).

In determining the radial position of pick up coils, the following electric circuit is used to feed half sinusoidal wave current (Fig. 4.4). The external inductance is inserted in addition to the ring inductance to adjust the current period to that in the presence of the core. Since the frequency dependence of the permeability of the core is rather generous, our experiments are made in the higher frequency range than the JFT-2 operation.

In the presence of the core no external inductance is used as shown in Fig. 4.4.

Under these experimental conditions, the resistance of the ring conductor does not matter since primary and ring currents are almost out

---

*) When the ring conductor is placed at the very center of the plasma column, magnetic surfaces are not concentric due to the toroidal effect. They are displaced towards outside of the torus.

of phase. Experiments are made in less than saturation of the core, and hence, a linear scaling can hold with respect to the ampere turns and the strength of the magnetic field.

§4.4 Experimental Results

Firstly, the primary winding and the ring conductor are set up without the iron core. The leakage magnetic field of this system is compared with those of other configurations. We may call it as "leakage magnetic field in the air core" in correspondence with (1) mentioned in §4.1. The vertical component of this field decreases with radius as illustrated in Fig. 4.5. Now we define an average magnetic field over the area of the pick up coil by $\langle B \rangle = \int BdS / \int dS$. When scaled to the JFT-2 tokamak, it is approximately equal to $\langle B \rangle \simeq 9.4$ Gauss/100 kA in the case of air core. This measured value is consistent with that obtained by numerical calculation.

Secondly, the experimental results in the presence of the iron core show $\langle B \rangle \simeq 172$ Gauss/100 kA , which corresponds about eighteen times larger than that of air core.

In spite of the double yokes of the iron core which seem to destroy the toroidal symmetry of the system, the leakage magnetic field is uniform in the toroidal direction within an experimental error, when the primary winding is located at the necks of the core leg as shown in Fig. 4.6a. However, when it is wound at the middle of yokes as in Fig. 4.6b, a strong non-uniformity appears and moreover, the absolute intensity of the leakage field increases (See Fig. 4.7).

A level of the leakage field is increased by about 34%, when the shielding plate is inserted which makes the radial distribution of the leakage field uniform. Its level becomes $\langle B \rangle = 230$ Gauss/100 kA .

When the magnitude of the secondary current is fixed, the ratio of the magnetic field by the ring current to that by the iron core with primary winding is less than 0.02, and this is the accuracy of the above mentioned data.

§4.5 Discussion and Concluding Remarks

Under the experimental conditions the half period of the current is about 0.8 msec which corresponds to the copper skin deapth of 2.6 mm and is smaller than the minor radius of the ring conductor. Therefore, the current distribution in it must show a strong skin effect. Considering the fact that the magnetic field strength is larger at the inner side

surface of the ring conductor than the outer, the skin current distribution is somewhat emphasized at the inner side. The above mentioned experimental results appears to be based on the fact that the current distribution in the ring conductor are not different between the two cases, that is, with and without the core. However, even if there exists any difference, it is nothing serious. The reason is that the current distribution is also a superposition of the two kinds. The one is the same as that of secondary current of air core, and the other is due to the leakage field. The former does not effect on the measurement, and the latter does on the measurement, but it is just what is wanted.

Strength of the vertical field necessary for the plasma equilibrium has been obtained independently by S. Yoshikawa[28] and V.D. Shafranov.[34] In the absence of the shell it is written as

$$B_v = \frac{I_p}{cR}\left(\ln\frac{8R}{a} - \frac{3}{2} + \frac{\ell_i}{2}\right) + \frac{2\pi c a^2 p}{RI_p} \qquad (4.2)$$

, where R and a are the major and the minor radii of the plasma, I_p is the plasma current, p is the plasma kinetic pressure and ℓ_i is an internal inductance of the plasma current, respectively. When the contribution by a plasma kinetic pressure is neglected, substitution of the JFT-2 parameters, $R = 90$ cm, $a = 25$ cm and $\ell_i = 1.5$, for example, gives

$$B_v = 288 \text{ Gauss/100 kA} \qquad (4.3)$$

However, experimental results show that the leakage vertical field is

$$\langle B_v \rangle = 230 \text{ Gauss/100 kA} \qquad (4.4)$$

On the other hand V.S. Mukhovatov and V.D. Shafranov[17] have calculated the force of attraction on the current-flowing ring by the core. Effective vertical field can be deduced from the force Fc described in their article, namely Bv is calculated to be

$$B_v = \frac{Fc}{2\pi RI_p} = 280 \text{ Gauss/100 kA} \qquad (4.5)$$

The difference between these two values of 230 and 280 Gauss may be due to the fact that the model taken by them does not represent the actual situation. Firstly, an infinite cylinder of the core and infinite permeability are assumed. Secondly, the effect of the magnetization by the primary winding is not considered.

The experimental results seem to show that the destruction of the

toroidal symmetry by the iron core is not serious as long as the primary winding is placed properly but that by the primary winding may cause an troublesome problem. It appears that the fruitful way in obtaining a toroidally uniform leakage field is to use axisymmetric winding. However, a precise conclusion may be postponed until detailed experiments for various models will be made.

Now, it is revealed that the displacement of the plasma column may be determined not only by an externally excited transverse field, but also by the leakage or the error field in the presence of iron core. Especially in shellless tokamaks, the leakage field plays an important role because of its intensity.

These discussions do not apply to the tokamak with conducting shells. Namely, the shell prevents the leakage field from affecting the plasma, and instead it makes vertical field by itself which suppress the plasma shift. From this point of view, similar measurements are made to know the absolute value, the toroidal uniformity and the radial distribution of the leakage field on the JFT-2 tokamak device with the shell. This problem will be discussed in Chapter 5, which follows.

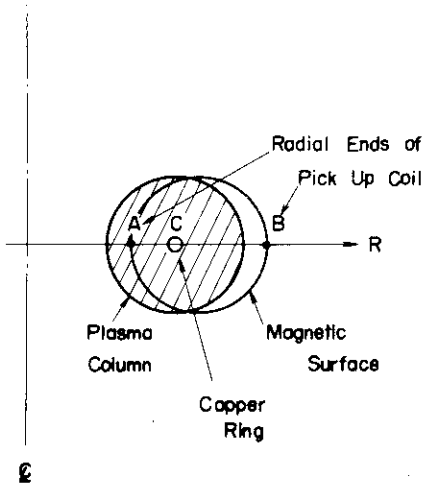

Fig. 4.1
Cross section of the plasma column, the simulated copper ring and a magnetic surface. A and B denote intersection positions of the magnetic surface with the median plane.

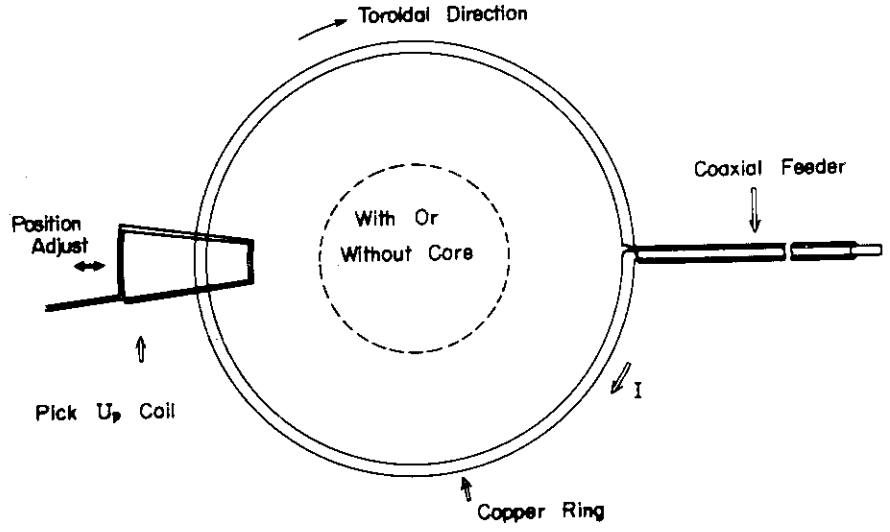

Fig. 4.2 Upper view of the copper ring conductor and one of the pick up coils.

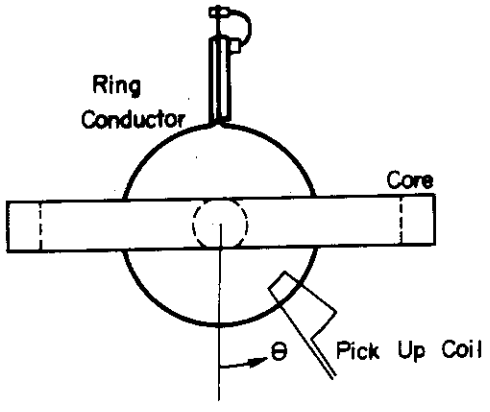

Fig. 4.3
Configuration of the measuring system and the iron core when it is viewed from the upperside.

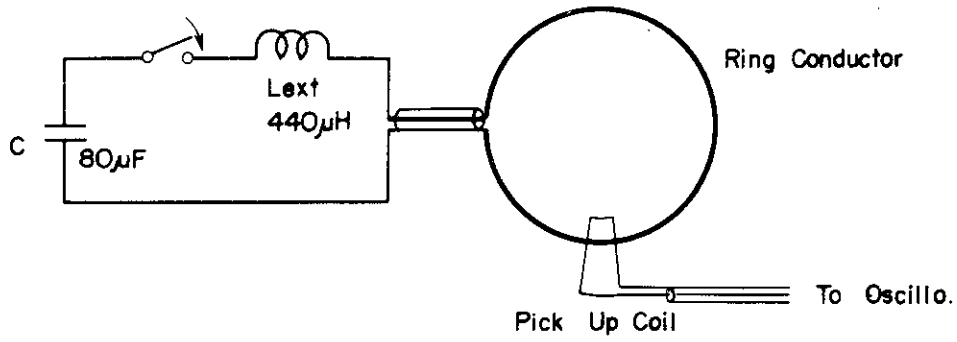

(a)

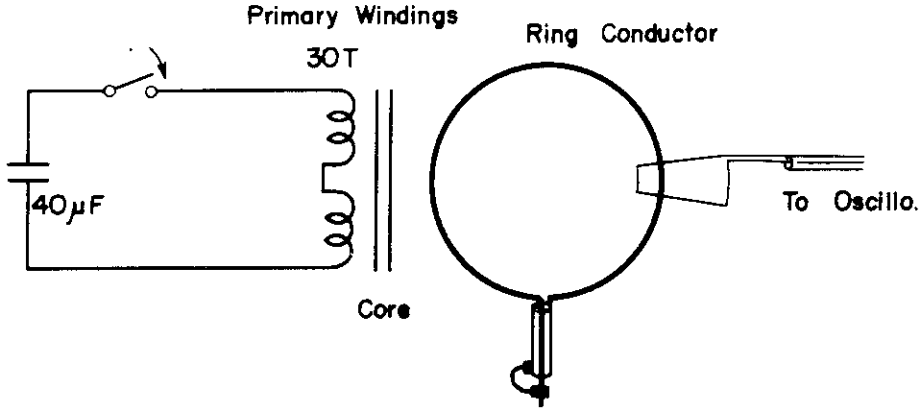

(b)

Fig. 4.4 Electric circuits used in the experiments. In the absence of the core, the ring current is fed through the coaxial feeder (a), whereas in the presence of the core the ring current is induced through the iron core (b). An external inductance is added in the case (a) to make the current period likewise in both cases.

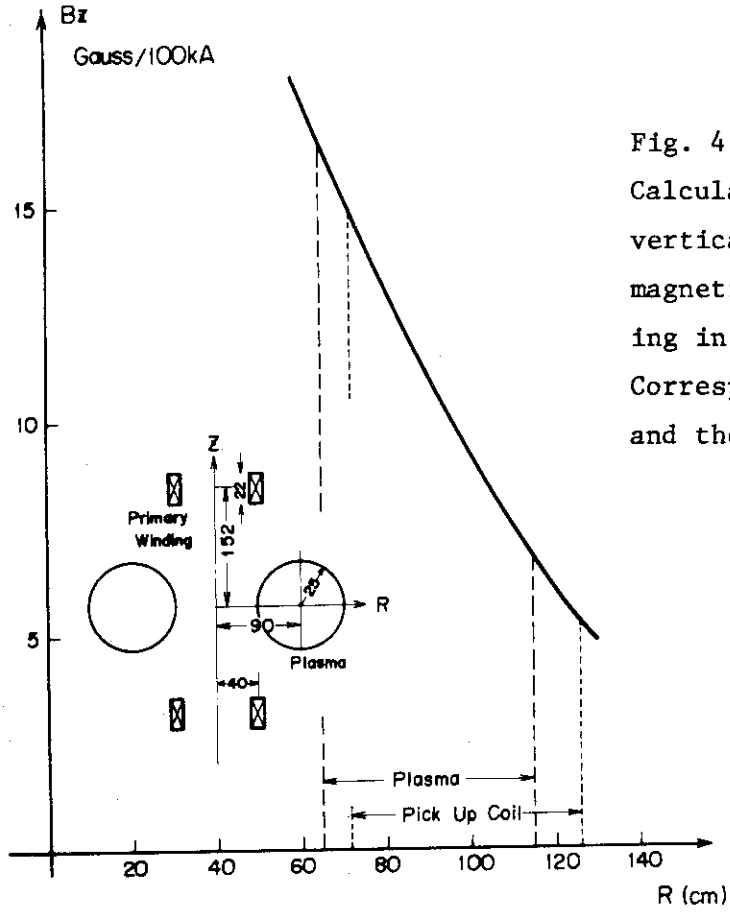

Fig. 4.5
Calculated radial distribution of the vertical component of the leakage magnetic field from the primary winding in the JFT-2 configuration. Corresponding positions of the plasma and the pick up coils are also shown.

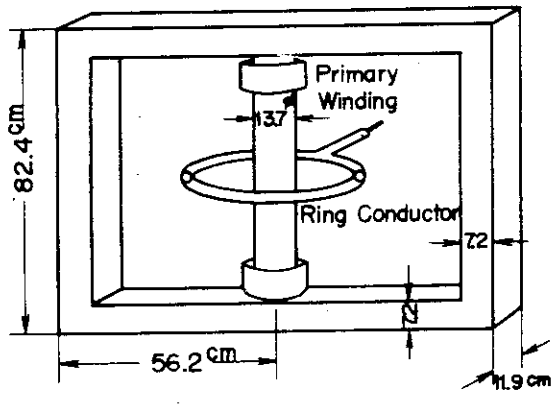

(a)

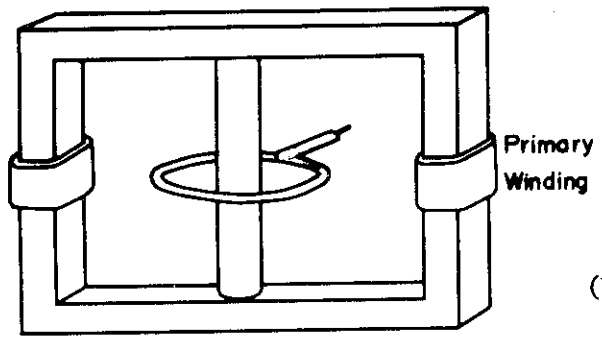

(b)

Fig. 4.6
Dimensions of the 1/5 model core of the JFT-2 device. Primary winding is located at the necks of the leg (a), and at the center of yokes (b).

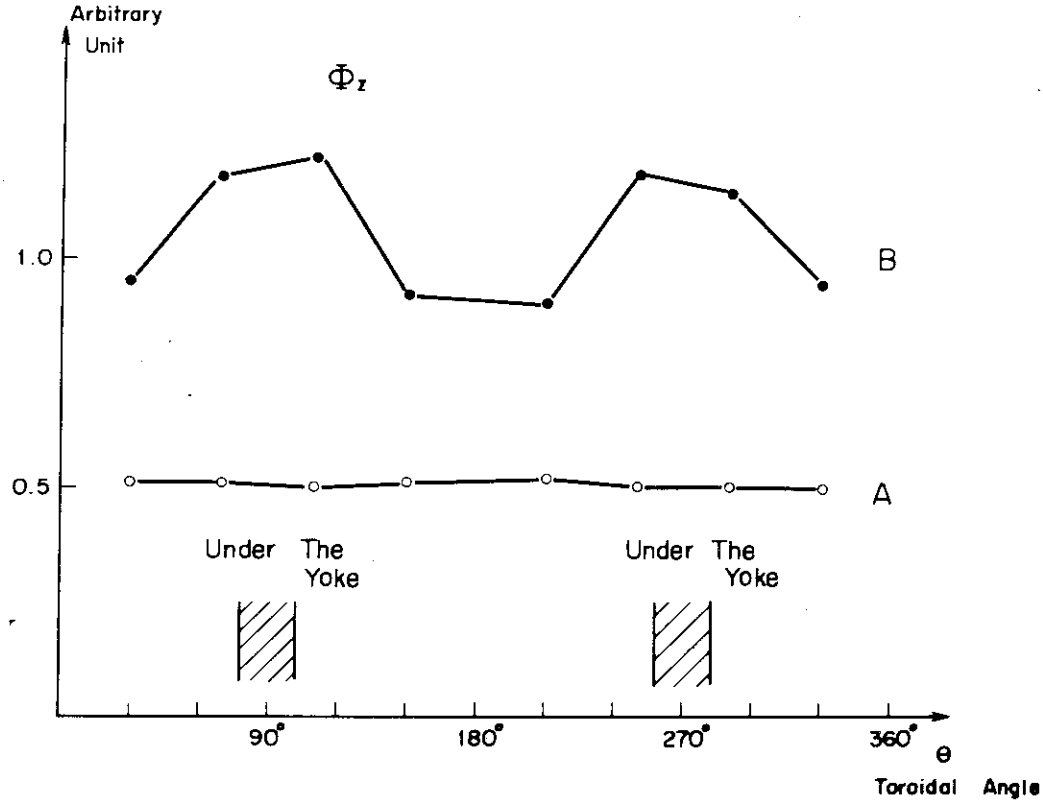

Fig. 4.7 Toroidal distribution of the vertical component of the leakage magnetic field in the presence of the secondary winding. The curve A and B correspond to the case (a) and (b) in Fig. 4.6, respectively.

CHAPTER 5

EFFECT OF THE CONDUCTING SHELL AND ITS GAP ON GENERATION OF THE VERTICAL MAGNETIC FIELD IN TOKAMAKS

§5.1 Introduction

The equilibrium of the plasma in tokamak devices with an electrically conducting shell is obtained by the vertical magnetic field generated by the eddy current flowing on a surface layer of the shell and by the external coils.[34)]

In usual tokamak devices,[3,5,13)] an electrically conducting shell takes an important role in creating most of the vertical field necessary for the plasma equilibrium and the residual vertical field is generated by the external coils. However, the shell should have at least one gap along the torus in order to induce an electric field on the plasma. The gap destroys the toroidal uniformity of the vertical field because the image current is prevented to flow along the torus at the gap. Although such a nonuniformity can be reduced simply by making the length of the shell gap infinitesimally small, evacuation system and plasma diagnostics demand an appropriate length of the shell gap in actual devices.

On the other hand, both theory[17)] and recent experiments[18)] predict that the leakage field from the iron core has the same order of magnitude of the equilibrating magnetic field of a plasma. Therefore, the leakage field may be expected to help in compensating the reduced vertical field near the shell gap. Some theoretical works have been performed with respect to the influences of the shell gap and the iron core under some approximations,[17,35)] but few experimental works have been reported.

In designing a toroidal device with a small aspect ratio, more attention should be paid to the influence of the shell gap. From this view point, distributions of the vertical fields near the shell gap are measured for the JFT-2 tokamak device by using a special pick up coil which is principally the same as described in the preceding chapter.[18)] The results are compared with approximate theories developed by V.S. Mukhovatov and V.D. Shafranov.[17)] Although measurements are carried out in the JFT-2 device, characteristics of the effect of the shell gap is not specific to the JFT-2.

§5.2 Method of Measurement

The configuration of the aluminum shell of the JFT-2 is shown in Fig. 5.1. A shell cap 7.35 cm wide can be attached to the shell to decrease

the gap length. An aluminum ring conductor 2.5 cm in minor radius and 90 cm in major radius is applied to simulate a plasma current (Fig. 5.2). The ring conductor consists of four parts which can be disassembled and reconstructed within an accuracy of ±0.1 cm about the major radius. It is supported by eight rollers at the shell gaps and is movable around the torus. On one of the parts, a coaxial current feeder is equipped so that the current may be fed directly or induced by interlinkage with the iron core.

A specially arranged pick up coil is used to measure the vertical fields except the field generated by the plasma current. The pick up coil made of thirty turns on an insulator plate is attached to the ring conductor in a median plane so that its radial ends may coincide with the intersection of a magnetic flux line by the ring current. By this method, the pick up coil is insensitive to the field by the ring current. Such an arrangement is made experimentally in the presence of only the ring conductor by adjusting the radial position of the pick up coil until the magnetic flux picked up becomes smaller than some critical value. This critical value is determined from the required accuracy of the measurement of ±2%. After the adjustment, the pick up coil is fixed to the ring conductor (Fig. 5.2) which is driven around the torus to measure the toroidal distribution of the vertical field.

In the first place, the effect of the shell gap is investigated. Four parts of the shell are assembled in the absence of the iron core just as shown in Fig. 5.1, and the current of about 20 kA is fed to the ring conductor which is set at the axis of the shell through the coaxial feeder from the capacitor bank. An external inductance is used to make the sinusoidal wave current of a half period of 15 msec. The effect of the shell cap is also investigated by attaching to and removing from the shell.

In the second place, the iron core is introduced to the system and the effect of the leakage magnetic field from the iron core is investigated. In this case, the ring conductor is electrically shorted and the current of 20 kA is induced by excitation of the primary winding of the current transformer. Thus the leakage magnetic field from the iron core entering through the shell gap is superposed to that by the shell in actual configurations. The intensity of the leakage field from the iron core is also measured separately in the absence of the shell.

§5.3 Experimental Results

A toroidal distribution of the vertical magnetic field by the shell is investigated by setting up the ring conductor at the axis of the shell. The distribution of the field averaged over the area of the pick up coil is measured in a range which covers a quarter of the torus. The results are shown in Fig. 5.3, in which the field intensity is normalized by the ring current at the respective time. Though the width of the shell gap is only 10.5 cm in this case, the effect of the gap extends as far as the central part of the shell. This figure also shows a relaxation of the skin effect of the vertical field due to the finite electrical conductivity of the shell. However, the curve at $t = 2$ msec after initiation of the sinusoidal coil current may be much the same distribution as a superconducting shell gives, since the time scale in observation is much shorter than the shortest characteristic skin time of 10 msec which is estimated by the relation $\tau = (4\pi\mu\sigma/c^2)(\ell/2)^2$ in Gaussian unit, where μ is the magnetic permeability, σ is the electrical conductivity and ℓ is the thickness of the shell. Therefore the non-uniformity of the toroidal distribution shown at $t = 2$ msec in Fig. 5.3 is not due to the finite conductivity of the aluminum shell but intrinsically due to the geometrical structure of the shell.

The effect of the shell cap is also investigated. The results are shown in Fig. 5.4 in comparison with the case without shell cap, indicating a slight improvement of the uniformity by the shell cap.

In the next place, the iron core is introduced in this system to evaluate the effect of the leakage field from the iron core. The results are shown in Fig. 5.5 which indicates that the intensity of the vertical field increases about 25% near the center of the shell and 170% at the gap. The valley in the toroidal distribution of the vertical field by the shell is almost buried and its uniformity is improved to about 10%. Fraction of the leakage field is obtained by subtracting the contribution by the shell from the measured field in the presence of both iron core and shell. The field thus obtained is indicated with a broken line in Fig. 5.5. For the same reason as mentioned above, i.e., the time interval of 2 msec after the initiation of sinusoidal coil current is shorter than any characteristic skin time, the leakage field detected inside the shell is caused by the bending of field lines at the gap. Namely, only a geometrical configuration of the shell and its gap is predominant in this time scale.

The absolute intensity of the leakage field from the iron core without

shell is also measured and is revealed to be 225 Gauss/100 kA irrespective of the toroidal position (See Fig. 5.5). In these measurements experimental conditions are chosen such that the magnetic flux density in the iron core may be lower than the saturation level. Therefore, the intensity of the leakage field is proportional to the ring current, as proved in the model experiment.[19)]

In the full assembly of the system, where present are the conducting shell, the iron core, primary coils shielding plates and the simulated plasma ring, the vertical component of the leakage field far apart from the plasma region is measured by the usual magnetic probes. Unlike former measurements, this is possible, since the azimuthal field by the plasma current does not disturb the measurement because of its rapid decrease with the distance. The purpose of this measurement is to serve data for the installation of diagnostic instruments and to get an idea of absorption of the leakage flux by the yoke. The results are shown in Fig. 5.6 in which a couple of directions are chosen, one in the direction beside the yoke, and the other nearly perpendicular to it. Azimuthal field by the plasma current is calculated for comparison.

§5.4 Discussion

Experiments described in the preceding section are performed by substituting an alminum ring of 2.5 cm in minor diameter for a corresponding plasma of 50 cm in minor diameter and 180 cm in major diameter. It is also noted that measurements have been made in a time much shorter than the skin time of the conducting shell, and therefore, the results can be compared with the theory[17)] in which the shell is assumed to be superconducting.

Firstly, we derive a theoretical intensity of the vertical magnetic field generated by the superconducting shell with an infinitesimally narrow gap and then compare it with the experiment. Secondly, using these results we derive effective gap length which are also compared with the theory.

It is well known that the vertical field necessary for the equilibrium of the plasma column is given as,[17)]

$$B_V = \frac{I_p}{cR}\left(\ln\frac{8R}{a} + \Lambda - \frac{1}{2}\right) \tag{5.1}$$

where I_p is the plasma current, c is the velocity of light, a is the minor radius, R is the major radius of the plasma column, and Λ is related to the internal inductance of the plasma ℓ_i and the poloidal beta β_p by a

relation $\Lambda = \beta_p + \ell_i/2 - 1$.

When the plasma column is surrounded by an ideally conducting shell with infinitesimally narrow gaps, vertical field $B_{v\ shell}$ is produced by the image current of the plasma current. This field is not sufficient to keep the plasma column in equilibrium at the center of the shell and consequently, it is necessary to apply an additional vertical field $B_{v\ add}$ given by[17)]

$$B_{v\ add} = \frac{I_p}{cR}\left\{\ln\frac{b}{a} + \left(1 - \frac{a^2}{b^2}\right)\left(\Lambda + \frac{1}{2}\right)\right\} . \qquad (5.2)$$

Then from the equilibrium relation, $B_{v\ shell} + B_{v\ add} = B_v$, we have

$$B_{v\ shell} = \frac{I_p}{cR}\left\{\left(\ell n\frac{8R}{b} - 1\right) + \frac{a^2}{b^2}\left(\Lambda + \frac{1}{2}\right)\right\} \qquad (5.3)$$

where b is the minor radius of the shell. Although eq. (5.3) is obtained by using relations which are originally derived for the equilibrium of the plasma, it can also be applicable to the ring conductor by putting $\beta_p = 0$. Now we substitute the dimensions of the JFT-2 shell and the simulated plasma current, i.e., R=90 cm, b=36 cm, a=1.25 cm and β_p=0, then we get $\ell n\ 8R/b - 1 = 1.99$ and $a^2/b^2 = 0.005$. Therefore the second term in the brackets in eq. (5.3) is negligible compared with the first term, since $(\Lambda + 0.5)$ is of the order of unity. Thus, in this case, $B_{v\ shell}$ should amount to 220 Gauss/100 kA.

On the contrary, the experimental result gives only 180 Gauss/100 kA even at the central part of the shell. This discrepancy seems to be mainly due to the effect of the shell gap, as is seen from the toroidal distribution of the vertical field by the shell (See Fig. 5.5).

These results will in turn determine the effective gap length as follows.

When we consider the effect of the shell gap, the field intensity averaged over the toroidal angle is important because this component leads to the displacement of the plasma as a whole. V.S. Mukhovatov and V.D. Shafranov have calculated the average intensity of the vertical field in the presence of the shell gap in terms of the effective gap length. The magnetic field inside the shell is generated either by external or by internal source. According to their expression, the field intensity inside the shell averaged along the toroid h_{ei} generated by the external source is connected with its field intensity h^0_{ei} in the absence of the shell by the following relation[17)]

$$h_{ei} = \frac{N\delta_{eff}}{2\pi R} h^{O}_{ei} \tag{5.4}$$

where N is the number of the shell gaps around the torus and is equal to 4 in our case. The effective gap length δ_{eff} is defined by

$$\delta_{eff} = \frac{\pi b}{\ell n(\alpha b/h)} \tag{5.5}$$

where α is a coefficient of the order unity and 2h is an actual gap length.

The enhancement factor $\delta_{eff}/2h$ versus actual gap length is shown in Fig. (5.7) for the dimension of the JFT-2. Since we now know the experimentally obtained leakage field from the iron core in the absence of the shell and its distribution along the torus inside the shell, we can determine an effective gap length δ_{exp} by the relation

$$\delta_{exp} = \frac{\pi R}{2} \frac{\int B_{in} d\phi}{\int B_{core} d\phi} \tag{5.6}$$

, where B_{core} is the leakage magnetic field in the absence of the shell, B_{in} is its fraction inside the shell given by the broken line in Fig. 5.5 and the integration in eq. (5.6) is performed from -45° to 45° with respect to the toroidal angle ϕ. For the present case, we obtain δ_{exp} = 50 cm. Such a consideration is also applicable to the vertical field generated by the shell. However, in this case we do not know the experimental value of the field intensity produced by the shell without gaps. Therefore we may use the theoretical value given by eq. (5.3). Using this value for B_{core} and the difference between theoretical and experimental values in Fig. 5.5 for B_{in}, we obtain δ_{exp}=51 cm in the case of a small gap length, i.e., with the shell cap, and δ_{exp}=61 cm without the shell cap.

These results are also shown in Fig. 5.7 in comparison with the theory. It is to be noted that in the case of the narrow gap, the theory is in good agreement with the experiment, while in the case of a wide gap, the theory overestimates the effective gap length by a factor of two.

On the other hand as mentioned in the preceding section, the weakened field by the shell due to the presence of shell gap is almost compensated by the leakage field from the iron core. Moreover, since its average intensity is so close to that given by eq. (5.3), the effect of the shell gap is not significant in the JFT-2 tokamak. However, it should also be noted that this is only a coincidence because the leakage field from the iron core may change with a different geometrical configuration of the iron core and the primary winding. Therefore, it may not be applied to

other tokamaks such as Oak Ridge ORMAK[36] or Princeton ST[5] which have primary windings at different positions.

Concerning the leakage field far from the plasma position, one finds that the level is increased by a factor of 2.5 - 4 in the direction apart from the yoke as compared with that of plasma current. However, it is significantly reduced due to absorption of the leakage flux by the yoke and this effect covers a fairly wide range of distance. These results suggests a method of diminishing leakage field in the design of future devices[37,38,39] where the diagnostic environment may be more severe.

§5.5 Conclusion

The effect of the shell gap on the vertical magnetic field inside the shell is investigated experimentally on the JFT-2 device. It is revealed that the effect of the shell gap extends as far as the central part of the shell and that the experimentally determined effective gap length is in good agreement with the approximate theory by V.S. Mukhovatov and V.D. Shafranov[17] for a gap width of about 10 cm, while there exists a difference by a factor of two for a gap length of about 25 cm. It should be also emphasized that the leakage magnetic field from the iron core plays an important role in compensating gap effect and as a result, the total vertical field is coincidentally just around the theoretical amount of the ideal shell without gaps, and its toroidal distribution approaches uniform.

The most significant effect which is remained unsolved is the scaling of these results with respect to the minor radius of the plasma. Namely, both theories and experiments so far have been concerned with the plasma with an infinitesimally small cross section. A plasma with larger cross section and high electrical conductivity may be expected to decrease the gap effect, since such a plasma will prevent the perturbed field from extending to the inside of the shell.

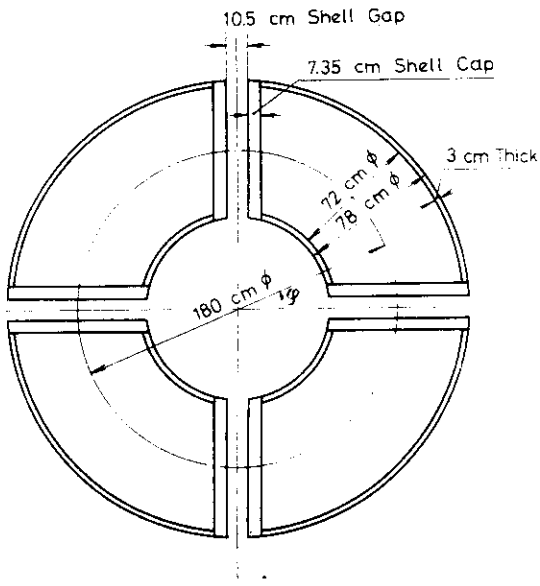

Fig. 5.1
Geometrical configuration of the shell and the shell cap of the JFT-2 tokamak (upper view).

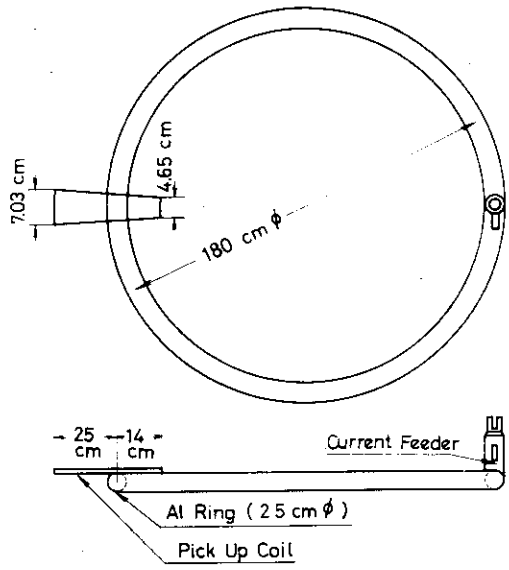

Fig. 5.2
Detection system for the measurement of vertical magnetic field. A pick up coil is fixed to the aluminum ring which simulates a plasma current.

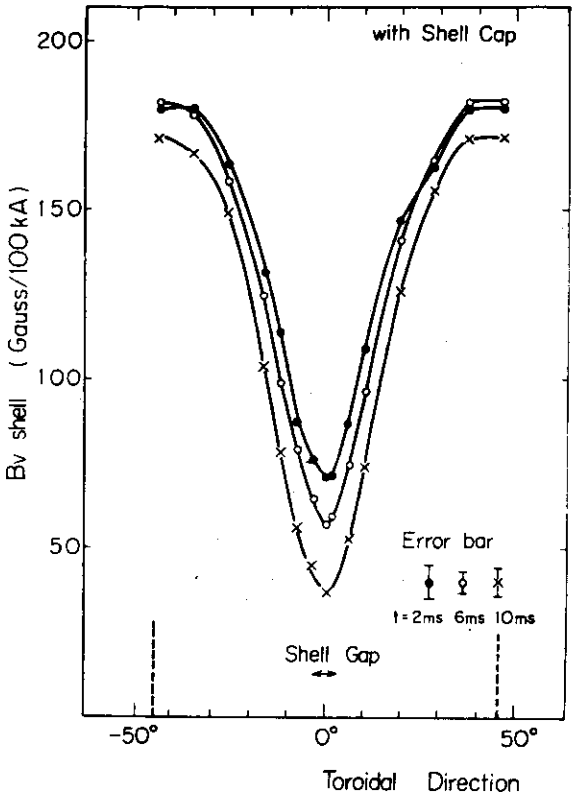

Fig. 5.3
Toroidal distribution of the vertical magnetic field generated by the image current in the shell, where t is the time after ignition of the simulated coil current.

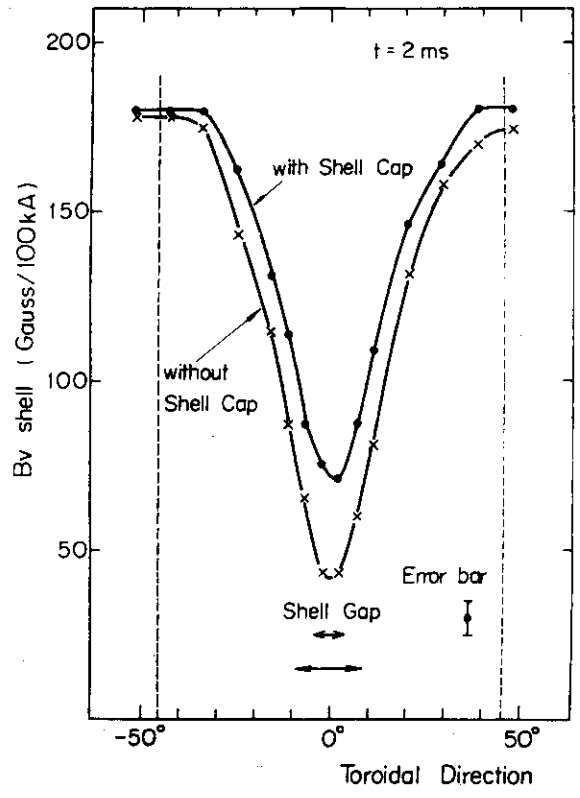

Fig. 5.4
Toroidal distribution of the vertical magnetic field generated by the shell at t = 2 msec with or without the shell cap.

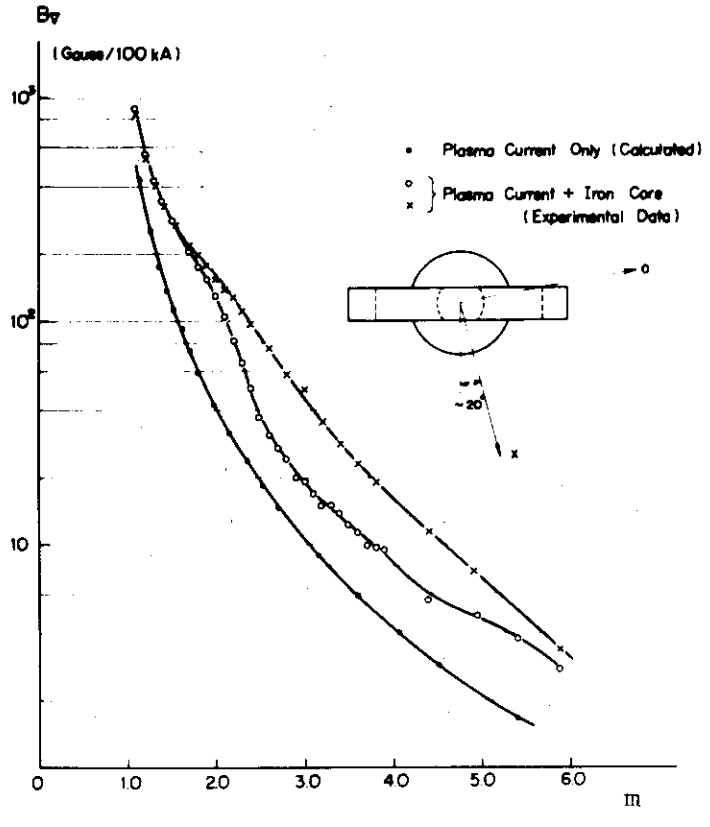

Fig. 5.6
Radial distribution of a vertical component of the leakage field due to the iron core and a plasma current measured by magnetic probes. Calculated vertical field by an "air core" plasma current are also shown by dotted points for comparison.

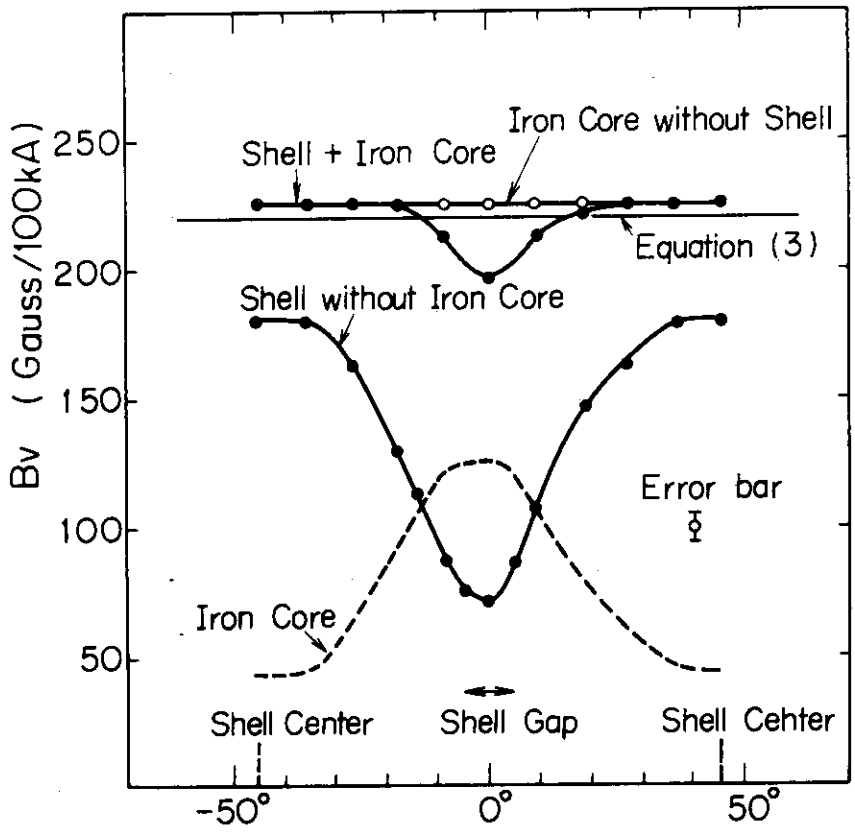

Fig. 5.5 Toroidal distribution of the vertical magnetic field generated by the shell and/or by the iron core. The distribution of the vertical field from the iron core is a result of subtraction of the contribution by the shell from the superposed vertical field. The leakage field from the iron core in the absence of the shell is also indicated. A theoretical value given by eq.(5.3) is shown for comparison.

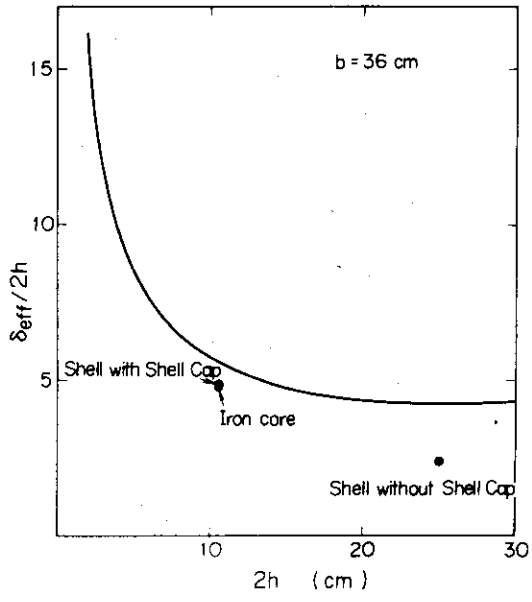

Fig. 5.7
An enhancement factor $\delta_{eff}/2h$ versus actual gap length 2h. A solid line is calculated by eq.(5.5). A white circle is obtained experimentally for the leakage field from the iron core and black points are obtained for the vertical field by the shell. Here the solid line is obtained by putting $\alpha = 1$ in eq.(5.5).

CHAPTER 6
SOAKAGE CURRENT ASSOCIATED WITH PULSED VERTICAL FIELD

§6.1 Introduction

The vertical control field in the JFT-2 tokamak device is composed of two magnetic field systems.[6] The one is generated by the continuous current and is called a D.C. vertical field. Four coils are placed outside the toroidal coil system between the two shielding plate (See Fig. 6.1). The other, so called a "pulsed vertical field", is generated by a set of coil assembly inside the shell with a time varying current (Figs. 6.2 and 6.3). The former which is measured by the Hall probe[22] is found to be quite uniform along the torus, although the presence of core yokes has been thought to destroy the toroidal symmetry. As for the latter, the shell has four gaps to accommodate with diagnostic and/or evacuation ports. For this reason, the pulsed vertical coils (See Fig. 6.4) have to traverse the torus along the edge of the shell in the poloidal direction. Thus the coils form so-called fractional turns. In order to reduce toroidal asymmetry of the vertical coils, the traversing parts are mounted outside the shell.

The installation of the pulsed vertical coils inside the shell is determined on the basis of the following reason. Provided that the coils were set at the outside of the shell, it takes a considerably long time for the vertical field to penetrate into the shell and hence, larger ampere turns would be required. Therefore, in the JFT-2 device, the pulsed vertical field is applied such that it cancels the constantly applied D.C. vertical field at the breakdown phase. The image current flows on the surface of the shell when the pulsed vertical field is energized. This current may have an advantage of improving the uniformity of the vertical field, whereas it simultaneously decreases the field intensity.

The most significant feature of this field system is the effect of soakage current due to finite conductivity of the shell combined with the presence of shell gaps. This effect had been pointed out by measurements[21] on the 1/5 model of the JFT-2 (See Fig. 6.5), and is confirmed this time on the JFT-2 device with more accurate measurements.[22]

§6.2 Method of Measurements

Magnetic probes, each of which consists of 2000 turns with an average radius of 5 mm, are mounted on a azimuthally rotating framework (See Fig.

6.6). The output signal is time integrated and is introduced to the syncroscope. This rotating framework is in turn attached to the toroidally movable axis and is scanned over the region which covers the whole range of the inside of the shell. On the rotating framework, a set of probes are mounted at three radial positions, and are capable of measuring the r, θ , and ϕ components of the vertical field, respectively. To avoid field disturbances due to the eddy current, the rotating framework is made of insulating material and other components are made of stainless steel no thicker than 6 mm in accordance with one tenth of the skin deapth. The measurement position can be adjusted by the electrical detector using photo-diode within errors of ±1 mm in the toroidal direction and $\pm 0.19^{\circ}$ in the azimuthal direction. Measurements have been carried out on the r, θ , and ϕ components of the pulsed vertical field at r=5 cm, 15 cm, and 25 cm, at every 5 degrees in θ and at 9 points in ϕ . Since the vertical coil is made symmetric with respect to $\phi = 45^{\circ}$, it is suffice to measure one eighth of the full torus.

§6.3 Experimental Results

Defining the r, θ , and ϕ coordinate as illustrated in Fig. 6.7, the measurements have been carried out covering the entire range of one period of the toroidal symmetry (one eighth of the full torus). The waveform of the coil current is changeable by six RL decay time constants after the ignition of the crowber switch (See Fig. 6.3). Measurements are made on three cases of decay time constants, namely τ_c = 6 msec, 14 msec and 26.8 msec. The magnetic coupling between pulsed vertical field and other field systems such as those by plasma current, by D.C. vertical coils and by the presence of transformer core may be weak because of their topological property. In Fig. 6.8 shown is the toroidal distribution of the vertical component B_v of the pulsed vertical field as a function of time. As is seen in this figure, the toroidal distribution becomes nonuniform as time proceeds. In particular, a strong nonuniformity appears in the case of longer decay time of the coil current. The vertical field persists near the center of the shell ($\phi \sim 45^{\circ}$) long after the decay of the coil current. These characteristics are consistent with those predicted by the measurements on the 1/5 model assembly.[21] Note that there exists a significant difference in the decay time of the vertical field between positions at the gap and at the center of the shell. The decay time near the gap is roughly equal to that of the coil current, which indicates a weak influence of the soakage

current. The decay time near the center, however, is much longer than that of the coil current. Typical decay times are shown in Fig. 6.9 in which the longest one extends to about 100 msec near the center of the shell in the case of τ_c=26.8 msec. The qualitative explanation of this phenomenon is given minutely in Reference 21. (See Fig. 6.10). A well known expression for the skin time $\tau \sim \mu\sigma(\frac{d}{2})^2$ is not appropriate for our use, where μ is the permeability, σ is the electrical conductivity and d is the thickness of the shell. Instead, it may fit reasonablly well, if one takes a form

$$\tau \sim \mu\sigma \frac{d}{2} \cdot \sqrt{\frac{\ell}{2} \cdot \frac{z}{2}} \qquad (6.1)$$

, where ℓ is the average length of the soakage currents in the azimuthal direction, and z is in the toroidal direction. Substituting the JFT-2 dimensions, $\ell \simeq 30$ cm, $d \simeq 3$ cm, and $z \sim 55$ cm, one finds

$$\tau \sim 130 \text{ msec}$$

which is not contradictory with the above measurements. Figure 6.11 shows the time variation of the toroidal component B_φ of the pulsed vertical field. The main source for the long persisting magnetic field is the presence of soakage current. The above results may well suggest that this soaking current loop diffuses toward the center of the shell.

Radial distributions of the vertical component are also shown in Fig. 6.12 in the case of two extreme positions, namely at $\phi = 3.2^\circ$ and at $\phi = 45^\circ$. In this figure, the intensity increases toward the coil and also it increases with the major radius R. The latter property which seems to be contradictory with our concepts of the toroidal effect, is in fact consistent with that obtained by numerical calculations performed by Takeda et. al.[6] assuming an infinite conductivity of the shell in the absence of shell gaps. Illustrated in Fig. 6.13 is the cross sectional view of the field distribution measured at $\phi = 45^\circ$ in the case of $\tau_c \sim 26.8$ msec. It is found that the toroidal effect compresses the magnetic flux to the outside of the torus, and consequently increases its intensity. Moreover, in the later stage of the coil current at t = 40 msec, the field intensities at $\theta = 90^\circ$ and 270° are appreciably stronger than those of other positions. This may be interpreted in terms of diffusion model of the soakage current loops described earlier.[21]

Radial components of the pulsed vertical field is important in view of island formation. This problem will be discussed in the following Chapter. Here, we only show the results of measurements at time t = 5 msec, 10 msec and 20 msec (See Fig. 6.14).

§6.4 Comparison with the Design Value and Concluding Remarks

Since the pulsed vertical field is generated by the fractional turns placed at the inside of the shell, it may be thought to be free from the influence of the iron core. In the design of this field, the most important unknown problem was the cooperative effect of finite conductivity with shell gaps. As is found by measurements in the later stage of the coil current, there is a strong nonuniformity of the vertical field along the torus due to the soakage current in the shell. However, in the relatively early stage, the field distribution is roughly uniform and can be compared with those obtained by numerical calculations[6] which assume an infinite conductivity of the shell in the absence of shell gaps. An example is given in Fig. 6.15 from which it is clear that vertical field is stronger and it increases toward the edge of the plasma at $r = 25$ cm in the case of measurement. Thus it may be concluded that it is difficult to regard the shell as superconducting, even in the initial stage of the pulsed vertical magnetic field.

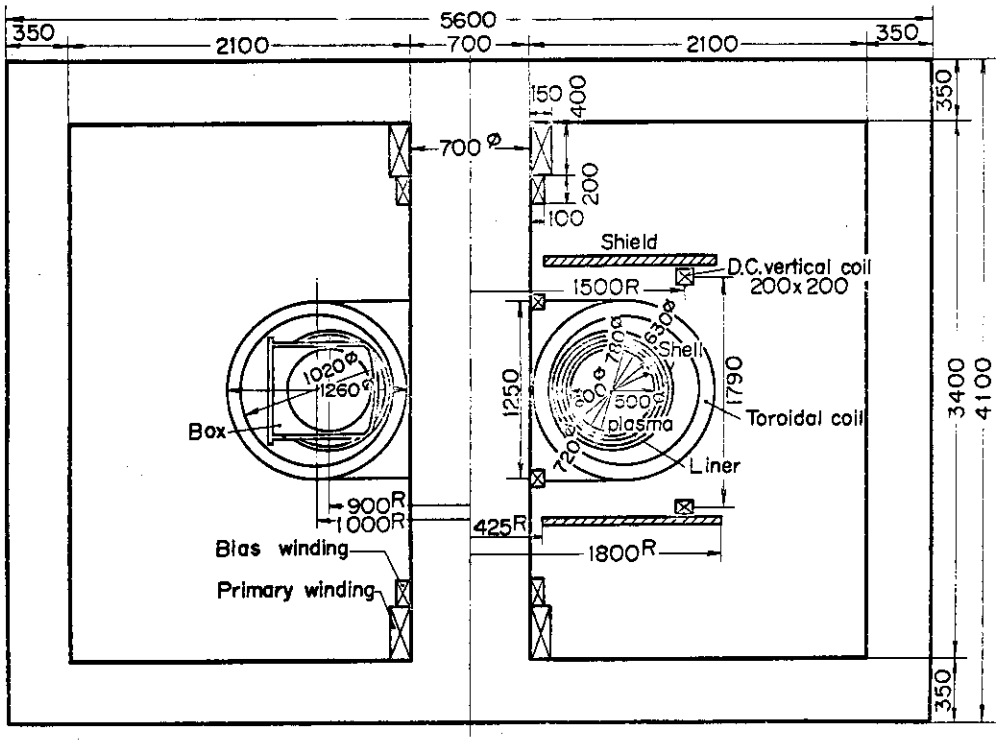

Fig. 6.1 Configuration of the JFT-2 magnetic system.

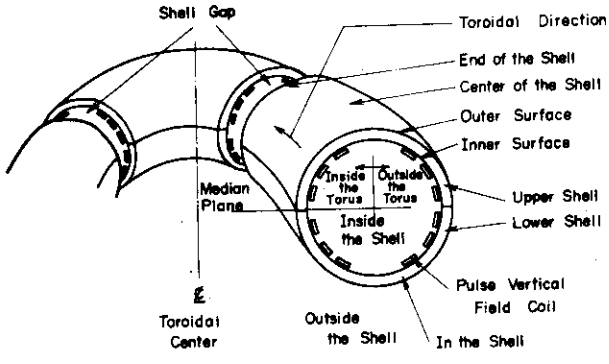

Fig. 6.2
Sketch of the shell and the pulsed vertical coils in the JFT-2.

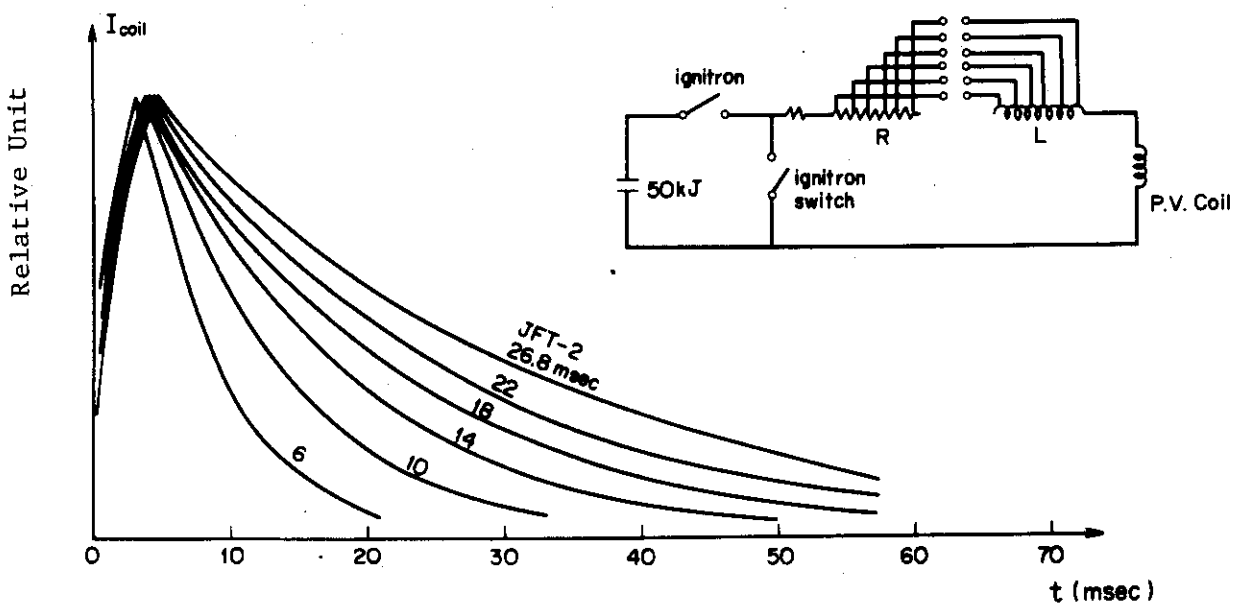

Fig. 6.3 Electric circuit used in the JFT-2 to provide various decay times of the pulsed vertical coil current, and the waveforms produced.

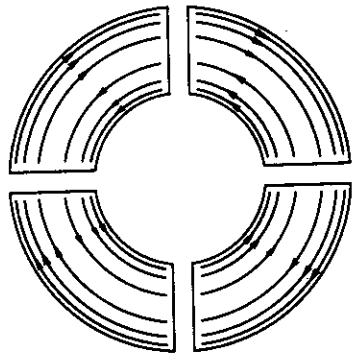

Direction of the Current
in the Pulse Vertical Field Coils

(a)

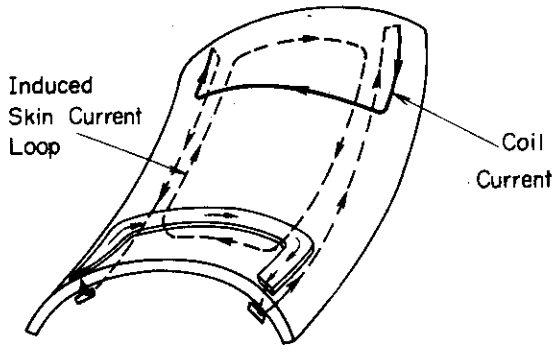

(b)

Fig. 6.4
Upper view of the shell and the current directions in the pulsed vertical coils (a) and typical current loops of the coil and the induced soakage current(b).

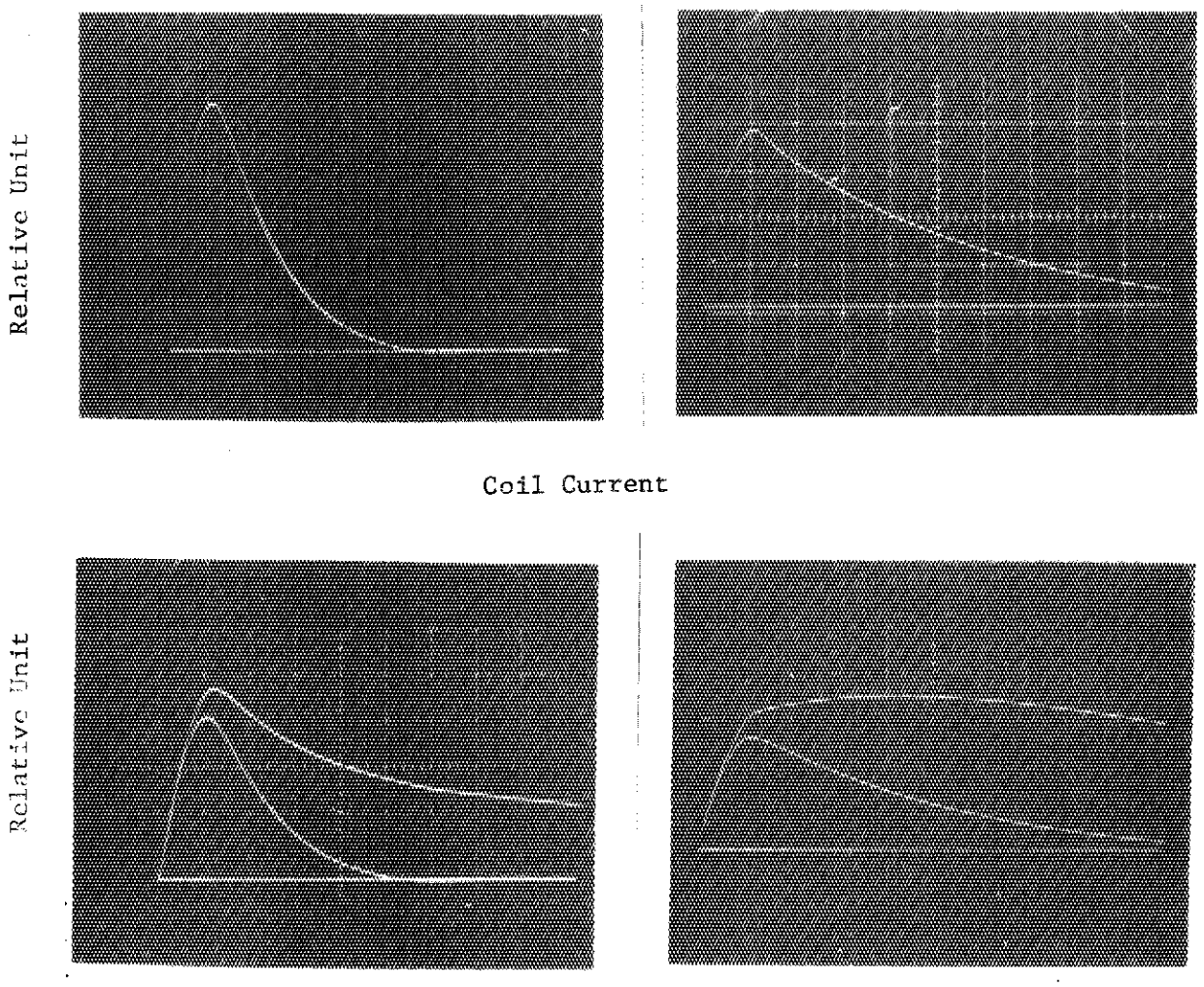

Fig. 6.5 Typical waveforms of the coil current (upper photographs) energized in the 1/5 model experiments with decay time constants of 250 and 890 μsec, respectively. The upper traces indicate the vertical field measured at the center of the shell (ϕ = 45°) whereas the lower at the gap (lower photographs). The time scale is 200μ sec/div. Short current pulse is chosen to scale the JFT-2 dimension in accordance with frequency and scale length dependences of the skin time.

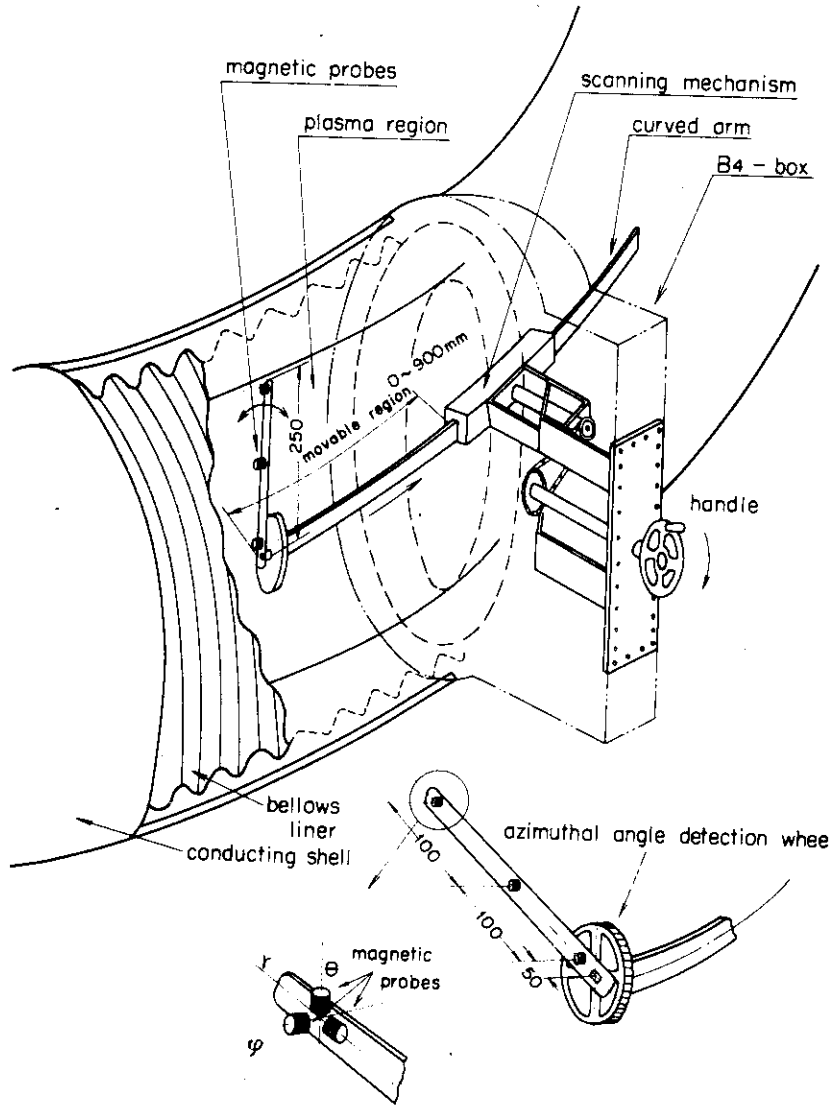

Fig. 6.6 Detection system for the pulsed vertical field.

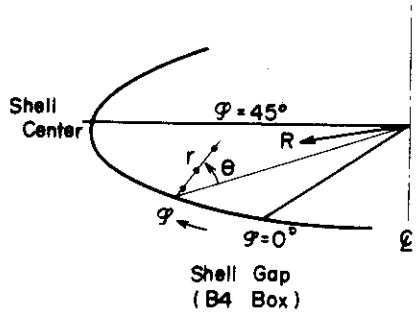

Fig. 6.7
Coordinate system for the measurement of the pulsed vertical magnetic field. The r = 0 axis is chosen to coincide with the center of the shell at R = 90 cm, and φ = 0° is the center of the gap.

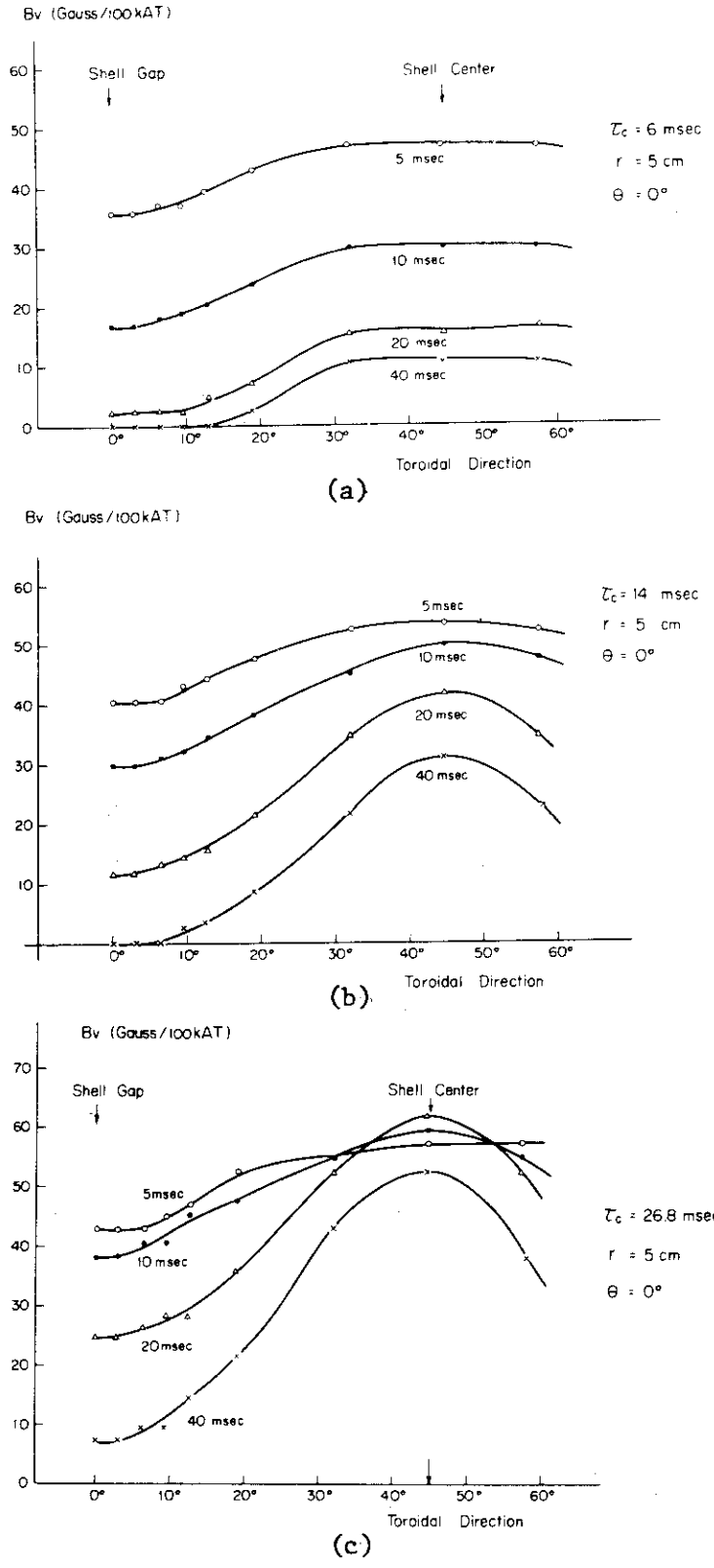

Fig. 6.8 Toroidal distribution of vertical components of the pulsed vertical magnetic field as a function of time. Measurements are made at r = 5 cm, $\theta = 0^{\circ}$ for coil current decay times of 6 msec (a), 14 msec (b) and 26.8 msec (c).

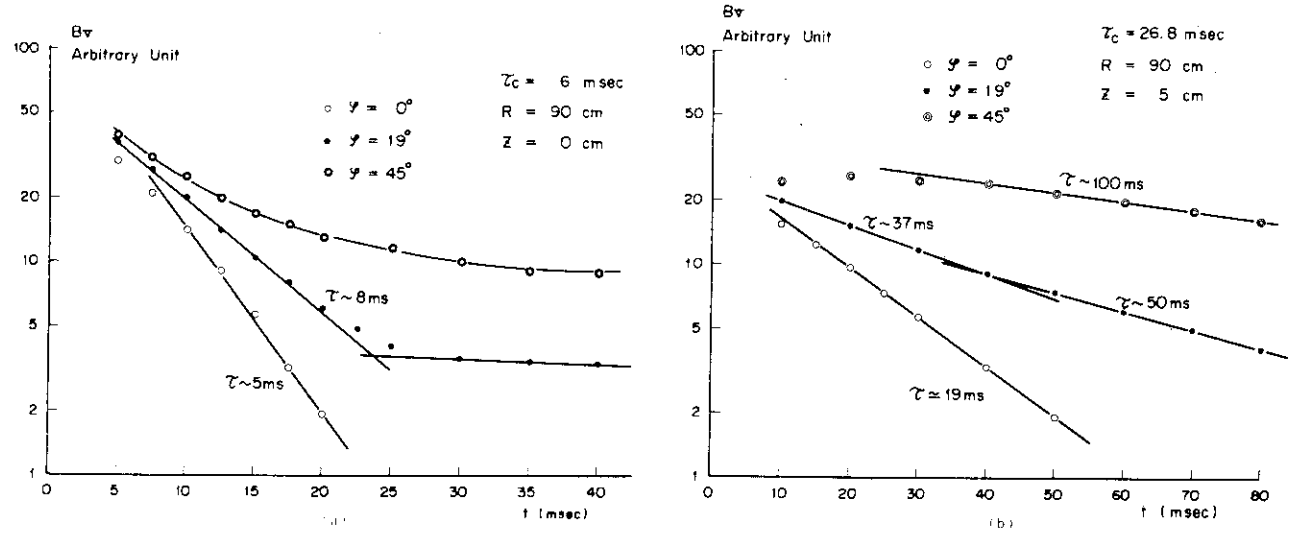

Fig. 6.9 Time behavior of the vertical component of the pulsed vertical field at three toroidal positions. The decay time at the gap is nearly equal to that by the coil current, while at the center it is much larger. Coil current decay times in (a) and (b) are 6 msec and 26.8 msec, respectively.

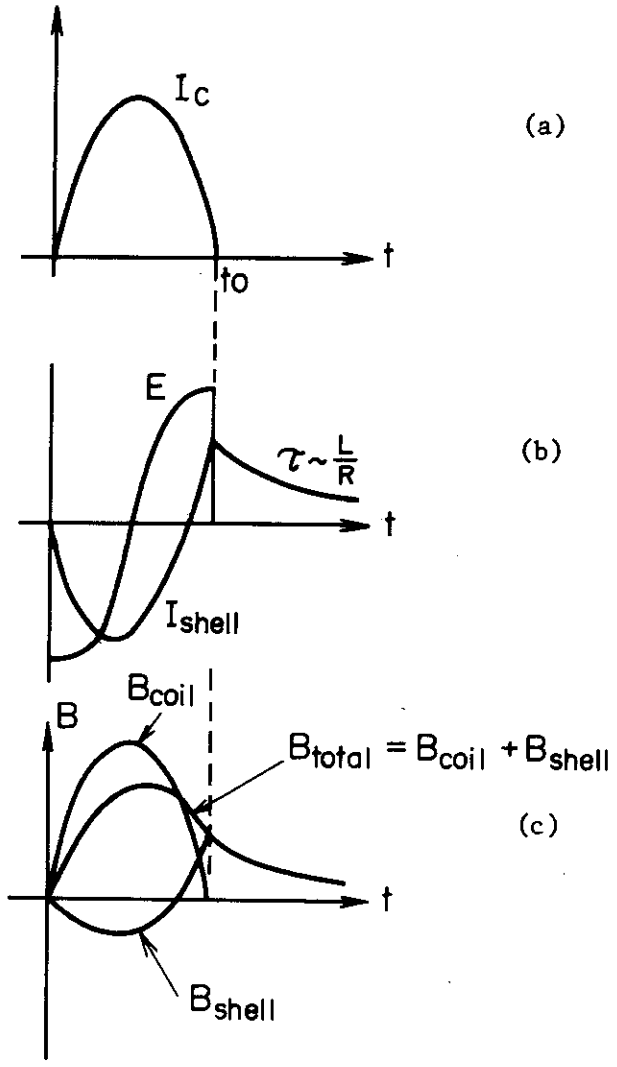

Fig. 6.10
Expected waveforms of the coil current I_c (a), induced electric field E on the shell surface and the soakage current I_{shell} driven by it (b), the superposition of the fields B_{coil}, B_{shell} generated by these currents that gives the measured waveform B_{total} (c). The phase lag of I_{shell} from the induced electric field is due to the inductive component of the soakage current. If the shell is superconducting, this phase lag is exactly $\pi/4$. The finite conductivity makes the phase lag less than $\pi/4$.

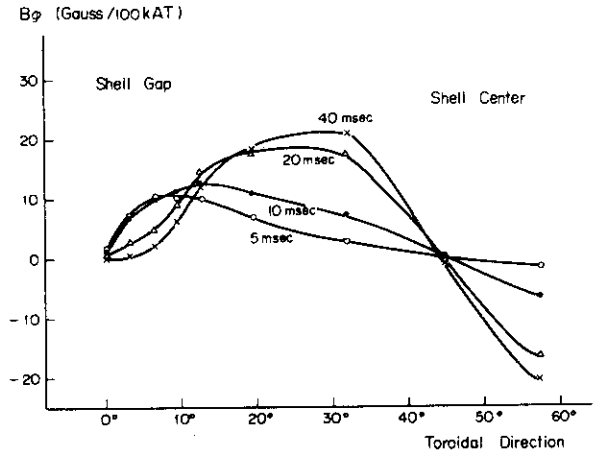

Fig. 6.11
Toroidal distribution of the toroidal component of the pulsed vertical magnetic field as a function of time, suggesting that the effective soakage current loop are shrinking toward the center of the shell.

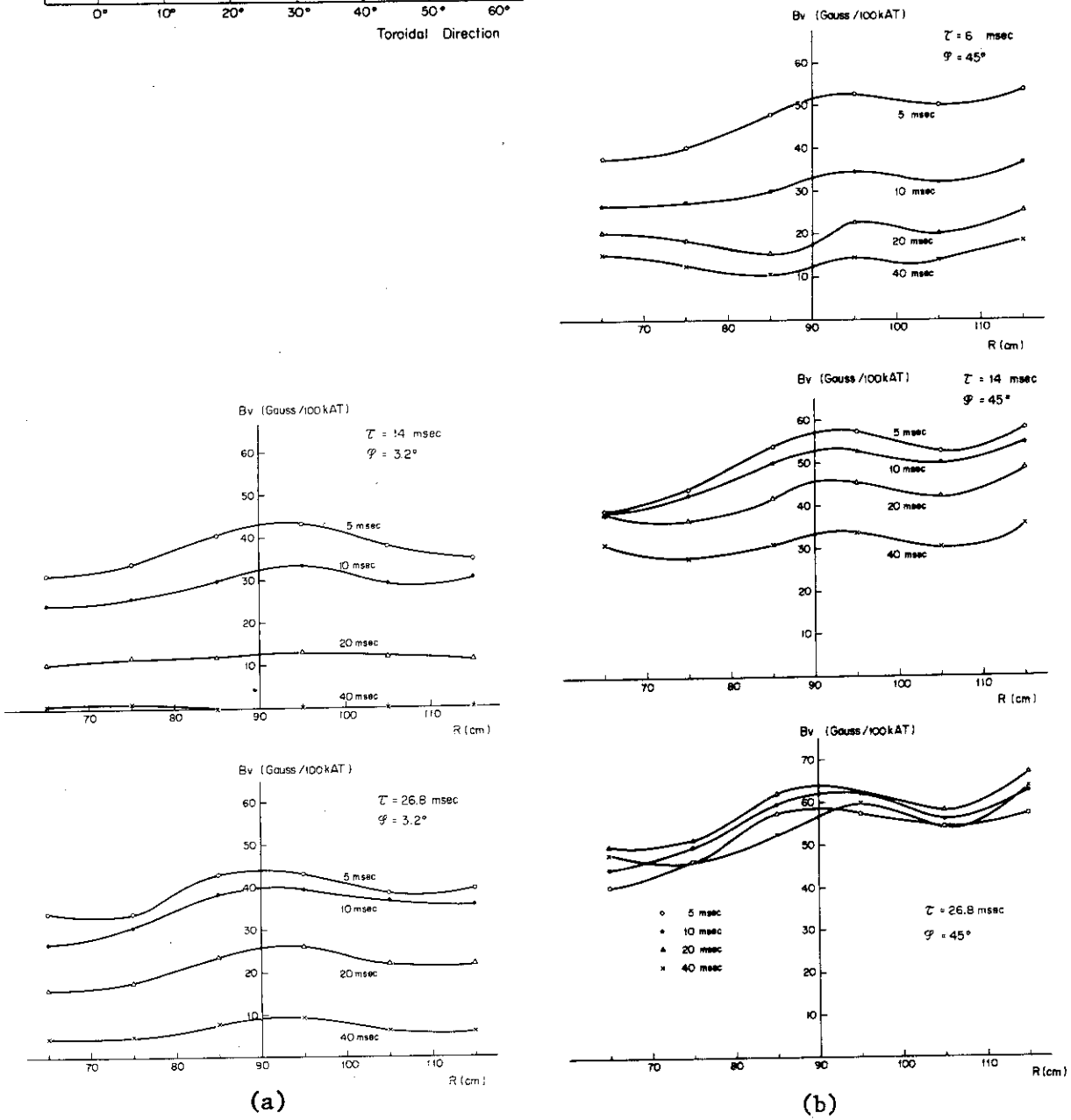

Fig. 6.12 Radial distribution of vertical components of the pulsed vertical field in the median plane at the shell gap (a), and at the shell center (b) for typical decay times of the coil current.

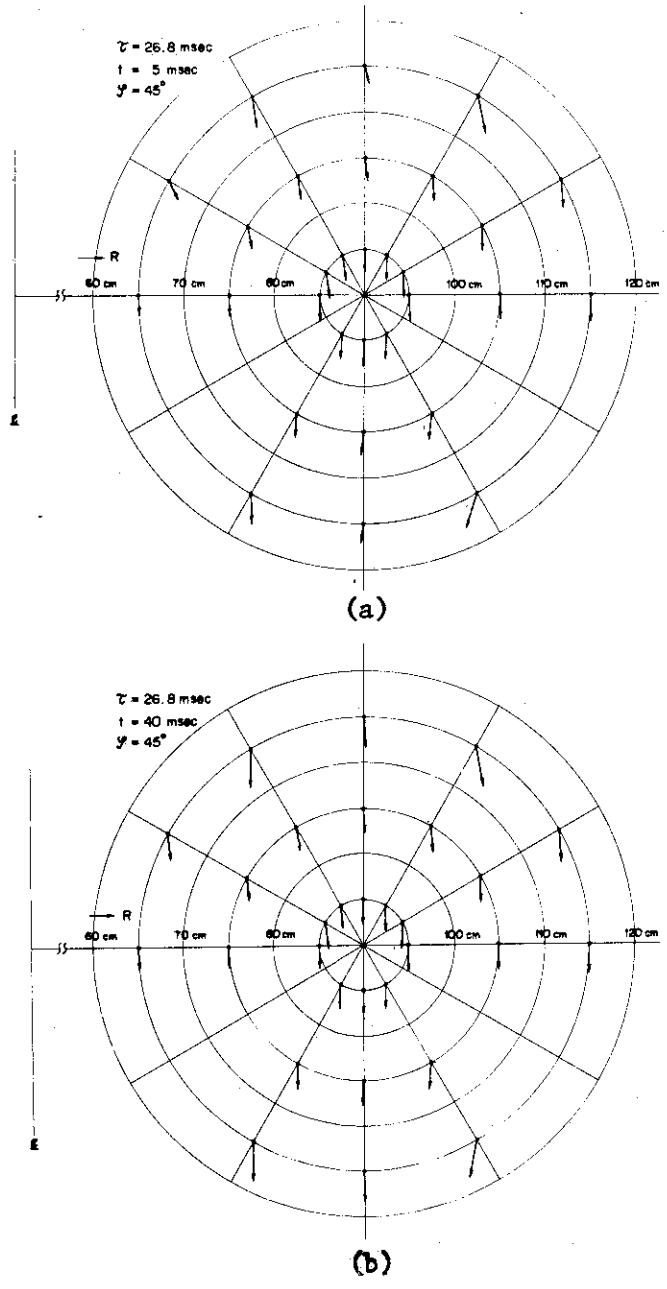

Fig. 6.13 Cross sectional view of the pulsed vertical field at t = 5 msec (a), and t = 40 msec (b) at the shell center. The arrow length indicates magnetic field intensity at each point. The decay time of the coil current is 26.8 msec in both cases.

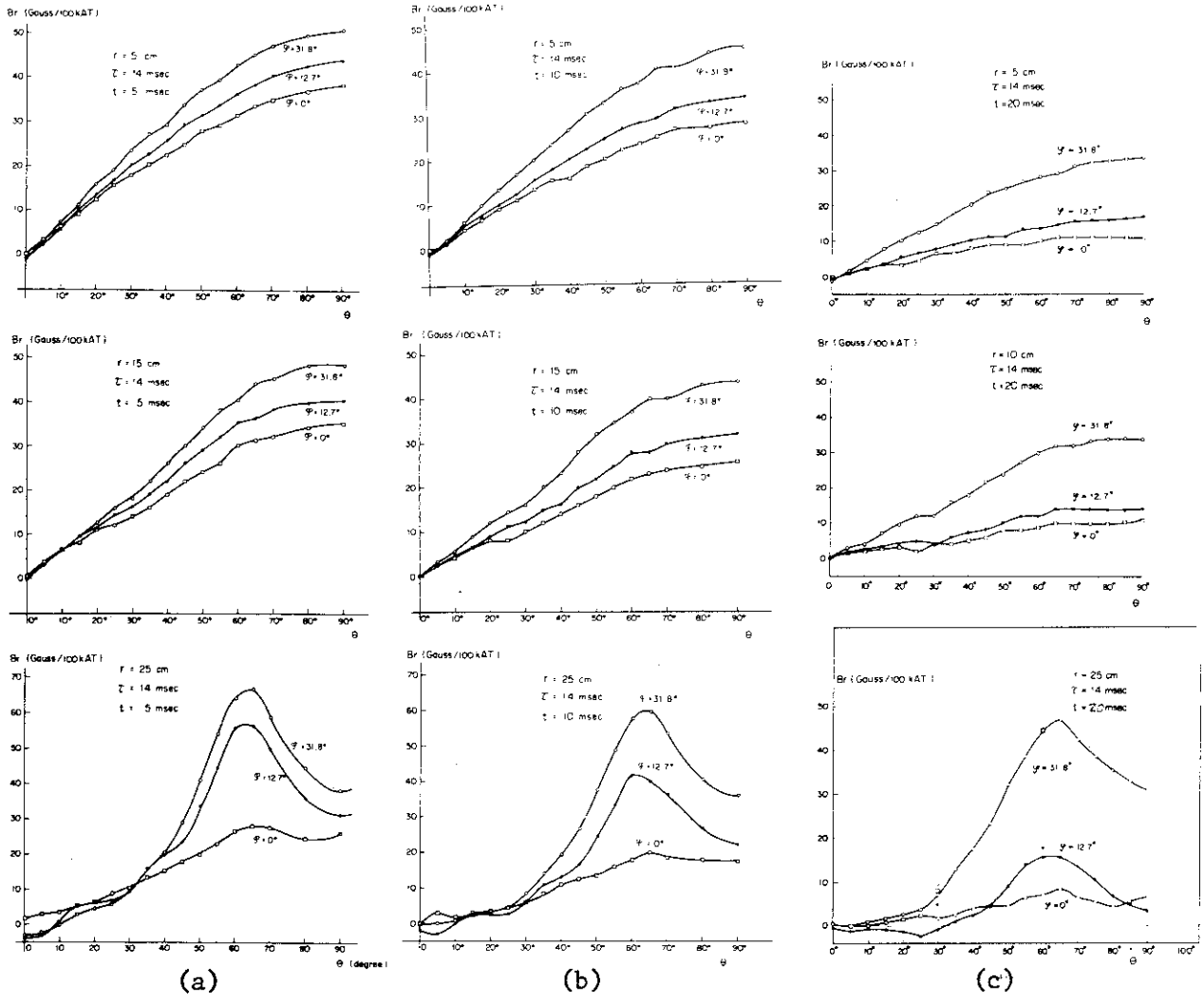

Fig. 6.14 Azimuthal distributions of B_r of the pulsed vertical magnetic field at t = 5 msec (a), 10 msec (b), and 20 msec (c). The decay time of the coil current is 14 msec in these cases.

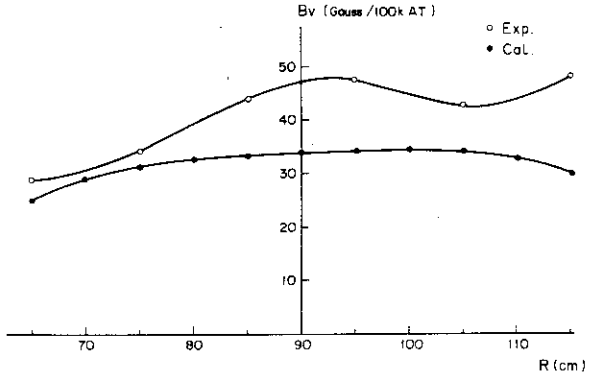

Fig. 6.15
Comparison of the radial distribution of the pulsed vertical magnetic field between measured and calculated values. The former is obtained at the center of the shell at t = 5 msec.

CHAPTER 7
MAGNETIC ISLAND FORMATION DUE TO ERROR FIELD IN TOKAMAKS[24]

§7.1 Introduction

Magnetic surfaces indispensable to high temperature plasma confinement in toroidal systems are assumed to exist in experimental devices. Theoretically such surfaces are known to exist only in the case of special symmetry, that is, toroidal symmetry or helical symmetry. A tokamak is one of the devices which satisfy such a condition. However, it is impossible to design and construct devices with a complete toroidal symmetry. In practical cases, the asymmetry results from shell gaps which are required not to short-circuit toroidal electric field and also from the holes in the shell to provide ports for diagnostics. These geometric disturbances give rise to magnetic error fields that disturb the toroidal symmetry. Especially important among these field perturbations are those in resonance with the period of magnetic lines of force. Perturbed magnetic lines of force may be inclined to drift towards the wall as they transit along the torus. However, the shear in magnetic surfaces helps reducing the effect of these disturbances, since the radial variation of the rotational transform restricts the resonance to a localized region. Thus magnetic error fields create islands in magnetic surfaces.[11,24] These islands have a deteriorating effect on the plasma confinement, since they enhance the transport of plasmas and facilitate the excitation of instabilities.[43] Physics of transport phenomena in the presence of magnetic islands have recently been investigated to some extent both in collisional and in collisionless regimes,[40,41,42] and they present anomalous diffusion coefficient of the plasma near the resonance surface.

In the present work, we are particularly interested in the role of external error fields on the island formation. Theoretical works[8,11] have been performed in the past on the island formation due to error fields. These analyses, however, are somewhat complicated and are lacking in physical pictures.

In this chapter, we present a simple analytical method to obtain the size of islands formed by the presence of resonant magnetic field and apply it to evaluation of magnetic island in the JFT-2 tokamak[6] at JAERI and ORMAK[36] at Oak Ridge, in particular, due to the pulsed vertical field associated with shell gaps. The results are then compared with those

obtained by numerical computation.

In §7.2, the width of islands is derived analytically in a general form in terms of the resonant component of magnetic field and the magnetic shear. Section 7.3 describes several examples of magnetic islands in JFT-2 and ORMAK. Some of the analytical estimates are confirmed by the numerical follow of the magnetic lines of force by the R.K.G. method.

§7.2 Analitical Estimate

We use the (r, θ, φ) coordinate system[29] to describe toroidal magnetic surfaces and magnetic lines of force, where r is the minor radius, θ and φ are the angular coordinates the short way and the long way around the torus, respectively. In the coordinate system, magnetic lines of force are given by

$$\frac{d\theta}{d\varphi} = \iota(r) \tag{7.1}$$

where $\iota(r)$ is the rotational transform of magnetic lines of force. Expanding $\iota(r)$ near $r = r_0$, the radius of resonant magnetic surfaces, eq. (7.1) can be rewritten as

$$\frac{d\theta}{d\varphi} \simeq \iota(r_0) + \frac{d\iota(r)}{dr}(r-r_0) = \iota_0 + \iota' x \tag{7.1a}$$

where $x = r - r_0$, $\iota_0 = \iota(r_0)$ and $\iota' = \left[d\iota(r)/dr \right]_{r=r_0}$. In the lowest order of the error field, equation of the magnetic lines of force is given by

$$\frac{dr}{rd\theta} = \frac{dx}{rd\theta} = \frac{B_r(r,\theta,\varphi)}{B_\theta(r)} \tag{7.2}$$

where $B_r(r,\theta,\varphi)$ is the radial component of error field. The θ -component of error field is small compared with the θ -component $B_\theta(r)$ of unperturbed field and is therefore neglected. Since the radial size of islands is small, we shall hereafter neglect the radial dependence of $B_r(r,\theta,\varphi)$ and $B_\theta(r)$. The value $B_r(r_0,\theta,\varphi)$ may be expanded in Fourier components

$$\begin{aligned} B_r(r_0,\theta,\varphi) = \sum_{m,n} \big(& (a_{m\cdot n} \sin(m\theta - n\varphi) \\ & + a'_{m\cdot n} \sin(m\theta + n\varphi) \\ & + c_{m\cdot n} \cos(m\theta - n\varphi) \\ & + c'_{m\cdot n} \cos(m\theta + n\varphi)) \end{aligned} \tag{7.3}$$

where $a_{m\cdot n}$, $a'_{m\cdot n}$, $c_{m\cdot n}$, and $c'_{m\cdot n}$ are the Fourier coefficients. Since it will be revealed that only the resonant component is important near the resonant

magnetic surface at $r = r_0$, we shall keep the first and the third terms in eq. (7.3) which satisfy

$$\frac{m}{n} \simeq \frac{1}{\iota_0} = q \tag{7.4}$$

where q is generally called by a safety factor. Finally one obtains simply

$$B_r(r_0, \theta, \varphi) = b_{m,n} \sin(m\theta - n\varphi + \beta) \tag{7.5}$$

where $b_{m,n} = \sqrt{a_{m,n}^2 + c_{m,n}^2}$ and $\beta = \tan^{-1}(c_{m,n}/a_{m,n})$.

Defining a new variable by

$$\alpha = m\theta - n\varphi + \beta \tag{7.6}$$

eq. (7.2) now takes a form

$$\frac{dx}{r_0 d\theta} = \frac{b_{m,n} \sin\alpha}{B_\theta(r_0)} \tag{7.7}$$

On the other hand from eqs. (7.1) and (7.6) we obtain

$$\frac{d\alpha}{d\theta} = -\frac{n}{\iota_0 + \iota' x} + m \tag{7.8}$$

Substituting eq. (7.7) into eq. (7.8) a nonlinear periodic equation is obtained:

$$\frac{d^2\alpha}{d\theta^2} = -n \frac{d}{d\theta}\left[\frac{1}{\iota_0}\left(1 - \frac{\iota'}{\iota_0} x\right)\right]$$

$$= n \frac{r_0 \iota'}{\iota_0^2} \frac{b_{m,n} \sin\alpha}{B_\theta(r_0)} = -A \sin\alpha \tag{7.9}$$

where

$$A = -\frac{n r_0 \iota'}{\iota_0^2} \frac{b_{m,n}}{B_\theta(r_0)} \tag{7.10}$$

Here we may assume $A \geq 0$ for convenience since in case of $A < 0$, by putting $m\theta - n\varphi + \beta = \alpha + \pi$ instead of eq. (7.6) we can easily deduce the following relation.

$$\frac{d^2\alpha}{d\theta^2} = A \sin\alpha = -|A| \sin\alpha$$

It can be seen that the behavior of a magnetic lines of force in a resonant error field is analogous to the motion of a particle in a periodic potential $U = A(1-\cos\alpha)$, if we regard α and θ as the position and the time, respectively.

Multiplied by $d\alpha/d\theta$ and integrated over θ eq. (7.9) is written in the usual energy integral form

$$\frac{1}{2}\left(\frac{d\alpha}{d\theta}\right)^2 = E - A(1-\cos\alpha) \tag{7.11}$$

where $\frac{1}{2}(d\alpha/d\theta)^2$ and $U = A(1-\cos\alpha)$ correspond to the kinetic and the potential energy, respectively, and $E = \frac{1}{2}(d\alpha/d\theta)^2_{\alpha=0}$ to the total energy. Putting $k^2 = E/2A$ $(k>0)$ we have

$$\left(\frac{d\alpha}{d\theta}\right)^2 = 4A\left(k^2 - \sin^2\frac{\alpha}{2}\right) \tag{7.12}$$

Characteristics of the solution of eq. (7.12) are well known.[44] Two types of solutions are possible as shown in Fig. 7.1. A particle with a sufficient energy moves across the periodic mountains towards larger $|\alpha|$ while the particle with $E<2A$ moves periodically within a limit of α. The latter corresponds to the islands of magnetic surfaces. This may indicate that dropping of other terms in eq. (7.3) is reasonable for island formation. Maximum excursion of the magnetic lines of force or the maximum size of islands δ is obtained at the boundary $k = 1$ of the two kinds. We obtain from eq. (7.7)

$$\delta = \int dx = \int \frac{r_o b_{m,n} \sin\alpha}{B_\theta(r_o)} \frac{d\alpha}{d\alpha/d\theta} \tag{7.13}$$

Using eq. (7.12), the integral in eq. (7.13) may be calculated and is equal to $4\sqrt{A}\frac{\iota_o^2}{n\iota'}$. As a result we have

$$\delta = \frac{4r_o}{\sqrt{m}}\sqrt{\frac{b_{m,n}}{B_\theta(r_o)}}\sqrt{\left|\frac{\iota_0}{-r_o\iota'}\right|} \tag{7.14}$$

In practical applications described in the following section we have to evaluate the resonant component $b_{m,n}$ of the radial component $B_r(r_o,\theta,\varphi)$ of the error field given in general Fourier series

$$B_r(r_o,\theta,\varphi) = \sum_{m;n'=0} \left(A_{m;n'}\cos\frac{2\pi m'\theta}{T_1}\cos\frac{2\pi n'\varphi}{T_2} + B_{m;n'}\sin\frac{2\pi m'\theta}{T_1}\sin\frac{2\pi n'\varphi}{T_2} + D_{m;n'}\cos\frac{2\pi m'\theta}{T_1}\sin\frac{2\pi n'\varphi}{T_2} + E_{m;n'}\sin\frac{2\pi m'\theta}{T_1}\cos\frac{2\pi n'\varphi}{T_2}\right) \tag{7.15a}$$

where T_1 and T_2 are the fundamental periods in θ and φ, respectively, m' and n' are integers and the Fourier coefficients are given as

$$
\begin{aligned}
A_{m'n'} &= \frac{4}{T_1 T_2}\iint B_r(r_o,\theta,\varphi)\ \cos\frac{2\pi m'\theta}{T_1}\ \cos\frac{2\pi n'\varphi}{T_2}\ d\theta\, d\varphi \\
B_{m'n'} &= \frac{4}{T_1 T_2}\iint B_r(r_o,\theta,\varphi)\ \sin\frac{2\pi m'\theta}{T_1}\ \sin\frac{2\pi n'\varphi}{T_2}\ d\theta\, d\varphi \\
D_{m'n'} &= \frac{4}{T_1 T_2}\iint B_r(r_o,\theta,\varphi)\ \cos\frac{2\pi m'\theta}{T_1}\ \sin\frac{2\pi n'\varphi}{T_2}\ d\theta\, d\varphi \\
E_{m'n'} &= \frac{4}{T_1 T_2}\iint B_r(r_o,\theta,\varphi)\ \sin\frac{2\pi m'\theta}{T_1}\ \cos\frac{2\pi n'\varphi}{T_2}\ d\theta\, d\varphi
\end{aligned}
\qquad (7.15b)
$$

In particular the error field symmetric with respect to $\varphi = 0$ axis gives $B_{m'n'} = D_{m'n'} = 0$ and the field symmetric with respect to $\theta = 0$ axis satisfies $B_{m'n'} = E_{m'n'} = 0$. In order for the magnetic field given by eqs. (7.15a) and (7.15b) to be rewritten in the form of eq. (7.3) the following relation should hold

$$
a_{m,n} = \frac{E_{m'n'} - D_{m'n'}}{2}\ , \quad a'_{m,n} = \frac{E_{m'n'} + D_{m'n'}}{2}\ ,
$$

$$
c_{m,n} = \frac{A_{m'n'} + B_{m'n'}}{2} \quad \text{and} \quad c'_{m,n} = \frac{A_{m'n'} - B_{m'n'}}{2} \qquad (7.16)
$$

where $m = 2\pi m'/T_1$ and $n = 2\pi n'/T_2$.

§7.3 Application and Comparison with Numerical Calculations

One of the most important sources of the error field in tokamak devices is the external or the internal field associated with shell gaps. Tokamaks with conducting shells should have such gaps to induce electric field on the plasma. Since the effective gap length is larger than actual gap length, we should use the former value as giving a pessimistic estimate.

The first example we consider is a configuration with four shell gaps which are mutually apart by $\pi/2$ in the toroidal direction and with multipole error field present only at the effective gaps. Namely, the error field over the effective gap length g is assumed as

$$B_r = B_o \left(\frac{r}{r_o}\right)^{L-1} \sin L\theta \tag{7.17}$$

where B_o is the field strength at the position half way between adjacent poles at $r = r_o$ and L is the number of poles. Substituting $T_1 = 2\pi$ and $T_2 = 2\pi/p$ into eqs. (7.15a) and (7.15b) gives

$$A_{m;n'} = B_{m;n'} = D_{m;n'} = 0$$

and

$$E_{m;n'} = \frac{4p^2}{(2\pi)^2}\int_0^{2\pi}\int_{-g/2R}^{g/2R} B_o\left(\frac{r}{r_o}\right)^{L-1}\sin L\theta \,.\sin m'\theta.\cos pn'\varphi \, d\theta d\varphi \tag{7.18}$$

where $p = 4$ is the number of periods along the torus and R is the major radius. Resonance occurs if

$$n' = \frac{n}{p}, \quad m' = m = qn = L \tag{7.19}$$

then we obtain

$$b_{m,n} = \tfrac{1}{2} E_{m;n'} = \frac{4B_o}{\pi n}\left(\frac{r}{r_o}\right)^{qn-1} \sin\left(n\frac{g}{2R}\right) \tag{7.20}$$

In the case of $q = 2$, eq. (7.20) becomes

$$b_{8,4} = \frac{B_o}{\pi}\left(\frac{r}{r_o}\right)^7 \sin\frac{2g}{R} \tag{7.21}$$

Substituting $B_o = 0.2$ Wb/m^2, $r_o = 36$ cm, $r = 20$ cm, $R = 90$ cm and $g = 20$ cm into eq. (7.21) and assuming a narrow plasma current channel at $r = 0$, we obtain from eq. (7.14)

$$\delta = 1.26 \text{ cm}$$

For comparison, magnetic surfaces are computed by following magnetic lines of force by means of the R.K.G method in the same configuration described above and are shown in Fig. 7.2. Here the magnetic lines of force returns to the same island in every other transit. The number of islands formed is equal to $m = 8$. The width δ is about 1.25 cm which is consistent

with the analytical estimate of 1.26 cm. However, islands produced by this multipole are shown only as a hypothetical example, since such an intense error field is unlikely to exist in the JFT-2 tokamak device.

As other typical examples which are more closely related to actual devices, we consider the island formation due to ohmic heating coils and pulsed vertical coils in ORMAK for which the number of minor periodicity is two. Resonant perturbation fields will be picked up on the basis of the simple model described in the preceding section. We use a straight cylindrical coordinate system neglecting toroidal effects. This simplification may not lose the intrinsic nature of the subject. We also assume that the conductivity of the shell is infinite i.e., time variation of the soakage current flowing in the shell is neglected. Although the latter assumption may not be valid for the room temperature shell in the later stage of the discharge, the recent measurement has shown that a liquid nytrogen cooled ORMAK shell is almost ideally conducting.[45] At the shell gap, perturbation fields due to the ohmic heating coils and the pulsed vertical field coils are present together with their image currents. There have been arguments on the effective length of the shell gap. V.S.Mukhovatov and V.D.Shafranov[17] have studied on this problem assuming a filament plasma current and infinite conductivity of the shell. Their evaluation turned out to be in reasonable agreement with the experiment for a narrow gap length.[20] However, in the case of high temperature plasma with a large bore, where its conductivity is comparable with the room temperature shell,*) external fields near the gap may considerably be prevented from penetrating into a plasma. Thus the effective gap length may in fact be narrower than that given by the above authors. Henceforth, we will use the latter value as representing the upper limit of the effective gap length.

In the cylindrical coordinate system (r, θ, ϕ), position and current intensity of the i-th coil are expressed by $(r_{ci}, \theta_{ci}, \phi_{ci})$ and I_i, respectively. The radial component of the magnetic field generated by a group of coils is given by

$$B_r = \sum_{i=1}^{N} \frac{\mu_0 I_i \, r_{ci} \sin(\theta - \theta_{ci})}{2\pi\{r^2 + r_{ci}^2 - 2r \cdot r_{ci} \cos(\theta - \theta_{ci})\}} \qquad (7.22)$$

where μ_0 is the permeability of the vacuum, N the number of coils and (r, θ) the resonant position in the present concern. Here we will assume

*) The conductivity of the plasma with temperature of 1 keV is comparable with that of the copper shell.

that the field is present only over the period of effective gap length. By the double Fourier expansion of this field we calculate their coefficients as

$$a_{m,n} = \frac{2}{T_1 T_2} \int_0^{T_1} \int_0^{T_2} B_r \cdot \sin\left(\frac{2\pi}{T_1} m'\theta - \frac{2\pi}{T_2} n'\phi\right) d\theta \cdot d\phi$$

and

$$c_{m,n} = \frac{2}{T_1 T_2} \int_0^{T_1} \int_0^{T_2} B_r \cdot \cos\left(\frac{2\pi}{T_1} m'\theta - \frac{2\pi}{T_2} n'\phi\right) d\theta \cdot d\phi \qquad (7.23)$$

, where T_1 and T_2 are the period of symmetry along θ and ϕ, respectively, m' and n' are integers. The safety factor q is related to these values by the relation

$$q = \frac{m'}{n'} \frac{T_1}{T_2} \qquad (7.24)$$

which is equivalent with that given by eq. (7.4).
Our present concern is the resonant component given by

$$b_{m,n} = \sqrt{a_{m,n}^2 + c_{m,n}^2} \qquad (7.25)$$

, which determines the width of islands as previously described.

Precisely, the actual complex field generated by various magnetic coils should be analyzed to obtain $b_{m,n}$, since this value does not have an additive property with respect to the superposition of different magnetic fields. However, in the case of ORMAK configuration where the resonant mode number m differes appreciably between ohmic heating coils and pulsed vertical coils, a mode-mode coupling is expected to be small. This situation enables us to calculate the resonant component separately in these two cases.

(1) Ohmic Heating Coils of ORMAK

Our first interest lies in the ohmic heating coils that are placed regularly in the θ direction outside the shell (See Fig. 7.3). Each coil is placed mutually apart from adjacent coils by 20 degrees. This is exactly a multipole field with a pole number of eighteen. The flux function of this field is then given by[46]

$$\Psi = \frac{\mu_0 I}{4\pi} \ell n \left[1 + \left(\frac{r}{r_c}\right)^{2\ell} - 2\left(\frac{r}{r_c}\right)^{\ell} \cos \ell\theta \right] \qquad (7.26)$$

where Ψ is the flux function, ℓ is the number of poles and is equal to 18 in this case, r_c and I are the radial position and the current of each coil, respectively. The radial field component at the position r is then given by

$$B_r = \frac{1}{r}\frac{\partial \Psi}{\partial \theta} = \frac{\mu_o I}{4\pi r} \frac{2\ell(\frac{r}{r_c})^{\ell} \sin \ell\theta}{1 + (\frac{r}{r_c})^{2\ell} - 2(\frac{r}{r_c})^{\ell} \cos \ell\theta} \tag{7.27}$$

and is approximated by

$$\simeq \frac{\mu_o I}{4\pi r} \cdot 2\ell (\frac{r}{r_c})^{\ell} \sin \ell\theta \tag{7.27a}$$

The last equation can hold under the assumption $r \ll r_c$ with a large ℓ. Owing to the theoretical analysis[17] it is a good approximation to assume that the radial magnetic field given by the above equation exists only over the effective gap length and $B_r = 0$ in the other part of the torus. As is imagined in eq. (7.24), the minimum azimuthal mode number of resonance is eighteen with a corresponding q values of 18/2, 18/4, 18/6, 18/8 etc. We treat the case in which the rotational transform angle of the magnetic lines of force during the passage through the gaps is small compared with the angle between two adjacent poles, namely,

$$\frac{2 g_{eff}}{qR} \ll \frac{2\pi}{\ell} \quad \text{or} \quad q \gg \ell \cdot \frac{g_{eff}}{\pi R} \tag{7.28}$$

where g_{eff} is the effective gap length and R is the major radius of the plasma. Since the ORMAK has two shell gaps, the dominant resonant components may appear in the case of m = 18 and q = 18/2, that is,

$$b_{m,n} = b_{18,2k} \leq b_{18,2} \lesssim |B_r| \cdot \frac{g_{eff}}{\pi R} \tag{7.29}$$

, where k is an integer and B_r is the radial component of the multipole field given by eq. (7.27). In this series of inequality, the last term gives the upper limit of the resonant components. Substituting the ORMAK dimensions into eqs. (7.28) and (7.29), namely, $I = 5 \times 10^3$ A (corresponding to the total ampere turns of 90 kA), $r_c = 0.32$ m, $g_{eff} = 0.52$ m (this is about five times larger than the geometrical gap length) and $R = 0.795$ m, we find

$$q \gg 3.8$$

and

$$b_{18,2} \lesssim 3.98 \times 10^{-6} \text{ Wb/m}^2$$

, where we intend to study the resonances at r = 0.2 m. This amount is one to two orders of magnitude smaller than what may cause islands of appreciable width. For the parabollic current distribution, for instance, the width of island is expected to be an order of 0.1 cm and can be neglected. Numerical Fourier analysis of the magnetic field of this geometry gives exact resonant components. The results are summarized in Table 7.1 from which one may conclude that resonant field components due to the ohmic heating coils in ORMAK do not make islands of a significant width.

(2) Pulsed Vertical Coils of ORMAK

The configuration of the ORMAK pulsed vertical field coils and their image currents is illustrated in Fig. 7.4. Since these coils are installed inside the shell, image currents are induced along the wall of the shell, while at the gap (precisely, over the effective gap length) no image currents are induced. Assumptions are made that image currents are equivalently replaced by a set of inverse current coils and that all the currents are filament-like. Since the radial components of this field is antisymmetric with respect to $\theta = 0$ as shown in Fig. 7.5, there are no resonent components when m is an even integer. Again the resonant components are obtained numerically and are summarized in Table 7.2 in which those for $q \leq 1$ are not listed.

Among them, the most important are $b_{5,1}$ and $b_{7,1}$. Their radial distributions are shown in Fig. 7.6, which indicates a rapid decrease of magnitude as they enter toward a plasma axis. We then evaluate the width of islands formed with these components using eq. (7.14). The square root of the inverse shear varies appreciably with radius as shown in Fig. 7.7 for typical current distributions. For instance, in the case of a parabollic current distribution, $\sqrt{\left|\frac{\ell_0}{-r\ell'}\right|} \sim 1$ at r = 0.2 m, while it is ~ 2.5 at r = 0.1 m. On the other hand B_θ is given by the equation

$$B_\theta = \frac{\mu_0 I_p}{2\pi a}\left(2\frac{r}{a} - \left(\frac{r}{a}\right)^3\right) \tag{7.30}$$

where a and I_p are the plasma radius and current, respectively. Putting the values r = 0.2 m, a = 0.23 m, I_p = 90 kA $\sqrt{\left|\frac{\ell_0}{-r\ell'}\right|} \sim 1$, m = 5 and $b_{5,1} = 7.63 \times 10^{-5}$ Wb/m^2, we find

$$\delta \simeq 1.1 \text{ cm}$$

for the corresponding B_t field of 0.84 Wb/m^2. Obviously one obtains the same size of islands at the same position with conditions, B_t = 1.5 Wb/m^2, I_p = 160 kA and I = 8.9kA per each coil.

Other typical values are presented in Table 7.3. In the above analysis we have used the effective gap length which is about five times larger than geometrical gap length. As discussed earlier, the applicability of this assumption is still uncertain for the high temperature plasma. Therefore, we also calculate resonant components in the case of geometrical gap length. Comparison is made between the two cases in Table 7.4 which indicates that $b_{m,n}$ is nearly proportional to the gap length under the condition given by eq. (7.28). Thus one may conclude that the width of islands due to the pulsed vertical coils in ORMAK is less than 1 cm and hence it may not cause deteriorating effects on the plasma confinement, but is not, of course, completely negligible.

(3) Pulsed Vertical Coils of the JFT-2

As in ORMAK, the toroidal symmetry of the pulsed vertical coils of the JFT-2 is destroyed by the presence of shell gaps. The current distribution of the vertical coils is also antisymmetric with respect to $\theta = 0$, while, unlike ORMAK, no currents exist at the gap as shown in Fig. 7.8. Image currents in the shell are substituted by a set of coil currents with inverse polarities at equal distances from the inner surface of the shell. These currents distribution $j(\theta, \varphi)$ is expanded in Fourier series with coefficients given by

$$A_{m',n'} = B_{m',n'} = D_{m',n'} = 0$$

and

$$E_{m',n'} = \frac{4}{\pi^2} \int_0^{\frac{\pi}{2}} \int_0^{2\pi} j(\theta, \varphi) \sin m'\theta \cdot \cos 4\, n'\varphi \, d\theta \, d\varphi \qquad (7.31)$$

From this expression, one finds $E_{m',n'} = 0$ if m' is an even integer. Resonance occurs when q is not an integer. For instance, the Fourier component of the coil currents which corresponds to the resonance of m' = 7, n' = 1 is written as

$$j(\theta, \varphi) = 7.43 \times 10^{-2} \, j_e \cdot \sin \frac{2g}{R} \sin(7\theta - 4\varphi) \qquad (7.32)$$

Then the magnetic field is obtained by solving a Laplace equation under the boundary conditions at r = b,

$$\begin{aligned} B_\theta^{II} - B_\theta^{I} &= \mu_0 K_z \\ B_r^{II} - B_r^{I} &= 0 \\ B_z^{II} - B_z^{I} &= -\mu_0 K_z \end{aligned} \tag{7.33}$$

, where B^I and B^{II} denote the region $0 < r < b$ and $r \geq b$, respectively, and K_z is the surface current density.
As a result we obtain (See Appendix I).

$$B_r^I = -7\mu_0 (kb)^2 K_7'(7kb)\ I_7'(7kr)\ j(\theta, \varphi)\ \cos\alpha \tag{7.34}$$

where

$$k = \frac{2\pi}{\lambda} = \frac{1}{Rq} \quad , \quad \cos\alpha = \frac{Rq}{\sqrt{b^2 + R^2q^2}}$$

, Kn' and In' are the derivatives of the modified Bessel functions.

Assuming an infinite conductivity of the shell and neglecting its curvature, we approximate the image current by substituting $b = b + \delta b$ instead of b in eq. (7.34), where δb indicates the separation distance between pulsed vertical coils and their image currents. Since B_r^I in eq. (7.34) has a b dependence like $b^2 K_7'(7kb)$, and since

$$\begin{aligned} &\{ b_2^2 K_7'(7kb_2) - b^2 K_7'(7kb) \} \\ &\quad = \{ (b+\delta b)^2 K_7'(7k(b+\delta b)) - b^2 K_7'(7kb) \} \\ &\quad \simeq 2b\,\delta b \left\{ K_7'(7kb) + \frac{b}{R} K_7'(7kb) \right\} \end{aligned} \tag{7.35}$$

, we finally have

$$B_r \simeq -14\mu_0 b^2 k^2 \left\{ \frac{\delta b}{b} K_7'(7kb) + \frac{\delta b}{R} K_7''(7kb) \right\} I_7'(7kr)\ j(\theta, \varphi) \cos\alpha \tag{7.36}$$

For the JFT-2 tokamak, putting b = 36 cm, R = 90 cm, $b^2k^2 = \left(\frac{b}{Rq}\right)^2 = 0.052$, $\frac{2g}{R} = \frac{2 \times 10}{90}$, $\frac{\delta b}{b} = \frac{18}{360}$, $K_7'(7kb) + \frac{b}{R} K_7''(7kb) = 7.22 \times 10^3$, $I_7'(7ka) = 5.57 \times 10^{-6}$ and $\cos\alpha \simeq 1$, we find

$$B_r \simeq 2.37 \times 10^{-10} \cdot j_e \tag{7.37}$$

In order to produce the vertical field of 100 Gauss, the current of 25 kA

should be fed to each coil. Therefore, j_e is given by

$$j_e = 3.1 \times 10^5 \quad A/m \tag{7.38}$$

Using these values, the resonant component Br is calculated to be

$$Br \simeq 7.35 \times 10^{-5} \quad Wb/m^2 \tag{7.39}$$

Then the width of islands at, for instance, r = 20 cm is evaluated for the parabollic current distribution as

$$\delta = \frac{4 \times 20}{\sqrt{7}} \sqrt{\frac{7.35 \times 10^{-5}}{0.111}} = 0.78 \text{ cm} \tag{7.40}$$

, where we have used a relation $\sqrt{\left|\frac{\ell_0}{-r_0 \ell'}\right|} \sim 1$. Since this is in the same order of magnitude of the ion Gyration radius, it may not cause a deleterious effect on the plasma confinement.

In the above analytical approach, the shell is assumed to be superconducting. In fact, the soakage current plays the most significant role on both time evolution and toroidal distribution of the vertical field as discussed earlier. Therefore, we will deal with this problem, by using time dependent spacial distributions of the vertical field which are obtained in vacuum by the probe measurements introduced in Chapter 5. Azimuthal and toroidal distributions of this field are already shown in Fig. 6.8. We will use the results which are extended to the whole angle in θ on the basis that toroidal effect appears weak and the vertical field coil is made symmetric with respect to the median plane.

Following magnetic lines of force in this field configuration, the formation of islands is investigated numerically. Again the integer n is chosen to be 4 because this is the basic period of the vertical field coils associated with gaps in the toroidal direction. Two examples corresponding to q = 3/4 and 7/4 are studied assuming symmetric plasma current distributions peaked at r = 0 or parabolic. Also assumed is that the current distribution of the plasma is not affected by the distortion of magnetic surfaces such as islands formation. Magnetic islands at r = 15 cm for q = 3/4 in the case of parabolic current distribution is shown in Fig. 7.9. Here the magnetic lines of force returns to the same islands in every three transits along the major circumference of the torus. Other examples of islands formed at r = 25 cm is shown in Fig. 7.10 in which resonance occures for q = 3/4 and q = 7/4. The current distribution is assumed either parabolic or peaked at r = 0.

On the other hand, by the double Fourier analysis of the radial component of the pulsed vertical field, we obtain radial distributions of $a_{m,n}$ and $c_{m,n}$ which are defined by eq. (7.23). The results for $a_{m,n}$ are shown in Fig. 7.11, while $c_{m,n}$ is always zero in this case. From this figure, one finds at r = 25 cm $b_{3,4} = 1.34$ Gauss and $b_{7,4} = 0.70$ Gauss per 100 kAT of the coil current which amounts to generate about 25 Gauss of the average vertical field at t = 20 msec. Using these values and putting the same conditions in numerical follow of field lines, we obtain with an aid of eq. (7.14), δ = 1.60 cm and 1.12 cm for q = 3/4 and q = 7/4 resonances at r = 25 cm corresponding to Figs. 7.10(a) and Fig. 7.10(b), respectively. These values are found very close to those given by numerical computation.

§7.4 Discussion

Formation of islands in magnetic surfaces in the presence of magnetic error field is studied. Among these, islands produced by multipole error field at the shell gaps are shown only as a hypothetical example, since such an intense error field is unlikely to exist in the JFT-2 tokamak device. However, the other examples which are concerned with ohmic heating field or pulsed vertical field are practical cases as met in the JFT-2 tokamak or Oak Ridge ORMAK. Since q(r) is generally an increasing function of r in tokamak plasmas, there may exist several resonant surfaces across the plasma, for instance, at $q(r_1) = 3/4$, $q(r_2) = 5/4$ and $q(r_3) = 7/4$ from inside to outside.

Theoretical work predicts that the size of islands increases in inverse proportion to the square root of the shear. Therefore, the field error should have a most deteriorating effect on the confinement for a flat current distribution of the plasma. Since eq. (7.14) is valid only for a small size of island we have to depend, in other cases, upon the numerical calculation described in §7.3 in studying magnetic surfaces. Fortunately, however, plasma current distributions in most cases should be reasonably peaked and the intensity of the resonant magnetic fields is considerably small, eq. (7.14) may still hold. On the other hand, it is rather easy to evaluate $b_{m,n}$ in designing a device and therefore it may be very convenient to use eq. (7.14) as a size of islands by the error field.

Appendix

We assume that the current distribution is expressed as

$$j(\theta,\varphi) = j_{m,n}\cos(m\theta - n\varphi) \tag{A-1}$$

The θ and z components of the current is then given by

$$K_z = j_{m,n}\cos\zeta \cdot \cos(m\theta - n\varphi) \tag{A-2}$$

$$K_\theta = j_{m,n}\sin\zeta \cdot \cos(m\theta - n\varphi) \tag{A-3}$$

where ζ is the angle between magnetic line of force and z axis and is determined by

$$\tan\zeta = \frac{b}{Rq}$$

Introducing a scalar potential ϕ which satisfies $\mathbf{B} = \nabla\phi$, together with a relation div $\mathbf{B} = 0$, we find an equation for ϕ.

$$\nabla^2\phi = 0 \qquad (0 < r < b, \quad r > b) \tag{A-4}$$

The general solution to eq. (A-4) is

$$\phi = G_{m,n}\cos(m\theta - n\varphi)\times\left[A_n \cdot I_n(mkr) + B_n K_n(mkr)\right] \tag{A-5}$$

with $B_n = 0$ at $0 < r < b$, and $A_n = 0$ at $r > b$.
Substituting above relation into eq. (7.24) we find

$$\frac{A_n}{B_n} = \frac{K_n'(mkb)}{I_n'(mkb)} \tag{A-6}$$

and

$$B_n K_n(mkb) - A_n I_n(mkb) = \frac{\mu_o j_{m,n}\cos\zeta \cdot b}{m \cdot G_{m,n}} \tag{A-7}$$

Combining eqs. (A-6) and (A-7) we get

$$G_{m,n}\cdot A_n = kb^2 \cdot K_n'(mkb) \cdot \mu_o j_{m,n}\cos\zeta \tag{A-8}$$

and finally we obtain

$$B_r = m\cdot\mu_o (kb)^2 \cdot j_{m,n}\cdot\cos\zeta \cdot K_n'(mkb)\cdot I_n'(mkr)\cdot\sin(m\theta - n\varphi) \tag{A-9}$$

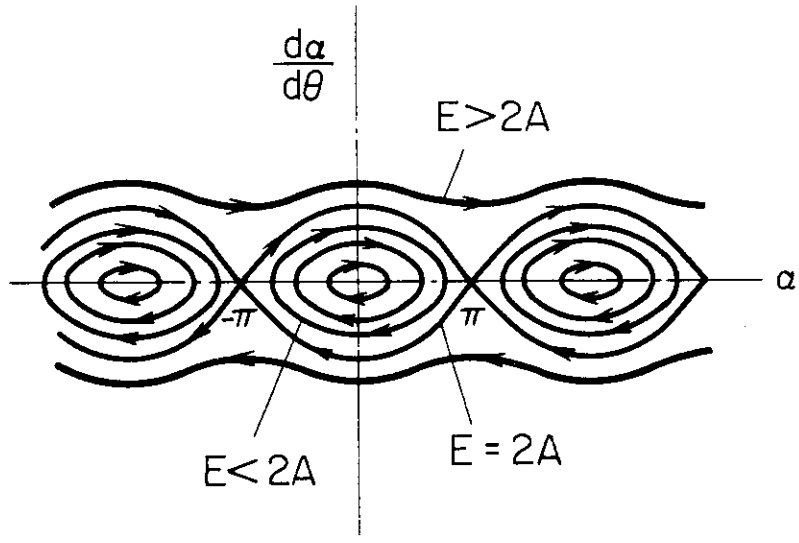

Fig. 7.1 Behavior of the magnetic lines of force in a phase space. Particles with E> 2A correspond to the magnetic lines of force outside the islands while particles with E<2A correspond to those inside the islands.

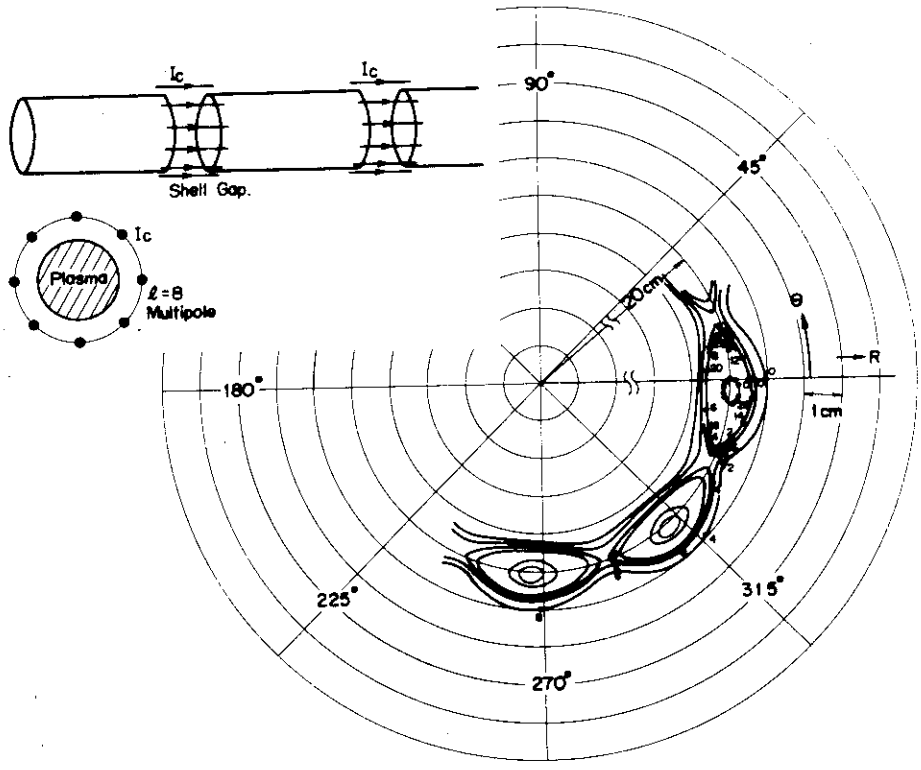

Fig. 7.2 An example of islands formation by the ℓ=8 multipole error field at the shell gaps. The current distribution is assumed to be peaked at r = 0 and also satisfy the relation, q = 2 at r = 20 cm. The integers indicate the number of transits of the magnetic line of force around the torus started from points at θ = 0

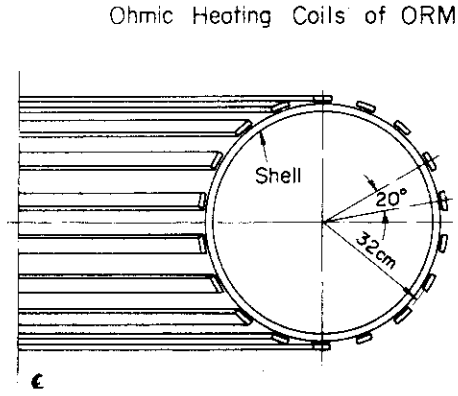

Fig. 7.3
Configuration of the ohmic heating coils of ORMAK.

Table 7.1
Dominant resonant components due to the ohmic heating coils of ORMAK at r = 20 cm. The current is 5 kA in each coil corresponding to the total ampere-turns of 90 kA. The effective gap length is 52.2 cm for ORMAK.

g_{eff} = 52.2 cm		I = 5 kA (I_p = 90 kA) r=20cm	
m	n	$q = \frac{m}{pn}$	$b_{m,n}$
18	1	9	3.7×10^{-6} Wb/m^2
	2	9/2	2.9×10^{-6}
	3	3	1.9×10^{-6}
	4	9/4	0.7×10^{-6}
	5	9/5	0.2×10^{-6}
	.	.	.
	.	.	.
	.	.	.
	.	.	.
	.	.	.

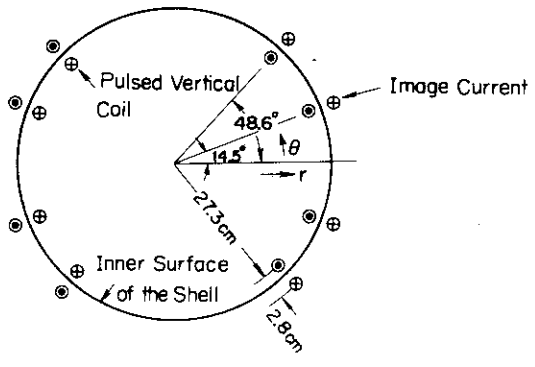

Fig. 7.4
Cross section of the pulsed vertical coils of ORMAK. Image currents are present only inside the shell.

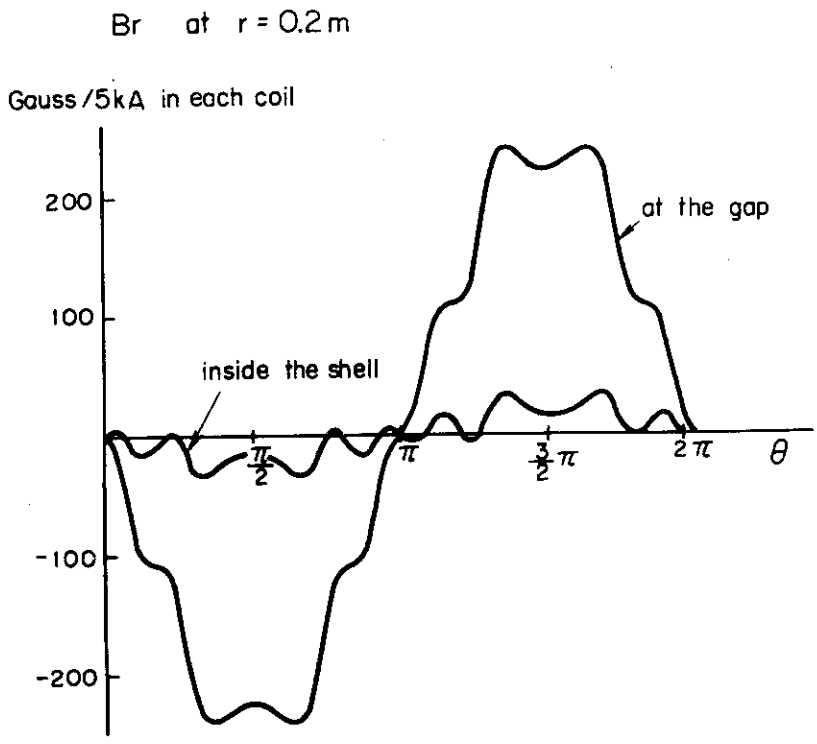

Fig. 7.5 Azimuthal distribution of the radial component generated by the pulsed vertical coils of ORMAK. The amount is significantly reduced inside the shell due to the presence of image currents as compared with that at the gap.

g_{eff} = 52.2 cm			I = 5 kA/each coil		
m	n	$q = \frac{l}{p} \cdot \frac{m}{n}$	$b_{m,n}$ r = 10 cm	r = 15 cm	r = 20 cm
3	1	3/2	0.28 Gauss	0.64	1.13
5	1	5/2	0.05	0.24	0.76
	2	5/4	0.04	0.19	0.60
7	1	7/2	0.03	0.29	1.66
	2	7/4	0.02	0.23	1.30
	3	7/6	0.01	0.14	0.81
9	1	9/2	0.002	0.04	0.43
	2	9/4	0.002	0.03	0.36
	3	9/6	0.001	0.02	0.20
	4	9/8		0.01	0.07
	.	.			
	.	.			
	.	.			

Table 7.2 Dominant resonant components due to the pulsed vertical coils of ORMAK at r = 10, 15 and 20 cm. The coil current of 5 kA can generate the average vertical field which can withstand the plasma current of 90 kA with a low plasma pressure.

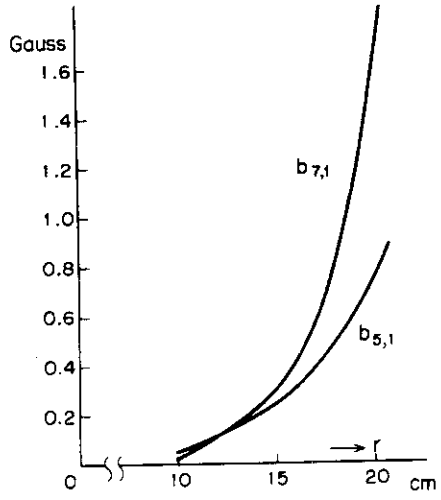

Fig. 7.6
Radial distribution of the typical resonant components, $b_{5,1}$ and $b_{7,1}$ in the pulsed vertical field.

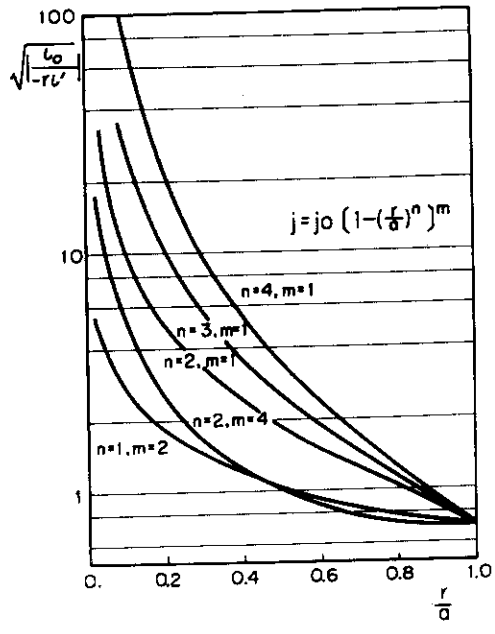

Fig. 7.7
Radial distributions of the square root of the inverse shear. Currents are assumed to be in proportion to $j_0(1 - (\frac{r}{a})^n)^m$.

resonant position	r = 10 cm	r = 20 cm
$q = \frac{5}{2}$	δ = 0.4 cm	1.1 cm
$q = \frac{7}{2}$	0.3 cm	0.7 cm

Table 7.3
Typical width of islands generated by $b_{5,1}$ and $b_{7,1}$ components of the pulsed vertical field of ORMAK.

r = 15 cm			I = 5 kA/each coil	
m	n	$q = \frac{m}{pn}$	$b_{m,n}$ g_{eff}=52.2 cm	g=10.2 cm
3	1	3/2	0.64 Gauss	0.16 Gauss
5	1	5/2	0.24	0.06
	2	5/4	0.19	0.06
7	1	7/2	0.29	0.08
	2	7/4	0.23	0.08
	3	7/6	0.14	0.07
9	1	9/2	0.04	0.01
	2	9/4	0.03	0.01
	3	9/6	0.02	0.01
	4	9/8	0.01	0.01

Table 7.4 Comparison of resonant components between the effective gap and geometrical gap length in the case of pulsed vertical field of ORMAK.

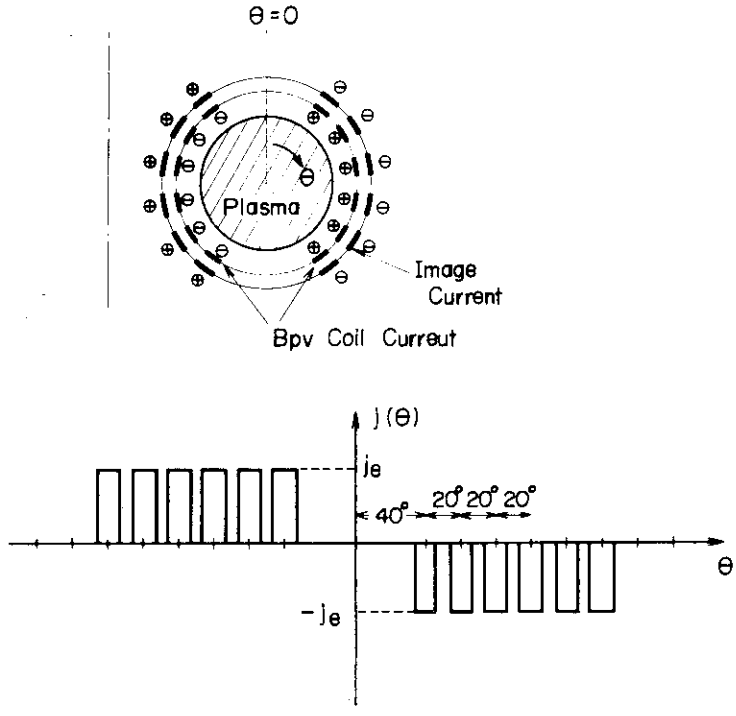

Fig. 7.8 Configuration of the pulsed vertical field coil provided in the JFT-2 tokamak. Azimuthal current distribution is also shown. Induced image currents flow in the opposite direction which do not exist at the shell gap.

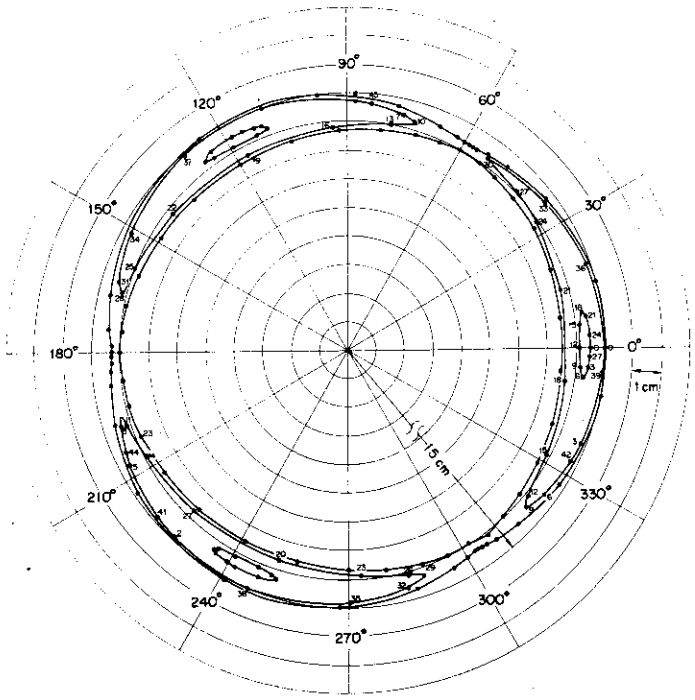

Fig. 7.9 An example of islands formed by a resonance with the pulsed vertical field in the JFT-2 at r = 15 cm for q = 3/4 in case of a parabolic current distribution. The plasma radius is assumed 25 cm with a plasma current I_p = 278 kA, toroidal magnetic field B_t = 10 kG and the average pulsed vertical field intensity $\langle B_{pv} \rangle$ = 108 Gauss.

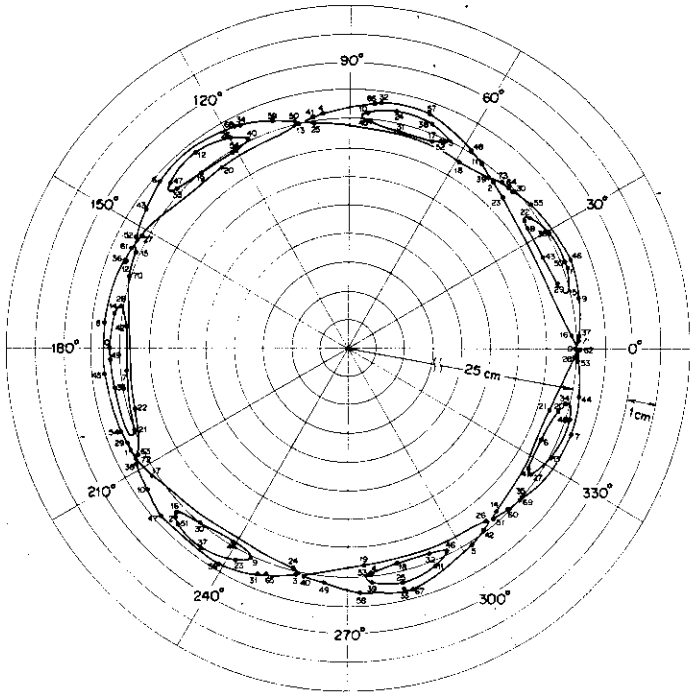

(a)

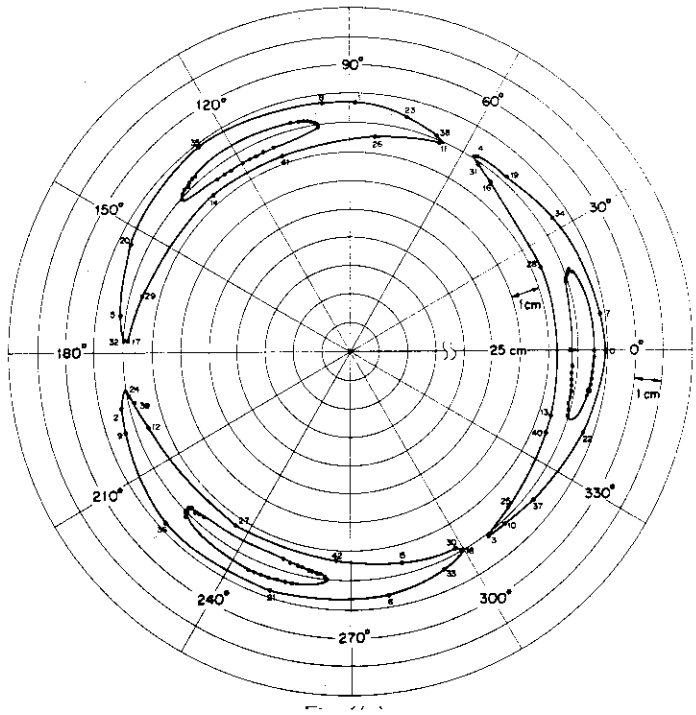

(b)

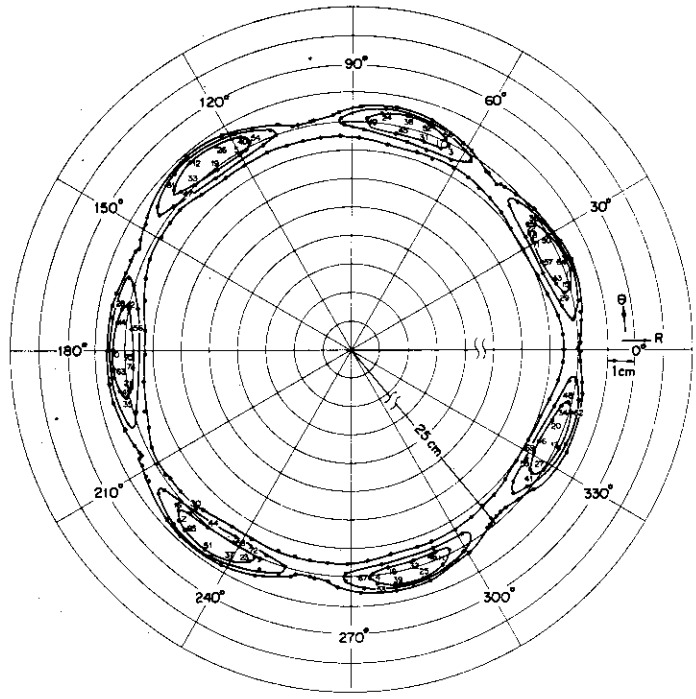

(c)

Fig. 7.10 Islands formed by the resonance with the pulsed vertical field in the JFT-2 tokamak at r = 25 cm. Cases (a) and (b) correspond to the islands in the case of the peaked current distribution centered at r = 0, and the case (c) to the parabolic current distribution under the condition

(a) $q = 7/4$, $I_p = 200$ kA, $B_t = 10$ kG, $\langle B_{pv} \rangle = 108$ Gauss

(b) $q = 3/4$, $I_p = 465$ kA, $B_t = 10$ kG, $\langle B_{pv} \rangle = 108$ Gauss

(c) $q = 7/4$, $I_p = 200$ kA, $B_t = 10$ kG, $\langle B_{pv} \rangle = 108$ Gauss

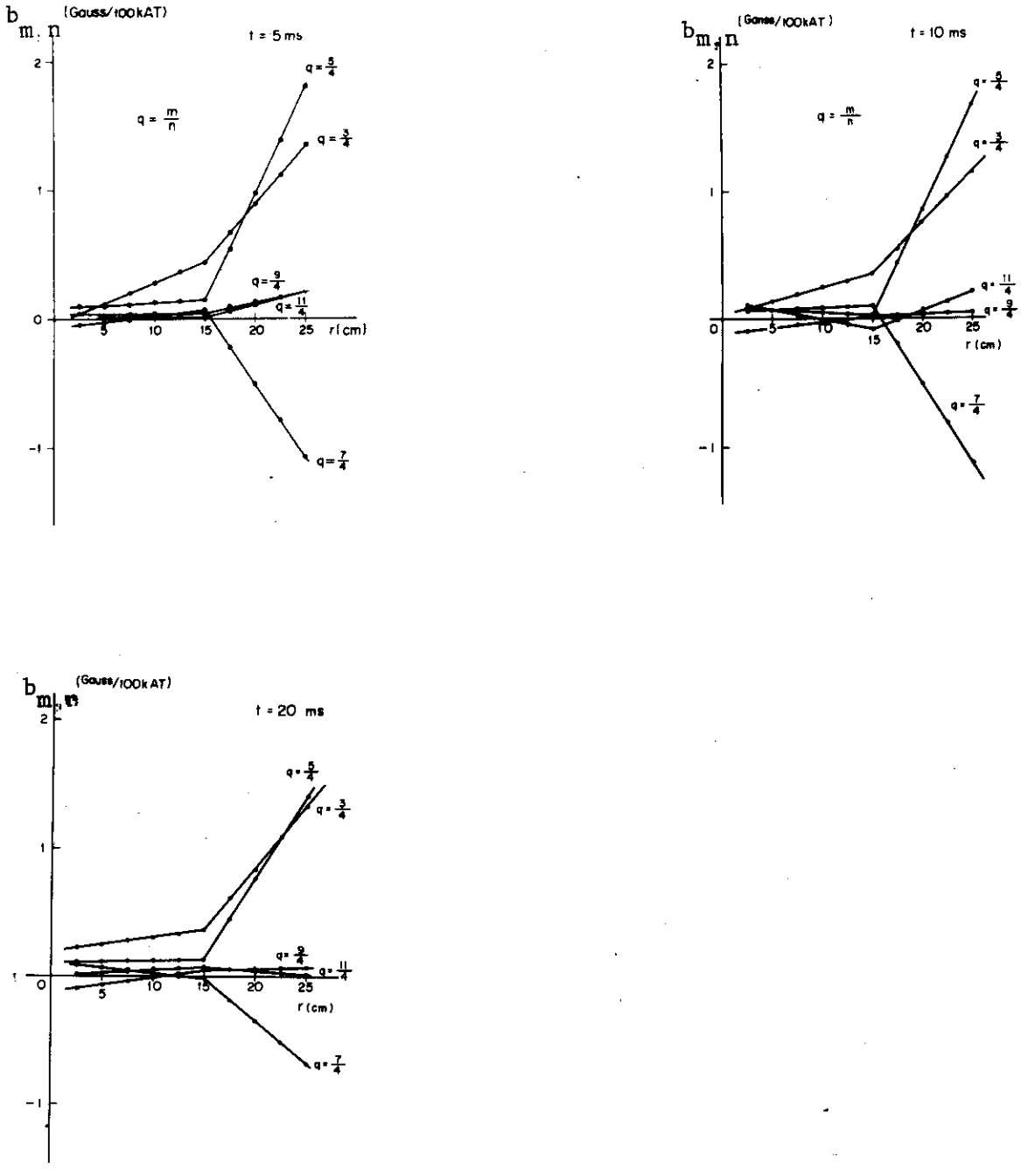

Fig. 7.11 Resonant component $b_{m,n}$ of the pulsed vertical field versus radial position for different values of q when the peak ampere-turns are equal to 100 kAT.

CHAPTER 8
INFLUENCE OF A MINOR PERIODICITY ON THE MAGNETIC ISLAND FORMATION IN TOKAMAKS[26)]

§8.1 Introduction

In designing toroidal magnetic traps, in particular, tokamak devices, it is very important to make systems as symmetric as possible. However, in actual cases, asymmetries arise from many engineering difficulties involved. For instance, discrete magnetic coils, diagnostic ports and evacuation ports easily destroy the symmetry. Such a configuration generally includes magnetic field perturbations in resonance with rotational transforms of the magnetic lines of force in a plasma. These perturbations are known to form islands in magnetic surfaces[8,11)].

Theoretical analyses[11,24)] predict that a width of islands is proportional to the square root of a ratio of resonant field component to azimuthal field and inversely proportional to the square root of the relative shear, namely, δ is given by

$$\delta = \frac{4r_0}{\sqrt{m}} \sqrt{\frac{b_{m,n}}{B_\theta}} \sqrt{\left|\frac{\iota_0}{-r_0\iota'}\right|} \tag{8.1}$$

, where r_0 is the radius of the magnetic surface concerned, m is a mode number in the azimuthal direction, $b_{m,n}$ is the radial harmonic component of the resonant magnetic field perturbations proportional to $\sin(m\theta - n\varphi)$, B_θ is the unperturbed azimuthal field intensity at $r = r_0$, ι_0 is the rotational transform and ι' is its derivative at $r = r_0$, respectively. This expression may well suggest the formation of fairly wide islands with only a small amount of resonant perturbation field. For instance, with $\sqrt{\left|\frac{\iota_0}{-r\iota'}\right|} \sim 1$, $b_{m,n}/B_\theta \sim 10^{-3}$ and $m = 2$, one obtains $\delta / r_0 \sim 0.1$. Since the factor $\sqrt{\left|\frac{\iota_0}{-r\iota'}\right|}$ is determined by the plasma current profile, there are only a few parameters left to be improved in decreasing the width of islands. Therefore it is needed to choose a small resonant component together with a large mode number m in the design of actual devices.

From this point of view, it is necessary to evaluate the resonant components which are included in a mixture of magnetic fields in the devices. Of course, the helical perturbations of the plasma current form islands,[42, 47,48)] but this internal effect should be attributed to the stability of plasma and therefore we do not intend to investigate this problem further in this article. Instead, we are particularly interested in the role of external fields in conjunction with shell gaps. Since the external fields are

shielded by the conducting shell, they can exist only at and near the shell gap. Under these conditions, we find that the minor periodicity along the torus which is essentially determined by the number of periodic shell gaps has an important meaning in the formation of islands. Some of the islands formation can be suppressed by a proper choise of this periodicity. Thus, the object of the present paper is to investigate a general rule of avoiding resonance and to confirm it on some examples with an aid of numerical calculations.

§8.2 General Feature

Any perturbation field which resonates with the rotational transform of magnetic lines of force makes islands in magnetic surfaces.[8,11,24] First of all, we describe a basic aspect of resonance due to the presence of helical magnetic perturbations whose pitch coincides with the rotational transform of unperturbed magnetic fields. Only the radial component of the perturbation field is responsible for islands formation. Fig. 8.1 illustrates the cross section of the magnetic surface where the coordinate system (r, θ) is fixed on the helical pitch of this perturbation field. In this coordinate system, the unperturbed magnetic lines of force on the resonant surface always stay at the same position in θ, while those on the non-resonant surface move around the axis. Then what happened in the trajectories of the magnetic lines of force in the presence of perturbation field is that those starting from any original position on the resonant surface experience the inward or outward drift due to the radial component of the magnetic field as they transit along the torus. Since the drift is of a cumulative nature, they make large excurtions from the original circular surface. In the case of shear free system (uniform plasma current distribution) this property is the most significant, since there are no suppressing mechanisms present. In this case, the magnetic surface coincides with that of perturbation field. However, in the general case where considerable amount of shear is present, a radial variation of the rotational transform makes unperturbed magnetic lines of force to drift in the opposite direction in θ in our coordinate system with respect to the resonant surface concerned. Thus the magnetic lines of force which have excursed from the resonant surface are then exposed to the azimuthal drift due to the shear and finally reaches the region where the sign of radial drift is opposite. This property confines the magnetic lines of force to some restricted region and consequently leads to the formation of islands.

Although there are generally no helical coils installed in tokamaks, the

toroidal asymmetry associated with the azimuthal non uniformity of the perturbation field can generate the helical components as illustrated in a past work.[23] Taking into account the fact that a conducting shell contributes to the shielding of external fields, we can idealize the model as follows; We assume that linear harmonic fields (for example, a line cusp or a multipole field) are present only at the shell gaps. In this configuration, the number of minor periodicity represented, in this case, by that of shell gaps along the torus has an important physical meaning. For instance, if only one gap is assumed to be present in combination with an $\ell = 2$ cusp field as illustrated in Fig. 8.2, the magnetic resonance occures at the $q = 2$ surface, because in every transit the magnetic line of force sees a radial drift in the same direction at the gap due to the applied perturbation field. Such an accumulation of the radial drift is the motive force of island formation; this is the basic aspect of magnetic resonance.

However, if the number of minor periodicity is two (two gaps), one cannot expect island formation because the direction of the drift at the other gap is just the opposite. Hence the radial drift can be canceled in a transit along the torus.

Thus, the condition for resonance is found to be

$$p \cdot q = \frac{\ell}{z} \tag{8.2}$$

, where p is the number of minor periodicity once around the torus, q is the safety factor which is an inverse of the rotational transform, ℓ is the number of poles of the perturbed harmonic magnetic field and z is an integer. The above simple relation enables us to find resonant cases. The results are summalized in Table 8.1 for the typical number of poles and minor periodicities. In this Table, the resonant cases for which q is less than unity are not included, because the presence of MHD instabilities overwhelms the stable plasma confinement in such a low q regime.[49] From this table one may find that the occurrence of resonance is slower for large number periodicities. In the case of four gaps ($p = 4$) for instance, there are no resonances for $\ell \leq 3$ and for $\ell > 3$ the occurrence of resonances is limited to the least number. In the case of one gap ($p = 1$), one has to worry about almost every resonant mode. Since a mode number m which determines the number of islands formed in the azimuthal direction on the resonant surface is expressed in terms of p,q and z by the relation,

$$m = p \cdot q \cdot z = \ell \tag{8.3}$$

, the width of islands becomes small with increasing p and q as suggested by eq.(8.1). Therefore, if the resonant field component $b_{m,n}$ is of the same order, resonances of the higher mode number in Table 8.1 are relatively unimportant. Furthermore, not all of the resonances in the table can occur in actual cases. It depends on the existence of the perturbation field and also on the plasma current distribution. For instance, if we assume a current distribution

$$j(r) = j_0\left(1 - \frac{r^n}{a^n}\right)^m \tag{8.4}$$

, where j_0 is the current density at the center, n and m are the integers and a is the radius of the plasma,
then we obtain

$$1 \leq \frac{q(r)}{q(o)} \leq \frac{n+2}{n} \qquad \text{for } m = 1$$

and also

$$1 \leq \frac{q(r)}{q(o)} \leq \frac{(n+1)(n+2)}{n^2} \qquad \text{for } m = 2 \ .$$

The upper limits of these ratios are generally in the range of 1 - 2 when n varies from 2 to 4 as shown in Fig. 8.3. Thus the number of resonant cases is limited by the current distributions. For a more peaked current distribution as is observed in the ST tokamak,[50] the distribution may be approximated by

$$j(r) = j_0\left(1 - \left(\frac{r}{a}\right)^2\right)^4 \tag{8.5}$$

In this case the ratio $q(r)/q(0)$ varies from 1 to 5. Thus one may envisage that the multi-island would easily be formed at the respective radial resonant positions.

§8.3 Numerical Study of the Minor Periodicity

In this section we again consider the influence of minor periodicity on the island formation. Predictions discussed in §8.2 will be confirmed by means of numerical calculations. Magnetic surfaces are obtained by projecting the magnetic lines of force traced by the R.K.G. method onto a fixed cross section. In the first place, we investigate the model where $\ell = 4$

cusp field are present over the effective gap distance (See Fig. 8.4). We assume a radial position of these coils of 30 cm from the axis, coil current of ± 10 kA, plasma radius of 25 cm, gap length of 20 cm and plasma current of 173.6 kA with its distribution expressed by $j_0(1-(\frac{r}{a})^2)^4$, which will make the outermost resonant surface ($q = 4$) at the plasma edge. Although these values are given artificially, it does not alter the qualitative characteristics of the island formation. Since the ratio $q(r)/q(0)$ varies from 1 to 5 as seen in Fig. 8.3, one can expect islands formation at $q = 4$, 2, 4/3, and 1 in the case of one minor periodicity ($p = 1$). The results are shown in Fig. 8.4 where formations of $m = 4$ islands are seen at the respective position. In cases of $q = 4/3$ and 1 resonances, the width of islands is too small to observe, but slight deformations of the magnetic surfaces can be identified. This can be explained by the following two reasons. Firstly, the amount of resonant components decreases very rapidly with decreasing radius as easily imagined from eq. (7.27) or from Fig. 7.6 in Ch.7, although the inverse of the shear increases. Secondly, validity of eq. (7.28) is uncertain, since phase mixing of the radial component at the gap as seen from traversing magnetic lines of force becomes prominent in lower q regime.

In the case of two gaps, however, the dominant islands at $q = 4$ disappear. A slight deformation of the resonant surface at $q = 4/3$ also disappears as pointed out by our predictions. The remaining $q = 2$ resonance can be clearly suppressed by doubling the number of minor periodicity from 2 to 4 as shown in Fig. 8.4.

The above examples may be considered to be a special case, since such a cusp field will hardly be applied in tokamaks. In more realistic cases, the perturbation field may be a multipole field where only unidirectional coil currents are present. Then we put a $l = 4$ multipole field at the gap with other dimensions left unchanged. The coil current is assumed to be 20 kA in this case. Numerical results are shown in Fig. 8.5 for the typical values of p. In contrast with the former cases, $m = 8$ islands appear at the $q = 4$ surface when p is varied from 1 to 2. The width of these islands is small as compared with that of $m = 4$ ($p = 1$) islands, although total length of the shell gap is doubled. In the case of $p = 4$, islands of $m=16$ and $m = 8$ appear at $q = 4$ and 2 surfaces, respectively. The width of islands is also decreased, in particular, the $m = 16$ islands become, in effect, negligible. The appearance of these modes is attributed to the nonvanishing higher resonent components contained in the multipole field. This situation would be understood by Fourier analysis described in the Appendix-II.

We have also calculated islands formations in the case of parabollic current distribution, where only q = 4 resonance can take place. Their characteristics are similar to those given above.

Above discussions will lead us to speculate islands formation asscciated with toroidal field ripple. Suppose we put a line current on z axis of a linear periodic toroidal field. This configuration does not make islands, since Br is azimuthally symmetric and does not include the harmonic component proportional to $\sin(m\theta - n\varphi)$. However, in the torcidal configuration, the situation differs a little bit. It was pointed out by numerical simulation[51] that islands are formed if the line current flows crossing the field lines, while they are not formed if the current flows completely along the field lines. The lowest resonance mode is given by n = p, m = qn, where p is the number of toroidal coils. In the JFT-2 tokamak, p = 16 so that the lowest mode is proportional to $\sin(16\theta - 16\varphi)$ for q = 1 and $\sin(32\theta - 16\varphi)$ for q = 2. Such high n mode harmonic components would hardly exist in general cases but one should note that the pole number of the control field should be different from the number of toroidal coils (In ORMAK, the number of ohmic heating coils is 18, while the number of toroidal coils is 56).

§8.4 Concluding Remarks

Islands formation is significantly suppressed by the increase of the number of minor periodicity. In the present work, the minor periodicity is represented by the number of gaps. However, it is not directly related to the latter, since in some cases, the perturbation field differs from one gap to another. For instance, a presence of yoke of the transformer core or of the current feeder of coils near one of the shell gaps may easily decrease this number. Thus as a guiding rule for the design of tokamaks, one may describe as follows; For a given number of gaps attention should be paid to make devices as periodic as possible.

In the course of our analysis, we have neglected the effects of deformation of the plasma current distribution due to the formation of islands in magnetic surfaces. One may envisage that the plasma pressure distribution tends to be uniform over the islands and as a result, plasma current will follow the flux line of the islands. Such a localized current filament may generate helical magnetic field components which in turn influence the width of islands. In the case of normal sheared system, $d\iota/dr < 0$, this effect works such that the magnetic field perturbations due to

the helical current tend to reduce the external resonant field irrespective of directions of toroidal magnetic field, of plasma current and of coil current. However, in the case of $d\ell/dr > 0$, the helical current will enhance the resonant component and consequently may significantly increase the island width. We are now continuing the effort on this subject together with a study of island formation due to neutral beam injection.

Appendix-II

Under the condition $q \gg \ell \cdot \frac{g_{eff}}{R}$ being valid, Fourier coefficients defined by eq. (7.23) are approximated by the integral with respect to θ, that is,

$$c_{m,n} = K B_{rc} \simeq \frac{1}{\pi} \int_0^{2\pi} B_r \cdot \cos m\theta \cdot d\theta$$

$$a_{m,n} = K B_{rs} \simeq \frac{1}{\pi} \int_0^{2\pi} B_r \cdot \sin m\theta \cdot d\theta$$

It is our purpose to examine whether the resonant component

$$b_{m,n} = K \sqrt{B_{rs}^2 + B_{rc}^2}$$

vanishes or not for the typical values of m and n.

In the case of multipole field, B_r is given by eq. (7.27), namely,

$$B_r = C \cdot \frac{\sin \ell\theta}{A - \cos \ell\theta}$$

, where $A \equiv \frac{1}{2}\left(\frac{r_c}{r}\right)^{\ell} + \frac{1}{2}\left(\frac{r}{r_c}\right)^{\ell}$ and $C \equiv \frac{\mu_0 I}{4r} \cdot \frac{\ell}{\pi}$

On the other hand B_r in the cusp field is expressed as

$$B_r = C \cdot \left[\frac{\sin \ell\theta}{A - \cos \ell\theta} + \frac{\sin \ell\theta}{A + \cos \ell\theta}\right]$$

$$\equiv B_r' + B_r''$$

, where $B_r' = C \cdot \frac{\sin \ell\theta}{A - \cos \ell\theta}$, $B_r'' = C \cdot \frac{\sin \ell\theta}{A + \cos \ell\theta}$

Using these equations we calculate resonant components which are summarized in the following Table A.

Thus the $\ell = 4$ multipole field contains higher mode components while $\ell = 4$ cusp field has only the fundamental mode.

Table A

	ℓ = 4 multipole	ℓ = 4 cusp
m = 4	$I_c = \frac{1}{\pi}\int_0^{2\pi} Br \cos m\theta \cdot d\theta = 0$ $I_s = \frac{1}{\pi}\int_0^{2\pi} Br \sin m\theta \cdot d\theta \neq 0$ $\sqrt{B_{rc}^2 + B_{rc}^2} = I_s \neq 0$	$\frac{1}{\pi}\int_0^{2\pi} Br' \cos m\theta \cdot d\theta = I_c = 0$ $\frac{1}{\pi}\int_0^{2\pi} Br'' \cos m\theta \cdot d\theta = -I_c = 0$ $\frac{1}{\pi}\int_0^{2\pi} Br' \sin m\theta \cdot d\theta = I_s$ $\frac{1}{\pi}\int_0^{2\pi} Br'' \sin m\theta \cdot d\theta = I_s$ $\sqrt{B_{rc}^2 + B_{rc}^2} = 2 I_s$
m = 8	$I_c = \frac{1}{\pi}\int_0^{2\pi} Br \cos m\theta \cdot d\theta = 0$ $I_s = \frac{1}{\pi}\int_0^{2\pi} Br \sin m\theta \cdot d\theta \neq 0$ $\sqrt{B_{rc}^2 + B_{rs}^2} = I_s \neq 0$	$\frac{1}{\pi}\int_0^{2\pi} Br' \cos m\theta \cdot d\theta = I_c = 0$ $\frac{1}{\pi}\int_0^{2\pi} Br'' \cos m\theta \cdot d\theta = I_c = 0$ $\frac{1}{\pi}\int_0^{2\pi} Br' \sin m\theta \cdot d\theta = I_s$ $\frac{1}{\pi}\int_0^{2\pi} Br'' \sin m\theta \cdot d\theta = -I_s$ $\sqrt{B_{rc}^2 + B_{rs}^2} = 0$
m = 16	$I_c = \frac{1}{\pi}\int_0^{2\pi} Br \cdot \cos m\theta \cdot d\theta = 0$ $I_s = \frac{1}{\pi}\int_0^{2\pi} Br \cdot \sin m\theta \cdot d\theta \neq 0$ $\sqrt{B_{rc}^2 + B_{rs}^2} = I_s \neq 0$	$\frac{1}{\pi}\int_0^{2\pi} Br' \cos m\theta \cdot d\theta = I_c = 0$ $\frac{1}{\pi}\int_0^{2\pi} Br'' \cos m\theta \cdot d\theta = I_c = 0$ $\frac{1}{\pi}\int_0^{2\pi} Br' \sin m\theta \cdot d\theta = I_s$ $\frac{1}{\pi}\int_0^{2\pi} Br'' \sin m\theta \cdot d\theta = -I_s$ $\sqrt{B_{rc}^2 + B_{rs}^2} = 0$

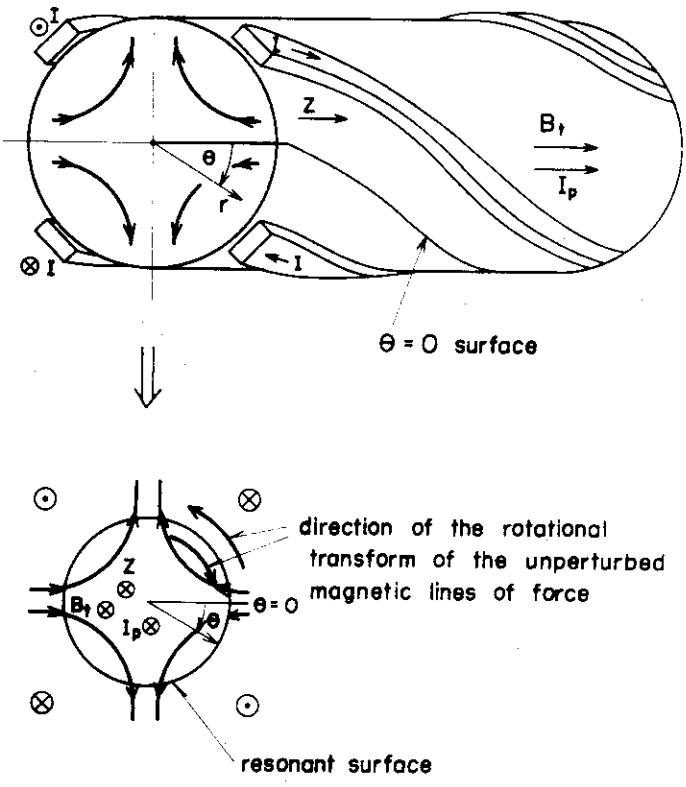

Fig. 8.1 Cross sectional view of the magnetic surface where cylindrical coordinate system (r, θ, z) is adopted with the axis on the moving frame of the external perturbation field.

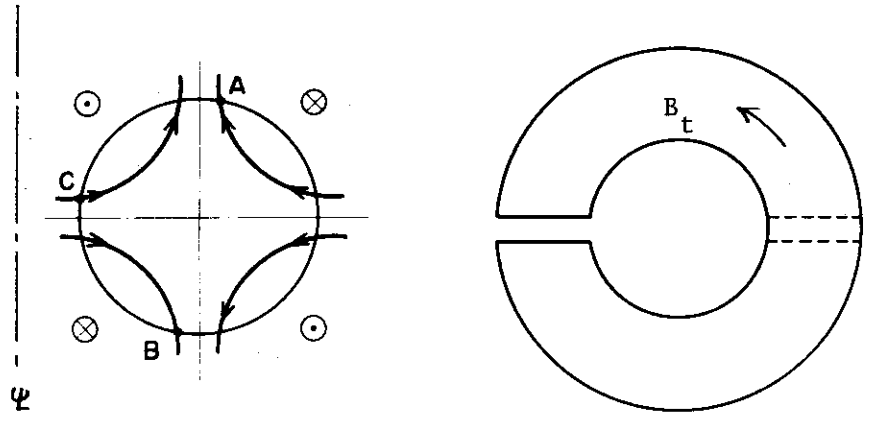

Fig. 8.2 Upper view of the conducting shell with one (or two) gap(s) (right) and cross section of the cusp type perturbed field at the gap (left). In the case of a single shell gap with q = 2, a magnetic field line starting from a point A returns to the opposite position (denoted by B) in every transit, and sees the same drift. While in the case of two gaps, the magnetic field line comes to the position where the direction of the drift is opposite (marked by C) in every half transit and experiences a cancellation in a complete transit.

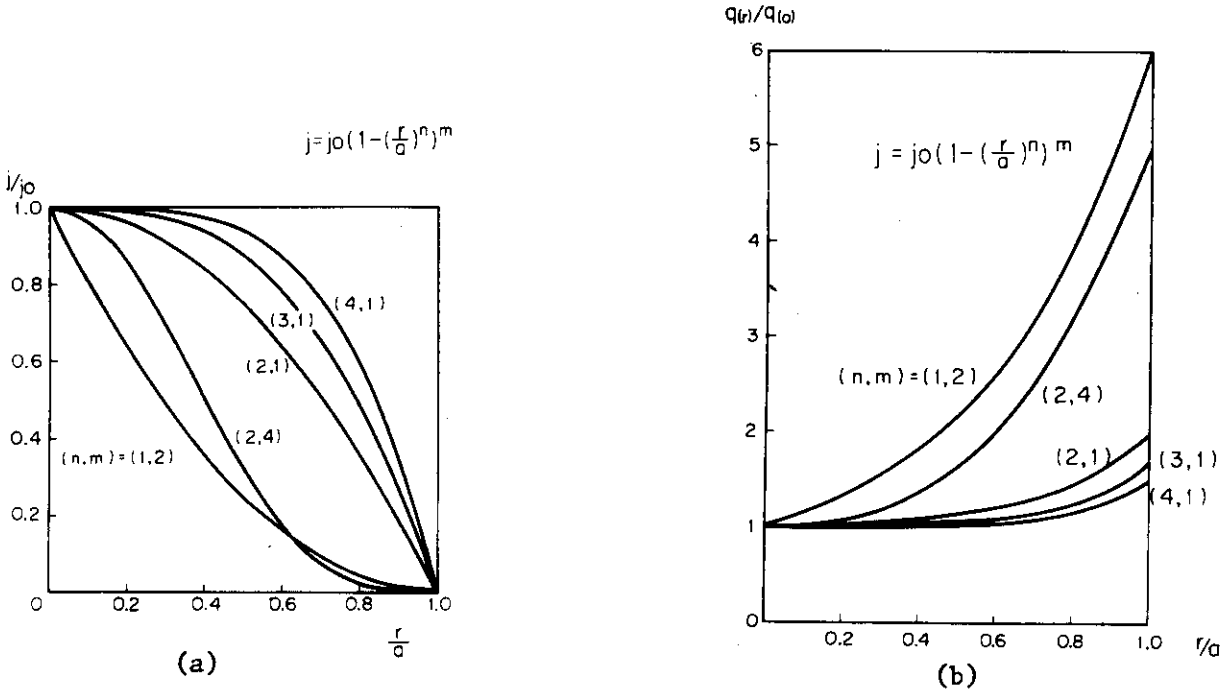

Fig. 8.3 Radial distributions of current (a),and safety factor (b). Currents are assumed to be in proportion to $j_0(1 - (\frac{r}{a})^n)^m$.

	ℓ = 1	ℓ = 2	ℓ = 3	ℓ = 4	ℓ = 5	ℓ = 6	ℓ = 7	ℓ = 8
p = 1	q = 1	q = 2 1	q=3, 3/2, 1	q=4, 2 4/3, 1	q=5, 5/2 5/3, 5/4	q=6, 3, 2 3/2, 6/5 1	q=7, 7/2, 7/3, 7/4, 7/5, 7/6, 1	q=8, 4, 8/3 2, 8/5, 4/3 8/7, 1
p = 2		q = 1	q = 3/2	q = 2, 1	q=5/2, 5/4	q=3, 3/2, 1	q=7/2, 7/4	q=4, 2, 4/3, 1
p = 3			q = 1	q = 4/3	q=5/3	q=2, 1	q=7/3, 7/6	q=8/3, 4/3
p = 4				q = 1	q = 5/4	q = 3/2	q = 7/4	q = 2, 1
p = 8								q = 1

Table 8.1 Resonant magnetic island formation due to harmonic perturbation fields in relation to the number of minor periodicities. Numbers of resonant cases are significantly reduced with an increase of minor periodicities.

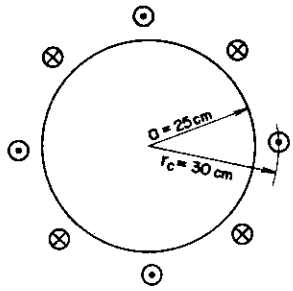

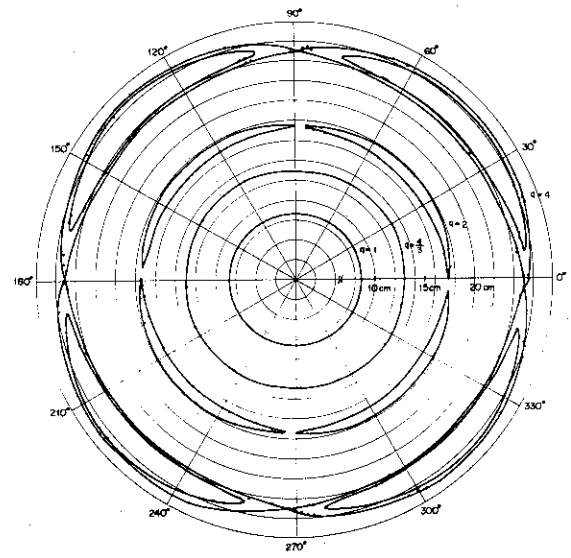

(a)

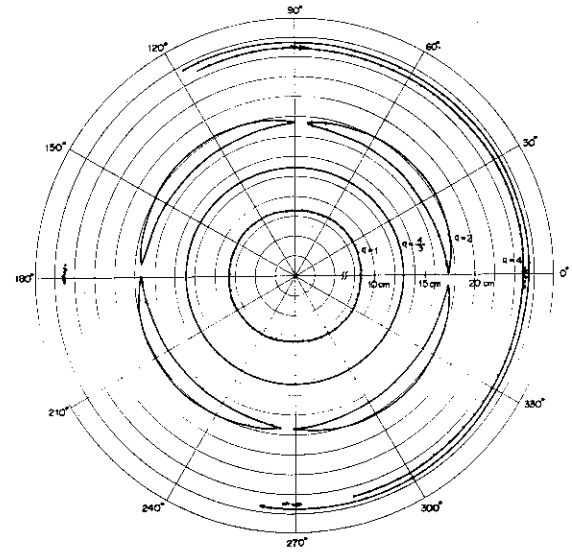

(b)

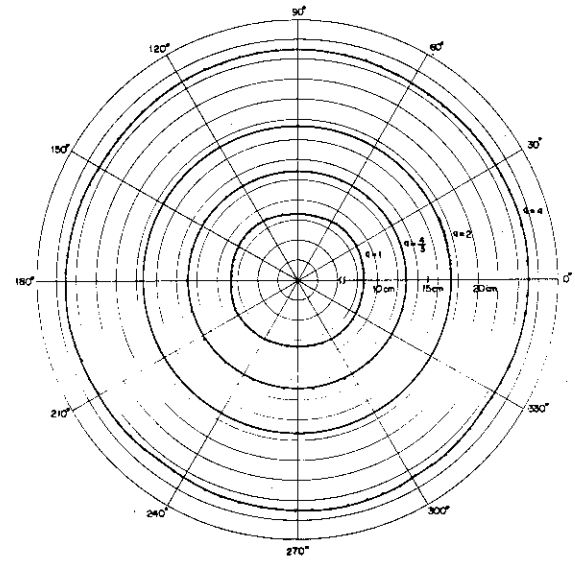

(c)

Fig. 8.4
Configuration of the $\ell = 4$ cusp field at the shell gap and resulting magnetic surfaces corresponding to the number of minor periodicities of one (a), two (b) and four (c). Assumed are the position of coils at r = 30 cm, coil current of $\pm$ 10 kA, plasma radius of 25 cm, gap length of 20 cm and plasma current of 173.6 kA whose distribution is expresses by $j_0(1-(\frac{r}{a})^2)^4$

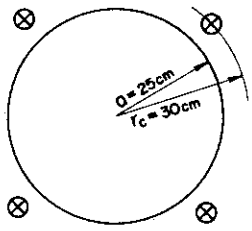

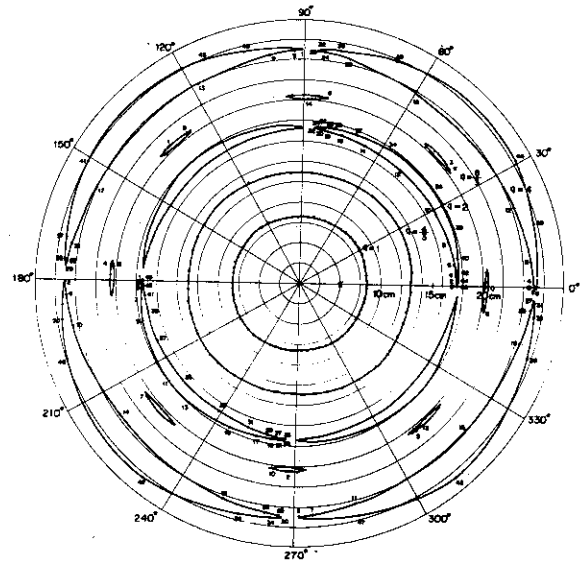

(a)

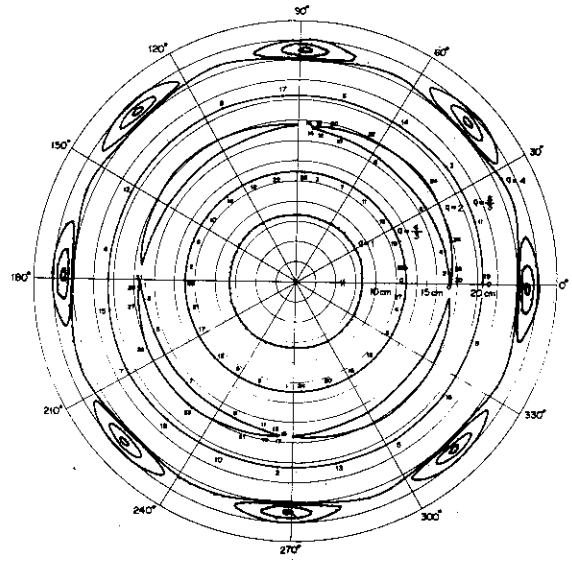

(b)

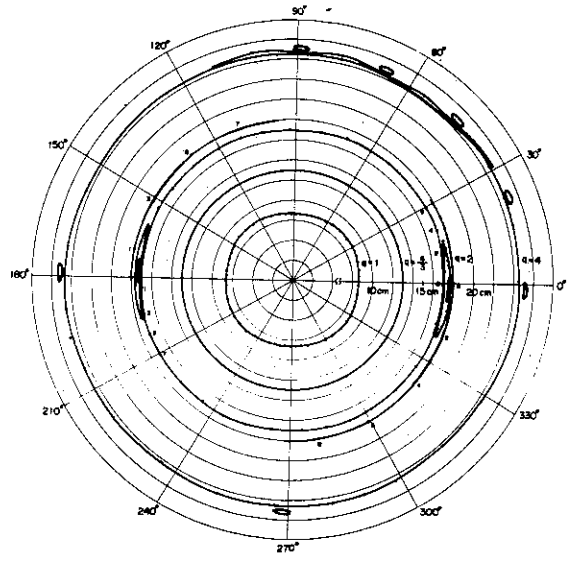

(c)

Fig. 8.5
Configuration of the $\ell = 4$ multipole field at the shell gap and resulting magnetic surfaces corresponding to the number of minor periodicities of one (a), two (b), and four (c). The difference is only the current of 20 kA per each coil with other parameters left unchanged.

CHAPTER 9
SUMMARY AND CONCLUSION

In the present thesis, the influence of the error field on plasma confinement in tokamaks is studied with a special emphasis on the designing view point.

In Chapter 2, the influence of the error field is crudely estimated in the initial breakdown phase. Firstly, any conceivable source which generates the vertical error field does not seriously affect the plasma confinement if the vertical control field is properly applied. The allowable radial component is estimated to be a few percent of the toroidal field intensity. This is easily satisfied in the usual coil assembling with knock pins. Secondly, the $\mathbf{E} \times \mathbf{B}$ drift due to charge separation causes a rapid plasma loss which overwhelms those by the error field, and requires a rapid formation of magnetic surfaces.

In Chapter 3, a global effect of the error field on the plasma column deformation is studied when closed magnetic surfaces are formed. Deformation of the circular magnetic surface in the presence of axisymmetric error field is found to be small unless the error field intensity becomes close to the azimuthal field intensity. Possible source of the generation of radial error field would be either the twist of the toroidal coil bases or the tilt of each coil to its extreme within machining errors of the knock pin and hole. A local bending of the plasma column due to shell gaps may be negligibly small but the outward expansion of the plasma hoop cannot be neglected. It is found to be proportional to the square root of the gap length and is easily compensated by the additional vertical field.

In Chapter 4, the leakage magnetic field from the iron core is studied in the presence of both primary winding and secondary one simulating plasma current. Using a special pick up coil, the leakage field is measured to be about 230 Gauss per 100 kA of the plasma current in the median plane, which is very close to what is necessary for the plasma equilibrium. In spite of the presence of core yokes, the toroidal uniformity is extremely good provided the primary winding is placed at the center pole. However, the toroidal distribution becomes poor when the primary windings are positioned at the yokes.

In Chapter 5, theoretical predictions by V.S. Mukhovatov and V.D. Shafranov[17] on the effect of shell gaps are confirmed experimentally. The gap effect on the internally or externally applied vertical field extends

as far as the central part of the shell. It is also clarified that the leakage magnetic field from the iron core plays a favorable role in compensating gap effect.

In Chapter 6, the time evolution of the pulsed vertical field is investigated by the probe measurements on the JFT-2. Due to the finite conductivity of the shell associated with shell gaps, a strong effect due to the soakage current is observed. The vertical field inside the shell persists long after the decay of the coil current.

In Chapter 7, the magnetic island formation due to error field is studied both analytically and numerically. The theory by M.N. Rosenbluth[11] is reconfirmed by a different simple analysis which gives the physical picture more clearly. Numerical calculations of magnetic surfaces are consistent with this analytical result. Several conceivable sources such as pulsed vertical field and ohmic heating field which may give large resonant components are investigated in this connection. Among them the pulsed vertical field has a possibility of forming magnetic islands with a width of the order of 1 cm.

In Chapter 8, the magnetic island formation is again discussed in relation to the minor periodicity along the torus. It is found that the islands formation is significantly suppressed by the increase of minor periodicities. This leads us to a rather surprising conclusion that the device should be made to have as many periodicities as possible. This is a significant implication in the design of future tokamaks.

We notice here that the following problems are left to be solved.

(i) Effect of the error field on the time evolving plasma including plasma-neutral interactions.

This problem is very important, since the production of an initial plasma strongly affects the stability of the later discharge.[36]

(ii) Diffusion loss of particles due to the magnetic field ripple.[52]

(iii) Self-consistent analysis of the magnetic island formation which includes interactions between the external field and the plasma deformation.

(iv) Excitation of internal helical perturbations by the external error field.

Most recently, the physics of the helical modes in the plasma has come to our interests in relation to external perturbation field.[43] Among them the disruptive instabilities may be the greatest concern. These problems will be attacked both experimentally and theoretically in near future.

ACKNOWLEDGMENTS

The author wishes to express his appreciation to Prof. K. Uo for his advice and constructive criticism during the preparation of this manuscript as well as to Prof. A. Iiyoshi and Assis. Prof. T. Obiki of Kyoto Univ.

He is also greateful to Dr. S. Mori of JAERI for his encouragement during the course of this research for years.

Detailed discussions with Drs. M. Yoshikawa of JAERI and S. Itoh of Nagoya Univ. and their suggestions in many stages of the work are gratefully acknowledged.

It is a pleasure to thank Messrs. N. Suzuki, T. Ohga and Dr. N. Fujisawa for their co-operation in the work.

The author also wishes to thank Dr. H. Shirakata for his encouragement and members of JAERI fusion research laboratory for their helps in taking data and for valuable discussions.

Many helpful discussions are also due to Drs. J.D. Callen, M. Murakami and J.A. Rome as well as encouragements by Dr. H. Postma of Oak Ridge National Laboratory.

Use has been made of the electronic computers FACOM 230-60 at JAERI and IBM 360-91 at Oak Ridge National Laboratory.

REFERENCES

1) L.A. Artsimovich et al : Plasma Physics and Controlled Nuclear Fusion Research 2 IAEA (1966) 595.
2) N.J. Peacock et al : Nature 224 (1969) 488.
3) L.A. Artsimovich et al : Plasma Physics and Controlled Nuclear Fusion Research 1 IAEA (1969) 17.
4) D. Dimock et al : Nuclear Fusion 13 (1973) 271.
5) W. Stodiek, D. Grove and J.O. Kessler : Plasma Physics and Controlled Nuclear Fusion Research 2 IAEA (1966) 687.
6) S. Itoh, T. Takeda, M. Ohta, N. Fujisawa, K. Inoue, M. Tanaka, M. Maeno, T. Tazima, S. Kunieda and S. Mori : Report of Japan Atomic Energy Research Institute, JAERI-memo 4048 (1970).
7) L.A. Artsimovich, et al. : Plasma Physics and Controlled Nuclear Fusion Research (Proc. 2nd. Int. Conf. Culham, 1965) 2 IAEA (1966) 595.
8) D.W. Kerst : Plasma Physics (Journal of Nuclear Energy, Part C), 4 (1962) 253.
9) A. Gibson : Physics of Fluids 10 (1967) 1553.
10) A. Gibson and J.B. Taylor : Physics of Fluids 10 (1967) 2653.
11) M.N. Rosenbluth, R.Z. Sagdeev, J.B. Taylor and G.M. Zaslavski : Nuclear Fusion 6 (1966) 297.
12) B.B. Kadomtsev : Soviet Physics JETP 25 (1967) 691.
13) S. Itoh, et al : Proc. of the 5th European Conf. on Controlled Fusion and Plasma Physics. (Grenoble, France, 1972) 3.
14) S. Itoh, et al : Proc. of the 3rd Inter. Symp. on Toroidal Plasma Confinement (München, 1973).
15) N. Fujisawa, et al : 5th Conf. on Plasma Physics and Controlled Nuclear Fusion Research, (Tokyo, 1974), CN33/A1-1.
16) S. Matsuda and M. Yoshikawa : Report of Japan Atomic Energy Research Institute, JAERI-M 4842. **in Japanese.**
17) V.S. Mukhovatov and V.D. Shafranov: Nuclear Fusion 11 (1971) 605.
18) S. Matsuda : Japan. J. appl. Phys. 12 (1973) 903.
19) N. Fujisawa, N. Suzuki, S. Matsuda, T. Ohga and S. Itoh : Report of the Japan Atomic Energy Research Institute, JAERI-M 4688.
20) S. Matsuda, N. Suzuki, T. Ohga and S. Itoh : Japan. J. appl. Phys. 13 (1974) 1604.
21) T. Ohga and S. Matsuda : Report of the Japan Atomic Energy Research Institute, JAERI-M 4748 (1972). **in Japanese.**

22) S. Matsuda, T. Ohga, N. Suzuki and N. Fujisawa : Report of the Japan Atomic Energy Research Institute, JAERI-M 5021. in Japanese.
23) S. Matsuda : Report of the Japan Atomic Energy Research Institute, JAERI-M 5298.
24) S. Matsuda and M. Yoshikawa : Japan. J. appl. Phys. 14 (1975) 87.
25) R.P. Feris, F.M. Hamzeh and A.J. Lichtenberg : Nuclear Fusion 13 (1973) 533.
26) S. Matsuda : ORNL TM-5114, and Japan. J. appl. Phys. 14 (1975) 2021.
27) L. Spitzer ; Physics of Fully Ionized Gases (Interscience Publishers, Inc., New York, 1956).
28) S. Yoshikawa : Physics of Fluids 6 (1963) 932.
29) A.I. Morozov and L.S. Solov'ev : Review of Plasma Physics (Consultants Bureau, New York, 1966) Vol. 2.
30) T. Takeda and S. Itoh : JAERI-memo 4186 (1970). in Japanese.
31) D.J. Rose and M. Clark : Plasma and Controlled Fusion (M.I.T. Press, Cambridge, 1961).
32) C.L. Longmire : Elementary Plasma Physics (Interscience Publishers, Inc., New York, 1963).
33) P. Papoular : Fontenay aux Roses Research Center Report EUR-CEA-FC-769.
34) V.D. Shafranov : Plasma Physics 5 (1963) 251.
35) T. Sometani and S. Itoh : Japan. J. appl. Phys. 11 (1972) 1181.
36) M. Murakami et al : Nuclear Fusion 14 (1974) 779.
37) JT-60 Program : IAEA Meeting of Specialist on Large Tokamak Experiments, July 4-11 1975, Dubna, USSR to be reported in Nuclear Fusion.
38) TFTR Program : ibid.
39) JET Program : ibid.
40) T. Ohkawa : Phys. Letters 38A (1972) 21.
41) P.H. Rutherford : Princeton Plasma Physics Laboratory Report MATT-975 (1973).
42) M. Wakatani : Japan Atomic Energy Research Institute Report JAERI-M 6124.
43) F. Karger, H. Wobig, S. Corti, J. Gernhardt, O. Klüber, G. Lisitano, K. McCormick, D. Meisel and S. Sesnic : IAEA Tokyo Conf. CN-33 A8-2 Nov. 1974.
44) C. Hayashi : Nonlinear Oscillation in Physical Systems (McGrow-Hill., New York, 1964).
45) R.J. Colchin : private communication.

46) T. ohkawa and W.D. Kerst : IL Nuovo Cimento 12 (1961) 784.
47) P. Chrisman, J. Clarke and J. Rome : Oak Ridge National Laboratory Report ORNL-TM-4501.
48) T. H. Stix : Phys. Rev. Letters 30 (1973) 833
49) V.D. Shafranov : Soviet Phys. Tech. Phys. 15 (1970) 175.
50) D. Dimock et al : Nuclear Fusion 13 (1973) 271.
51) W. Stodiek et al : CN-28/C-10.
52) T.E. Stringer : Nuclear Fusion 12 (1972) 689.